University of Alberta

EROSION-CORROSION IN SIMULATED OIL SAND SLURRY TRANSPORTATION

By

SIVA RATNAM SANKARAN ©

A thesis submitted to the Faculty of Graduate Studies and Research in partial fulfillment of the requirements for the degree of **Master of Science**

in

Materials Engineering

Department of Chemical and Materials Engineering

Edmonton, Alberta

Spring 2004

Library and Archives Canada

Published Heritage Branch

395 Wellington Street
Ottawa ON K1A 0N4
Canada

Bibliothèque et Archives Canada

Direction du Patrimoine de l'édition

395, rue Wellington
Ottawa ON K1A 0N4
Canada

Your file Votre référence
ISBN: 0-494-05676-2
Our file Notre référence
ISBN: 0-494-05676-2

NOTICE:
The author has granted a non-exclusive license allowing Library and Archives Canada to reproduce, publish, archive, preserve, conserve, communicate to the public by telecommunication or on the Internet, loan, distribute and sell theses worldwide, for commercial or non-commercial purposes, in microform, paper, electronic and/or any other formats.

The author retains copyright ownership and moral rights in this thesis. Neither the thesis nor substantial extracts from it may be printed or otherwise reproduced without the author's permission.

AVIS:
L'auteur a accordé une licence non exclusive permettant à la Bibliothèque et Archives Canada de reproduire, publier, archiver, sauvegarder, conserver, transmettre au public par télécommunication ou par l'Internet, prêter, distribuer et vendre des thèses partout dans le monde, à des fins commerciales ou autres, sur support microforme, papier, électronique et/ou autres formats.

L'auteur conserve la propriété du droit d'auteur et des droits moraux qui protège cette thèse. Ni la thèse ni des extraits substantiels de celle-ci ne doivent être imprimés ou autrement reproduits sans son autorisation.

In compliance with the Canadian Privacy Act some supporting forms may have been removed from this thesis.

While these forms may be included in the document page count, their removal does not represent any loss of content from the thesis.

Conformément à la loi canadienne sur la protection de la vie privée, quelques formulaires secondaires ont été enlevés de cette thèse.

Bien que ces formulaires aient inclus dans la pagination, il n'y aura aucun contenu manquant.

Canada

ABSTRACT

Erosion-corrosion is a significant concern especially in oilsand slurry transportation in long pipelines from excavation mines to extraction plants and tailing lines. Extensive research has been conducted on slurry flow erosion-corrosion and the influences of various parameters and the mechanism. However difficulties have arisen concerning the impact of flow, its control and mitigation in actual slurry pipelines. This study investigates the impact of erosion, corrosion and its synergistic effect in a simulated pilot scale two phase slurry flow-loop and with rotating cylinder electrode. Electrochemical, weight loss, limiting current measurements and microscopic analysis were completed to separate and identify the erosion-corrosion effect with temperature, flow rate and sand concentration. This study also discusses flow assisted corrosion, synergistic effect mechanism and proposes a unique technique to control the erosion-corrosion in slurry transportation.

KEYWORDS

Erosion, corrosion, erosion corrosion, slurry flows, oilsand, model, mechanism, flow loop, wear, cathodic protection.

ACKNOWLEDGEMENTS

This work is a collaborative effort between the industry and the University. The author gratefully acknowledges the keen interest and generous support from Syncrude Canada and the financial support from COURSE.

Author wishes to thank all the supervisors to provide facilities, personnel and scientific environment that enable him to successfully purse this research program with complete freedom and enthusiastic support.

Special thanks go to Tim Revega of Syncrude research, Artin Afacan, Andree keong, Robert Scott, Walter Boddez, Clark Bicknell, AnnMarie Brereton, Jiong Cai, and M.H.Wong of University of Alberta

Many thanks to Stefano Chiovelli of Syncrude research for his great support and friendship throughout this study.

Finally, I would like to acknowledge my wife for her belief in me and her undying devotion and support in whatever I chose to do.

NOMENCLATURE

a	Atomic weight
i	Current density
D	density of the material in
N	Number of equivalent exchanged
E.R	Erosion penetration rate
W	Sand production rate
V_m	Fluid mixture velocity
d_p	Sand size in micron
d	Pipe diameter
ρ_m	Fluid mixture density
D	Diffusion coefficient
m	Mass fraction of dissolved oxygen
ρ	Density
M_{Fe}	Molar mass of Fe
ρ_{Fe}	Density of Fe
C_{bO2}	Bulk concentration of oxygen
k_m	Wall mass transfer coefficient
P	Average penetration rate in mils per year
W	Weight loss in grams
A	Initial exposed surface area of the test piece in square inch
T	Exposure time in hours
S_m	A geometry dependent constant specified by Salama

X	Slurry concentration
Ds	Dry bulk density of Sand
Dw	Density of water
i_{corr}	Corrosion current density
ne	Reacted electrons
F	Faraday constant
MFe	Average molecular weight of the pipe material
ρ_{Fe}	Density of the pipe material
v_{plant}	Actual oilsand slurry transportation velocity
T_{plant}	Actual oilsand slurry transportation temperature
mp	Average mass of a single particle
χ	Slurry concentration
v_m	Mean slurry velocity
V_p	Particle velocity can be couple to flow velocity
α	Impact angle
V_{cr}	Critical velocity pipeline steel
P	Flow stress
Mp	Average particle weight.
$C_{O2_b_rot}$	Bulk concentration of oxygen in the rotating cylinder
$C_{O2_b_plant}$	Bulk oxygen concentration in oilsand slurry pipeline

TABLE OF CONTENT

1. INTRODUCTION 1

1.1 The problem 1
1.2 Definitions 2
1.3 Objective 3
1.4 Economy 4

2. LITERATURE REVIEW 5

2.1 Measurement of Corrosion and Erosion 5
2.2.1 Linear polarization 7
2.2.2 Electrochemical Impedance Spectroscopy (EIS) 8
2.2.3 Electrochemical Noise Measurements (ENM) 9
2.2 Morphology 9
2.3 Parameters that affect erosion-corrosion 9
2.3.1 Oxygen concentration 9
2.3.2 Velocity 10
2.3.3 Impingement angle 11
2.3.4 Slurry concentration and distribution 11
2.3.5 Materials properties 12
2.4 Mechanism 12
2.4.1 Corrosion mechanism 13
2.4.2 Flow mechanism 15
2.4.3 Erosion mechanism 17
2.4.4 Erosion-corrosion 19
2.5 Slurry simulations in the past 20
2.6 Erosion-corrosion model predictions 22
2.6.1 Flow models 22
2.6.2 Erosion models 23
2.6.3 Corrosion model 25
2.7 Past proposed solutions 26
2.7.1 Cathodic protection 26
2.7.2 Inhibition 27
2.8 Summary of literature review 27

3. MATERIALS AND METHODS 29

3.1 Slurry flow-loop 29

3.1.1 Test piece holder design 31
3.1.2 Specimen cleaning and weighing 32
3.2 Test material 33
3.3 Slurry simulation 33
3.4 Corrosion and synergistic effect measurements 34
3.5 Mass transfer simulation 36
3.6 Calibrations 37
3.7 Assumptions and validations 38
3.8 Flow-loop operating procedure 39
3.9 Calculations 39
3.9.1 Corrosion rate 39
3.9.2 Density 40
3.9.3 Measurement errors 41

4. RESULTS AND DISCUSSION 42

4.1 Oxygen diffusion 42
4.2 Oxygen concentration 43
4.3 Corrosion and Synergistic effect 44
4.4 Erosion-Corrosion 48
4.1.1 Effect of sand concentration 48
4.1.2 Effect of slurry velocity 53
4.1.3 Effect of temperature 55
4.5 Comparison with previous studies 58
4.6 Morphology 59
4.7 Accuracy of the measurements 63

5. MECHANISM AND MODELING 67

5.1 Corrosion 67
5.1.1 Mechanism 67
5.1.2 Diffusion rate (k_d) 68
5.2 Erosion 72
5.3 Synergistic effect 74

6. MITIGATION OF EROSION-CORROSION 78

6.1 Control of temperature 78
6.2 Reduction of oxygen 78
6.3 Preferential protection 81

7. CONCLUSIONS AND RECOMMENDATIONS 84

8. FUTURE WORKS 87

LITERATURE CITED 93

APPENDIX I 99

APPENDIX II 102

LIST OF FIGURES

Figure 1.1 : Schematic erosion-corrosion pattern 2

Figure 2. 1 : Effect of sand on erosion-corrosion in aerated/ de aerated water 10
Figure 2.2 : Corrosion rate and the breakaway velocity (extracted from Chexal, 1996).. 11
Figure 2.3 : Three major modes of erosion (Walker & Roco)..... 16

Figure 3.1 : Slurry flow-loop to simulate the oil-sand transport line..... 29
Figure 3.2 : XRD Analysis of C.P deposits 30
Figure 3.3 : Reverse osmosis filter unit (Petwa)..... 30
Figure 3.4 : Test piece holder design for flow-loop weight loss measurements..... 32
Figure 3.5 : Cathodic protection criteria for erosion measurements..... 32
Figure 3.6 : Micrograph of silica sand..... 34
Figure 3.7 : Sand distribution 34
Figure 3.8 : Tafel polarization diagram and the corrosion current extrapolation 35
Figure 3.9 : On-line corrosion measurements..... 36
Figure 3.10 : Open circuit potential 36
Figure 3.11 : The rotating cylinder electrode to measure the oxygen diffusion rate 36
Figure 3.12 : Corimass meter calibration for flow rate..... 38
Figure 3.13 : Slurry density to weight percentage conversion diagram 41

Figure 4.1 : Limiting current test with rotating cylinder electrode..... 42
Figure 4.2 : Saturated oxygen concentration in the flow-loop..... 43
Figure 4.3 : Slurry oxygen concentration change with in a test in the flow-loop..... 44
Figure 4.4 : Corrosion measurement at 22°C (Weight loss vs. Electrochemical)..... 45
Figure 4.5 : Corrosion thickness at 2.5 m/s and 32°C after 22 hrs without sand..... 46
Figure 4.6 : Electrochemical measurement at 32°C and 1.5 m/s (With & without sand). 47
Figure 4.7 : Effect of sand concentration at different velocities at 22°C..... 48
Figure 4.8 : Effect of sand concentration at different velocities at 32°C..... 49
Figure 4.9 : Effect of sand concentration at different velocities at 42°C..... 50
Figure 4.10 : Effect of slurry concentration on erosion, corrosion, synergy 51
Figure 4.11 : Ave. erosion-corrosion change with temperature @ 5% sand increase 52
Figure 4.12 : Effect of slurry velocity on erosion, corrosion and synergy at 32°C 54
Figure 4.13 : Erosion-corrosion change with temperature @ 0.5 m/s velocity increase .. 55
Figure 4.14 : Effect of temperature on erosion, corrosion and synergy at 2 m/s..... 56
Figure 4.15 : Contribution of erosion, corrosion and synergism (2m/s, 8% sand 32 °C) 56
Figure 4.16 : Temperature on erosion-corrosion at 2 m/s..... 57
Figure 4.17 : Micrograph of the corrosion at 2.5 m/s and 32°C after 22 hrs 59
Figure 4.18 : Erosion-corrosion after 30 hrs..... 59
Figure 4.19 : Flow path and micro-pits at the clean surface (after 30 hrs)..... 60
Figure 4.20 : Erosion-corrosion surface profile along the circumference. 60
Figure 4.21 : Erosion-corrosion surface roughness along the flow direction..... 61
Figure 4.22 : (a,b) SEM images of erosion at along the circumference 62
Figure 4.23 : SEM image of erosion ploughing scars on the flow-loop specimen..... 62
Figure 4.24 : Flow-loop reciprocating pump rotor 63
Figure 4.25 : Temperature variation in the erosion-corrosion test at the flow-loop 64

Figure 4.26 : Temperature deviations in the erosion-corrosion test at the flow-loop..... 65
Figure 4.27: Velocity variation in the erosion-corrosion test at the flow-loop..... 65
Figure 4.28 : Velocity deviations in the erosion-corrosion test at the flow-loop 66

Figure 5.1 : Schematic representation of the equilibrium corrosion process..... 68
Figure 5.2 : Limiting current test with rotating cylinder electrode..... 69
Figure 5.3 : Schematic O_2 diffusion and flow profile in rotating cylinder 69
Figure 5.4 : Schematic O_2 diffusion, flow profile and oxide layer near pipe wall 70
Figure 5.5 : Limiting current and corrosion current with velocity 71
Figure 5.6 : The difference between limiting and corrosion currentwith velocity 89
Figure 5.6 : Sand impact velocity (v_p) and the mean slurry velocity..... 73
Figure 5.7 : Shear fore with flow velocity for a single particle impact 74
Figure 5.8 : Stress distribution of a single particle impact 75
Figure 5.9 : Single particle impact simulation..... 76

Figure 6.1 : Schematic erosion-corrosion distribution along the slurry line..... 79
Figure 6.2 : Schematic potential / pH diagrams..... 80
Figure 6.3 : Schematic representation of oxygen removal by accelerating the corrosion 81
Figure 6.4 : Flow profile 81
Figure 6.5 : Preferential protection anode position and current distribution 82
Figure 6.6 : Preliminary preferential protection design 83

Figure 8. 1 : Proposed slurry flow-loop modification..... 88
Figure 8.2 : The difference between limiting and corrosion current.....88

1. Introduction

Alberta is rich in oil, oilsand and natural gas reserves and these industries constitute a major portion of the provincial economy. Intensive research has been carried out on excavation, transportation and extraction of oilsand for the last four decades. Transportation and distribution of slurry through pipelines called hydrotransport has become widely accepted practice since the first significant North American slurry pipeline built in 1957 (Hale, 1976). The oilsand industry has used hydrotransport technology to transport tailing materials for many years while oilsand hydrotransport is a more recent development.

Transportation of oilsand by hydrotransport has two main benefits. They are the ease of transportation from any excavation mine site to an extraction plant and oilsand conditioning. This means while the mixtures of oilsand and water flows through the pipeline, large lumps of oilsand are broken down and bitumen is separated from the oilsand. This is an environmentally friendly method and *Kyoto* protocol-proof way of transporting oilsand. However erosion-corrosion becomes a significant concern in oilsand transportation where oilsand is transported through long pipe lines with slurry concentration up to 50%.

Different terms were used in slurry flow related corrosion in pipelines. Erosion cavitations, flow induced corrosion, abrasion, scouring wear, erosion wear etc. latter the trend was to add the word corrosion and hence erosion-corrosion, cavitations corrosion etc. This reflects the realization that corrosion could play a decisive part in damage mechanism, a fact that long went unrecognized by many.

1.1 The problem

In single phase pipe flow, substantial internal erosion and corrosion, called flow-induced-corrosion, occur most frequently in disturbed flow conditions such as near inlet, exit, bends or weld joints of the pipeline. It results in clusters of deep pits usually up to few

inches on the downstream side from the disturbance. This is accelerated by the presence of even a small amount of sand and has been noticed in several pipelines in Alberta.

NACE qualitative guidelines for oil field operation recommended that average general corrosion rate of 10 mpy (0.254 mm/y) or pitting rate of 15 mpy should be treated at severe. However our results and the actual oilsand plant studies show a minimum erosion-corrosion rate of 250 mpy (6mm/y) or more. This is a potential problem because of increased pressure drops, unplanned shut down and catastrophic failure following severe attack.

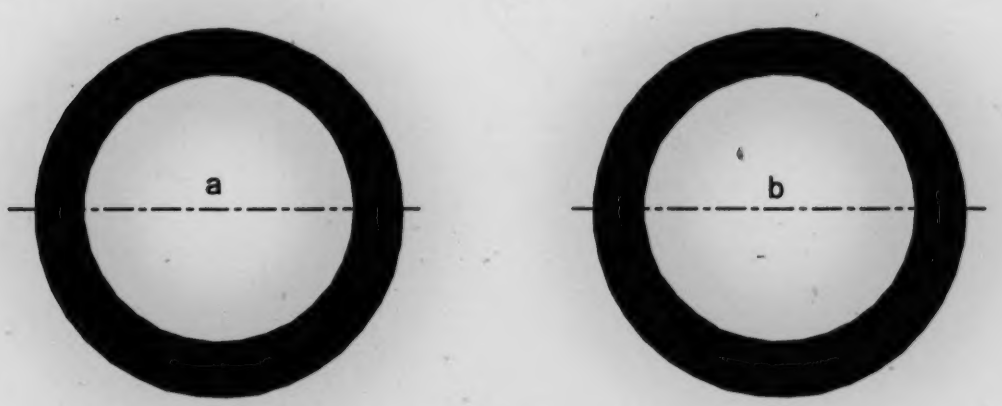

Figure 1.1 : Schematic erosion-corrosion pattern

Small amount of sand rolling on the bottom of the pipeline cause severe damage at the 6 o' clock position in oil exploration and transportation lines as shown in Figure 1.1a. In oilsand slurry transportation, severe erosion-corrosion pattern was noticed in the bottom half of the pipeline as in Figure 1.1b. Sometimes froth flow on top of the slurry causes severe attack at 2 o' clock and 10 o' clock position similar to the tidal zone corrosion observed in the steel piles in jetties and off-shore platforms.

1.2 Definitions

For this study and future references, *Corrosion* is defined as the material loss due to corrosion attack in pipeline carrying aerated saline water without sand. This term consists

of instantaneous corrosion or pure corrosion measured by electrochemical measurement and corrosion due to flow effects.

Based on ASTM-G15-99b (2000), *Erosion-corrosion* is defined as a synergistic process involving both erosion and corrosion in which each of these processes affected by the simultaneous action of the other and thereby accelerated. This is caused by the effect of corrosion, erosion and synergistic effect.

The rate of metal loss when the electrochemical corrosion is eliminated by cathodic protection is defined as erosion.

Synergistic effect is the rate of material loss resulting from the interaction of erosion and corrosion processes. This term consists of increased corrosion due to base metal erosion, increased corrosion due to oxide layer erosion and micro-stress-corrosion as defined in this study.

1.3 Objective

The objective of this research is to evaluate the effects of slurry-induced erosion-corrosion and find out a cost-effective solution to mitigate or reduce the erosion-corrosion in slurry pipeline.

The Strategy

To effectively achieve the above objective, the following strategies were adopted.

- A review of the literature including the characteristics of erosion-corrosion along with possible impact on long pipeline slurry transportation
- Simulate appropriate lab scale and pilot plant scale slurry flow
- Investigate the potential impact of various flow parameters, material properties on erosion-corrosion and separate the erosion, corrosion and synergistic effect due to slurry flow.

- Find out the cause and mechanisms of erosion-corrosion and developed a model for erosion-corrosion
- Finally once the underlying problems have been identified, develop an innovative approach to mitigate erosion-corrosion

Therefore this study will identify the new concepts, models, mechanisms and technological approaches and make recommendation to mitigate slurry erosion-corrosion and communicate the results to major oilsand industries.

1.4 Economy

A gradual improvement of oilsands economics has occurred over the past 90 years of applied research and 36 years of commercial production. Syncrude started 3.4 million barrels of crude oil in its first year production in 1979 and targeted 85 million barrels for year 2003. Presently oilsand extraction cost $12 to $16 US a barrel whereas oil produced using conventional methods costs roughly US$10 a barrel. Again this may vary until the details and cost impacts of the Federal government's *Kyoto* Protocol are known.

There are about 175 billion barrels of proven reserves in Alberta's oilsand, the world's largest resource of oil outside Saudi Arabia. Another 150 billion barrels could be extracted once new and more efficient extraction technologies are developed. Many companies plan to transport oilsand from excavation mine to extraction plant by pipelines in near future and there is a tremendous need and potential benefit to alleviate the effect of erosion-corrosion.

2. Literature Review

Although the transportation of solids in the form of slurries is basically older than history- *'the blood circulation system in mammal'* the research of erosion-corrosion in slurry transportation was initially undertaken in the 1950s.

In order to provide a comprehensive background for research, the specific corrosion problem or problems related to both erosion and corrosion are identified and reviewed in this chapter. Once the underlying problems have been identified, it will subsequently be possible to build a model to predict, a method to control and a program to monitor erosion-corrosion in slurry transportation. There is no doubt that the pipelines carrying slurry disrupts and deteriorates the pipe material much faster than single phase flow. Appropriate construction methods, broader application of corrosion-resistant materials and the application of improved erosion-corrosion related technical practices, along with compatible flow control procedures, can only be implemented once the short-term and long-term effects of slurry flow are known.

To-date many investigators have studied erosion-corrosion in simple pipeline geometries such as elbows, tees and straight pipelines (Postlethwaite 1976, Nesic 2001, Wood 2001). All of these studies indicate that erosion rate is proportional to velocity, sand concentration and many other factors including fluid properties, flow regime, pipe material, sand characteristics etc. The extent of corrosion and conditions that cause erosion-corrosion depends on fluids moving at high velocity, solids in suspension, direct impingement and the level of turbulence.

2.1 Measurement of Corrosion and Erosion

To understand the damage mechanism, it is important to evaluate the relative amount of material loss due to erosion, corrosion and the synergetic effect. Corrosion and synergistic effect can be regarded as the main reasons for the removal of material in aggressive slurry flow conditions. The removal of material caused by erosion-corrosion can be defined as:

$$V_T = V_E + V_C + \Delta V \qquad 2.1$$

Where:

V_T = the total removal of material due to erosion-corrosion

V_E = component resulting from mechanical wear or erosion only.

V_C = the damage of material due to corrosion only

ΔV = the synergistic amount of corrosion and erosion. It can be calculated from the above equation 2.1

ΔV could be further divided into two parts as corrosion-induced erosion and erosion induced corrosion.

$$\Delta V = (\Delta V_E + \Delta V_C) \qquad 2.2$$

Where:

ΔV_E = the accelerative component of erosion damage by corrosion and is called erosion or wear increment

ΔV_c = the accelerative component of corrosion loss by erosion and is called corrosion increment

The synergistic effect between corrosion and erosion increases proportionally to load. In aqueous conditions there is no significant effect of corrosion on erosion and therefore it can be assumed that the term ΔV_E is negligible (Postlethwaite 1986)

Erosion-corrosion rate can either be determined by direct thickness measurements or inferred from weight loss measurements by laboratory and pilot plant simulation. The weight loss technique was preferred by many studies as it is well proven, reduces the overall duration of test, and yields accurate information on both the amount of material removed and manner in which wear takes place (Ferrini, 1982). Some materials however, absorb water and may affect the values obtained from the weight loss measurements. This can be avoided by carefully drying the sample before and after the test.

Electrochemical techniques to measure and monitor corrosion is well-known and have been widely used for many different applications. These measurements are used for a

comparative purpose in laboratory tests and some cases for direct corrosion measurements. These results often provide corrosion rates in terms of electrical current. Although conversion of these current values to either mass loss rates or penetration rates is based on Faraday's law, these calculations can be complicated for alloys and metals with multiple valence values.

Furthermore corrosion can be accelerated during liquid solid impingement test by the application of potential (+600 mV SEC) positive to E_{cor}. The proportion of mass loss that could be attributed to the accelerated pure corrosion can be calculated from the current measured during the test at +600 mV (Neville , 1999)

In light of these, it is important to understand these electrochemical techniques and their applications. The techniques considered in this study are described below for easy reference.

2.2.1 Linear polarization

Linear polarization is based on complex electrochemical theory. For industrial applications it was simplified to a very basic concept. In fundamental terms, a small voltage called polarization potential is applied to an electrode in the solution. The current needed to maintain a specific voltage shift (typically 20 mV for linear polarization resistance and 100 mV for Tafel plots) is directly related to the corrosion on the surface. By measuring the current, corrosion rate can be derived. This is a more powerful tool than either coupons or ER probes which measure metal loss.

The recent electrochemical instruments automatically convert the corrosion current into corrosion rate. Current density ($\mu A/cm^2$) can be converted into corrosion rate or penetration rate in mm/year (Jones D.A, 1996).

$$R = \frac{0.00327(a.i)}{(n.D)} \qquad 2.3$$

Where:

R = corrosion rate, mm/y

a = atomic weight, g

i = current density, $\mu A/cm^2$

D = density of the material, g/cm^3

n = number of equivalent exchanged

The proportionality constant 0.00327 becomes 0.129 for mpy and 3.27 for μm/yr.

Anodic polarization and potentiodynamic tests are used to determine the kinetics of electrochemical corrosion process under conditions of solid free liquid flow and solid liquid impingement. Most observation shows that the corrosion current in static solution is much lower than the corrosion current after the erosion in static solution. Most of the oxide film was broken during erosion and the metal surface is much active after erosion. These techniques appear to work well for clean systems and are difficult in gases or water-oil emulsions where fouling of the electrodes may prevent the measurements.

2.2.2 Electrochemical Impedance Spectroscopy (EIS)

EIS is an electrochemical method in which either AC signal or AC impedance is used. This signal is applied to an electrode, here a corroding metal, and the response is measured. Usually, a small voltage signal is applied and the resulting current is measured. The measuring equipment, process the current-time and voltage-time measurements separated by different resistance such as the solution resistance and the polarization resistance. At lower frequencies different types of processes occur over different time scales at different frequencies. Consequently it may be possible to identify the diffusion effects or adsorption / desorption phenomena.

Bonnel (1983) used impedance measurements to study the electrochemical behavior and corrosion of carbon steel in 3% NaCl solution using rotating disc electrode. Both steady state and transient measurements were collected and showed that oxygen transport takes place not only in the liquid phase but also through porous layer of the corrosion products.

2.2.3 Electrochemical Noise Measurements (ENM)

Fluctuations of potential or current, typically of low frequency (<10Hz) and low amplitude is called electrochemical noise, It originates in part from the natural variations in electrochemical rate kinetics during corrosion process. They include partial Faradic currents, adsorption/desorption processes, surface coverage, and particularly in the case of localized corrosion, the initiation of pits and mechanical effects resulting from erosion and cracking process. Measurements were typically acquired by monitoring the evolution of a corrosion process on two or more coupled electrodes without the application of an external signal.

Shirazi et al (Shirazi, 2000) used this acoustic monitoring technique in slurry erosion-corrosion studies in one inch diameter stainless steel pipe elbows. They also showed a direct correlation between the particle impact velocity and the noise measurement. Using this correlation they predicted the erosion rate for an elbow.

2.2 Morphology

The microstructures of the surfaces of the erosion-corrosion specimens correlated with metal loss rates. The use of SEM made it possible to observe what had physically occurred on eroded surfaces. This also shows that the texture of the eroded surface of metal exposed to a liquid-solid medium and gas-solid medium are quite different. Correlating this information with measured material loss will establish the surface degradation mechanisms, but is more complicated than analytical modeling (Levy, 1995).

2.3 Parameters that affect erosion-corrosion

2.3.1 Oxygen concentration

Oxygen influences erosion-corrosion in three ways; control corrosion rate, corrosion potentials and be present as gas bubbles. The saturation concentration of dissolved oxygen decreases with increasing temperature and increasing concentration of other

dissolved species. It has been suggested that the corrosion of pipeline carrying aerated slurries is under oxygen mass transfer control and that the rate of mass transfer is enhanced under erosion conditions (Postlethwaite 1986, Shirazi 2000).

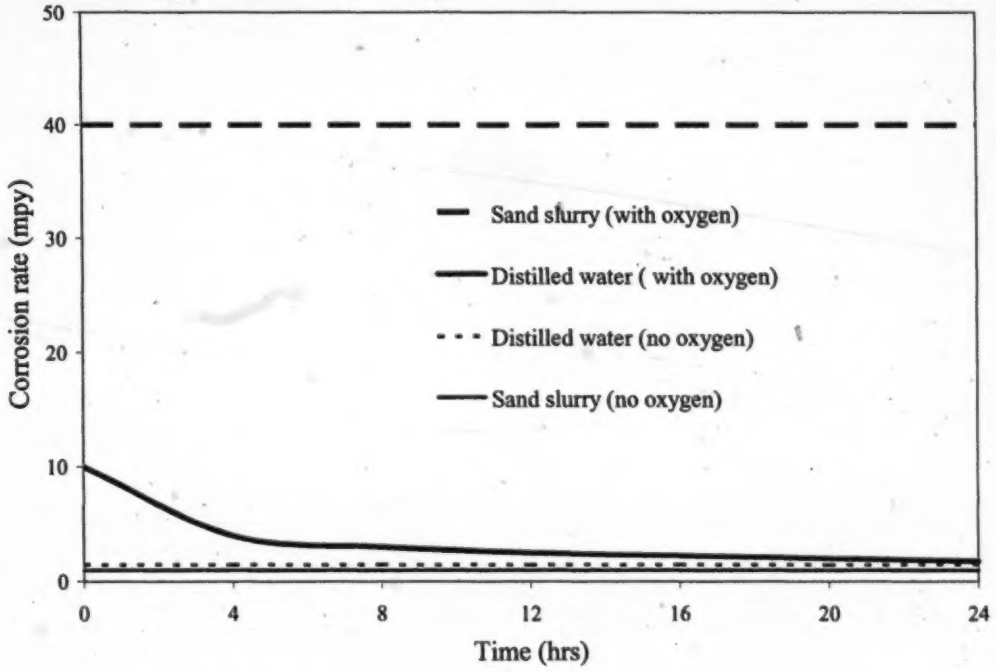

Figure 2. 1 : Effect of sand on erosion-corrosion in aerated/ de aerated water

The Figure 2.1 extracted from Edward et al (Edward, 1975) shows the corrosion rate is substantially increased by sand particle in the presence of oxygen. However the addition of sand in the absence of oxygen does not change the corrosion rate. When the environment is corrosive only, the solids erode the protective film and increase the corrosion rate (Edward, 1975)

2.3.2 Velocity

In slurry transportation, flow velocity is of more importance than for single-phase flow and when the velocity is too low, solids could settle out and start forming a bed at the bottom of the pipe. On the other hand, when the velocity is too high the solids could erode the inside surface of the pipe at an unacceptable rate and of course increase the

friction losses and the pumping requirements. Therefore, establishing the critical velocity and operating it at this velocity is very important in slurry pipelines (Husband, 1986). A plot of corrosion rate versus flow velocity is typically of the form shown in Figure 2.2. At a certain velocity, the so called critical or break away velocity (Chexal, 1996) a steep rise in corrosion rate occurs and is corresponds to the conditions wherein the film has been eroded through in certain areas.

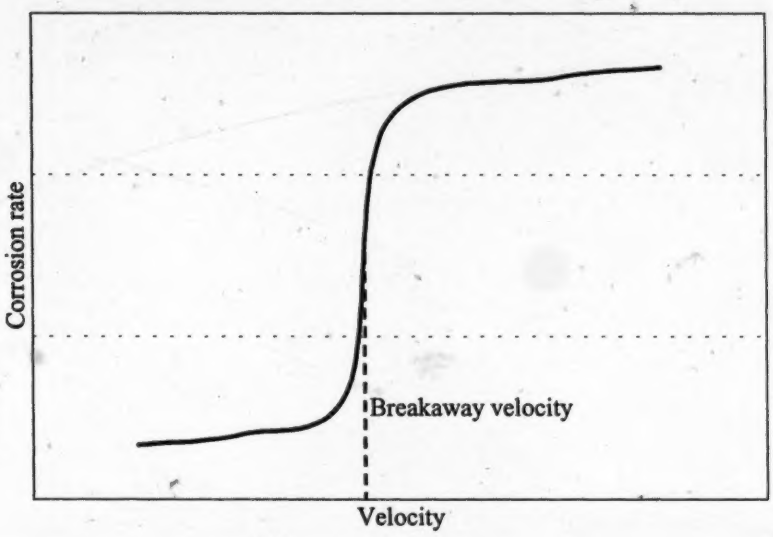

Figure 2.2 : Corrosion rate and the breakaway velocity (extracted from Chexal, 1996)

2.3.3 Impingement angle

The erosion is governed by the angle of impact of the solids and the strength and ductility of the pipe wall. In most slurry pipelines, the angle of impact is expected to be small, the pipe wall is ductile. Weight loss measurements in the laboratory by Burstein (Burstein, 2000) demonstrate that the synergistic effect between erosion and corrosion is enhanced by more oblique angle of impact than normal incidence

2.3.4 Slurry concentration and distribution

Concentration affects the flow regime and thus the erosion-corrosion distribution. Slurry erosion rates increase with increasing particle concentration up to a limit and the effect decreases with increasing particle concentration due to particle interaction. For slurries

with fine particles, higher concentrations may produce a more uniform velocity distribution in the flow of slurry and consequently less wear. The large particles are carried in fine particle slurry, the fine tends to reduce or cushion impacts of the large particles with pipe wall (King, 1991). Also for fully developed flows erosion rates varied linearly with the particle concentration from 0 -5 % mass concentration (Postlethwaite, 1993).

2.3.5 Materials properties

In pipelines, the erosion of metal surface results from the dynamic action of moving particles. Depending on the flow condition, the erosion can be either deformation wear (impact wear) or cutting wear (sliding wear). Both these wear occur when the solid particles are harder than the pipe surface. Thus making pipe wall harder than solid particles can eliminate the abrasive wear. However the most common abrasive particle silica, similar to oilsand, with a hardness of about 800kg/mm^2 and much greater hardness than most common pipeline materials of hardness varies between 200 to 800kg/mm^2 (Edward, 1975). Neville et al (2001) shows that micro-hardness is not the overall controlling factor in erosion-corrosion of various grade stainless steels. The resistance of a metal against the flow induced localized corrosion totally depends on the property of its protective layer of corrosion products.

Increase in Vickers hardness of steel by heat treatment has virtually no effect on erosion. There is considerable evidence in the literature (Levy 1995) to support the idea that higher strength and hardness do not result in a grater erosion resistance within families of alloys and surface hardening do not improve the erosion-corrosion resistance.

2.4 Mechanism

Erosion-corrosion caused by flowing slurry is not totally understood, despite many experimental and modeling studies to evaluate the interactions between mechanical and electrochemical mechanisms and the damage.

Slurry erosion-corrosion of passive materials is characterized by the mechanical perturbation of the passive film. The localized impacts of small abrading particles in suspension in a flowing corrosive fluid leading to transcendent corrosion phenomena include passive film breakdown.

2.4.1 Corrosion mechanism

Three basic forms of rusts may appear with dissolved oxygen (DO) in water (Bruce, 2002).

$$Fe + H_2O + 1½\ O_2 \rightarrow 2\ \alpha, \beta \text{ or } \gamma\text{-}FeO(OH) \qquad 2.4$$

If the water is nearly saturated with DO, hematite (Fe_2O_3) is often present, but if there is not much DO, other oxide form of magnetite (Fe_3O_4) will be present in the water. The beta form is the most often associated with water containing high chloride. It predominates over the other phases when the chloride content is high. When CO_2 is present the reaction that most predominates at moderate temperature of up to ~80°C is

$$Fe + H_2CO_3 \rightarrow FeCO_3 + H_2 \qquad 2.5$$

And the corrosion product above this temperature is magnetite (Fe_2O_3).

The γ-FeO(OH) is unstable and will quickly transform to magnetite by either of the following reactions.

$$3\ \gamma\text{-}FeO(OH) + e \rightarrow Fe_3O_4 + H_2O + OH^- \qquad 2.6$$

$$Fe2+ + 8\ \gamma\text{-}FeO(OH) + 2e \rightarrow 3Fe_3O_4 + 4H_2O \qquad 2.7$$

Pipeline internal corrosion caused by slurry flow is an electrochemical phenomenon and requires an anode, a cathode, a conductor between anode and cathode and electrolyte solution. The half cell electrochemical reaction at the pipe wall is:

Anodic reaction $2Fe \rightarrow 2Fe^{2+} + 2e^-$ 2.8

Cathodic reaction $O_2 + 4e^- + 2H_2O \rightarrow 4OH^-$ 2.9

Precipitation at the pipe wall

$$2Fe^{2+} + 4OH^- \rightarrow 2Fe(OH)_2 \qquad 2.10$$

Chemical oxidation near the pipe wall

$$2Fe(OH)_2 + ½\ O_2 \rightarrow 2Fe(OH)_3 \qquad 2.11$$

The overall reaction at is

$$2Fe + 1½O_2 + 3H_2O \rightarrow 2Fe(OH)_3 \qquad 2.12$$

The oxygen reduction is the main cathodic reaction in neutral slurries and the rate of reaction is controlled by oxygen diffusion. The final corrosion products are in the form of hydrated ferric oxide, magnetite or hematite.

Disturbed flows caused by sudden expansion, weld joint, erosion, etc. can induce formation of electrochemical cells due to difference in shear stress, aeration, pH and produced anodic and cathodic regions (Postlethwaite, 1991).

The electrochemical corrosion mechanism induced by liquid or slurry flow can be in the following ways (Heitz 1991)

- Supply of reactants or removal of intermediates or products by mass transfer and the rate-determining step is diffusion. It is generally more or less uniform.
- Erosive action on the metal surface by removal of surface layer, passive layers, or base metal, thus producing a more reactive surface, which leads to the formation of new layers.
- Stabilization of surface layers by increased mass transfer which cause the solubility product of the layer to be surpassed closer to the surface, thus causing better adherence.

Although these forms are present in the context of aqueous corrosion, proper identification of the type of corrosion and analysis of corrosion products is very important in identifying the corrosion mechanism. Spot test corrosion products using acid and magnetism as indicators for certain compounds are useful but often mislead; energy dispersive spectrometer EDS is used to identify the elements and the not compounds. X-ray diffraction (XRD) analysis is used to positively identify and understand the corrosion products and by application of the relevant equation, it is possible for one to establish a complete understanding of the cause of corrosion in a system. (Bruce, 2002)

From the x-ray analysis of corrosion products at 0 m/s and 0.5 m/s in a Jet impingement rig test, Nanjo (1990) shows the corrosion products at 0 m/s mainly considered reddish brown corrosion products Fe_2O_3 and FeOOH and were in the state of suspension during the test. Dissolved oxygen easily reached a metal surface and generates products of large oxidation number. In case of flow field, the main components of corrosion products were Fe_3O_4, which is blackish brown color and small amount of Fe_2O_3 and FeOOH. The corrosion products sticking tightly inside and around pits suppressed dissolved oxygen from diffusion. Therefore iron oxide of smaller oxidation number Fe_3O_4 could be formed. On the other hand, dissolved oxygen was supplied to the upper layer of Fe_3O_4 and iron oxide and hydroxide or large oxidation number species such as Fe_2O_3 and FeOOH could be formed.

2.4.2 Flow mechanism

"*Many researchers in erosion are interested in the mechanism by which particles remove the material rather than the fluid mechanics aspects. However, in some cases, the calculation of particle trajectories in a fluid stream rather than material selection has been the key to solving major erosion problems*" (Iain Finnie, 1995)

The transport of solid particles in slurry is either by sliding, rolling and jumping on the bottom of the pipe or dispersed in suspension. The slurry can be in laminar or turbulent flow, however the turbulent flow regime is encountered in most part of the industrial applications handling water.

Critical deposition velocity is very important parameter in designing pipe flow of settling slurries. It is defined as the velocity at which a stationary bed of particles appear at the bottom of pipe. The detailed study by Shook (Shook, 2000-b) can be used to calculate this.

The pipe material removed can be either by one or combination of the following particle dynamics pattern wear mechanism (Roco, 1988, Walker 1998)

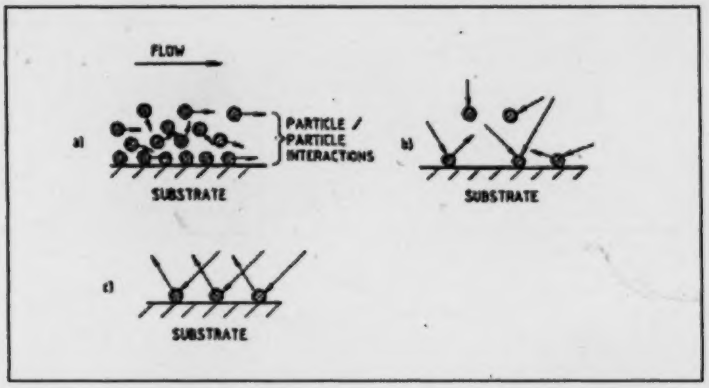

a) - Sliding bed
b) - Random impact
c) - Directional impact

Figure 2.3 : Three major modes of erosion (Walker & Roco)

Friction caused by Coulombic contacts, as shown in Figure 2.3 (a), is predominant when the sliding bed flow pattern occurs as well as when suspension flows are close to the critical sediment velocity.

By random impact we mean by collisions from random directions between solids and the wall as shown in Figure 2.3 (b). The turbulent velocity fluctuations of solids caused by fluid/solid and inter particle interactions play the major role in the straight pipe sections. Directional impact, caused by the mean separation velocity between solid and liquid, Figure 2.3 (c) develops in elbows, sections with contractions joints etc. The same mechanism can be expanded to other slurries handling equipments and the flow pattern determines which erosion wear mechanism is predominant.

The particulate wear mechanism is a stochastic process at particle scale and two steps explain the wear pattern via stochastic analysis. The first step is to investigate the motion of the particulate system in the vicinity of the bounding surface. The second step is the modeling of impact events at particle scale. Particles of random size and shape impact roll and slide on the wall with random velocities under various impingement angles, while the in-homogeneities of the exposed material and surface have random distributions. Therefore, the material removal is defined by a probability distribution function. (Roco, 1988)

By using the kinetic theory for large particles and at the boundary slip condition, one can determine the interaction energy between particles and the wall as a function of the mean solid velocity profile close to the wall. The supported load and dispersive stress were recently introduced to differentially describe and numerically evaluate the particle –wall interaction stresses by Coulombic friction and collusions respectively. Modeling the impact event is the second step in the analysis at particle scale.

Depending on the energy or frequencies of the particle hitting the surface, Heitz (1991) considered the chemo-mechanical effects and categorized them as follows:

I. The particle energy is too small to damage even the passive layer of a passivated metal or the impact events are too rare to have a measurable effect on the metal weight loss rate. Flow effects can only be effective via mass transfer.

II. The particle energy is sufficient to account for damage to the passive or other surface layers and to deform the outer regions of the base metal mechanically. The activated surface of the metal corrodes in the presents of aggressive agents. Erosive wear and corrosive rates are of the same magnitude. Damage and healing kinetics of passive or other layers are involved. Behavior of ferrous material is strongly determined by alloy composition. In materials with two phase structures (e.g. harden alloys with chromium carbide) local corrosion on a micro scale is observed.

III. The particle energy is so great that the base metal is preferentially eroded and the attack is mainly erosive wear. It can be shown that in turbulent tube flow with sand particles the mechanical energy of an impinging particle exceed the energy necessary to the formation of *micro furrow* (trough) by a factor of 1000.

2.4.3 Erosion mechanism

Deformation wear occurs when the particles kinetic energy causes local stresses higher than the yield strength of the pipe. Cutting wear occurs when the particles have sufficient energy to shear the local surface.

Iain Finnie (Finnie 1960) in an important contribution in this field compared the particle to the cutting edge of a tool which moves into the specimen surface causing plastic deformation of the material and removal of the formed debris. He evaluated his theoretical results with experimental data in which the particle velocity and angle of attack were strictly controlled. His correlation was good for ductile specimens at small angles of attack and known as cutting wear and accompanied by plastic deformation of the surface material. His theoretical relationship, however make no predictions for the erosion which occurs under normal attack on such materials (Levy, 1995)

Bitter (Bitter, 1964) also made a theoretical analysis of the problem. In addition to cutting wear he allowed for deformation wear which is associated with the repeated blows suffered by the specimen and which eventually cause cracking and spalling of surface material. It is this deformation wears which accounts for the erosion at normal attack in ductile materials and which is not accounted in the Finnie's analysis. (Levy, 1995) Bitter's theoretical work is exhaustive and extremely intricate, accounting for the elastic as well as for the plastic properties of the particle and specimen materials.

Levy (Levy, 1995) proposed another mechanism called the *platelet mechanism*. This approach was developed by physically observing the surface of an eroding ductile material at the microscopic level. The mechanism consists of sequential plastic deformation processes that account for all separate occurrences resulting in the overall surface degradation.

Particles initially impact a stress-free surface and cause craters of three distinct types: indentation, ploughing and smear craters. As the particles continue to impact, there is a general microscopic roughening of the surface because of plastic deformation caused by the large localized stress in the immediate areas of the particle impact. Eventually the particle impact crater and their attendant platelets completely cover the surface. At this time, particle no longer have a fresh surface to impact against, a gradual increase in frequency of smear-type craters with platelet formation starts and measurable erosion or the actual material loss starts.

2.4.4 Erosion-corrosion

The combination of erosion and corrosion results in more severe attack than would be realized with either mechanical or chemical corrosive action alone.

The material loss rate can be significantly accentuated when the passivity of the material such as stainless steel and Ni based alloys is breached by a mechanical influence. The material can make transition into a regime which consists of active and passive sites on the surface which depend on the mechanical influence, frequency and the extent of impacts by sand or other impacting species (Neville, 2001-b).

Post-experimental observations facilitated with light optical microscopy and scanning electron microscopy show that erosion-corrosion generally can be marked by its appearance in the form of shallow pits, horse-hoe-shaped groves, or other local phenomena correlated with the direction of flow (Heitz 1991, Neville, 1999). Affected areas are usually free of deposits and corrosion products, although they can sometimes be found if erosion-corrosion occurs intermittently or if the liquid flow rate is relatively slow.

Matsumura et al (Matsumura, 1995) suggested that corrosion is accelerated by erosion through the destruction of passive film by the particle impact followed by dissolution of the surface, leading to the elimination of the work-hardened layer as well as to an increase in the surface roughness. Both of these effects then allow impacting particle to penetrate more deeply into the material and cause greater corrosion damage.

Postlethwaite et al (Postlethwaite, 1986) compare two different erosion-corrosion mechanisms. Based on the studies in slurry pipeline carrying sand and similar abrasive slurries they proposed the following mechanism:

The erosive effect of solid particles prevents the formation of rust which normally reduces the diffusion of oxygen to the corroding surface. Therefore the corrosion proceeds at a high rate in the absence of such rust films. From his experimental studies

he has found that there was no significant effect of corrosion on erosion in aqueous conditions and assumed that this term can be negligibly small and concluded that erosion-corrosion in slurry pipelines carrying aerated slurries of sand and similar materials is under oxygen mass transfer corrosion control, with corrosion being the dominant mode of material loss. Postlethwaite et al further argued that any measures to prevent such corrosion of straight slurry pipeline should be concentrating on controlling the corrosion component rather than on choosing erosion resistant piping.

2.5 Slurry simulations in the past

Rotating electrode and slurry pot test are the well-developed laboratory scale tests used to evaluate the erosion-corrosion. However to simulate the real industrial erosion-corrosion problems, different pilot scale studies were carried out and some of the units relevant to this study are discussed below.

Postlethwaite (1986), Edward (1975) and King (1991) used to simulate slurry flow by making a flow-loop and with entry length of 60 diameters to allow fully developed flow similar to this study. Different types and shapes of test specimens were used to measure periodic weight losses. Postlethwaite et al used 50mm long and 10mm wide curved pipe cuttings. Corrosion measurements were obtained from electrochemical anodic and cathodic curves and polarization resistance measurements. The analyses included wear rate, morphology, mass transfer rate, etc.

Cathodic protection was employed mainly as a tool to determine the pure erosion contribution but it also illustrated large potential benefits in reducing the total material loss in liquid impingement up to extremely high velocities.

The slurry conditions were met by maintaining around 1 to 3% NaCl solution using tab water with up to 20% by volume, 30 – 50 mesh silica sand and run for the period of 100 hours and kept saturated with dissolved oxygen at various velocities from 2 to 6 m/s. They have obtained high wear rate in the range of 6 to 25 mm/y. The pH values of these solutions were approximately 7.0.

Shirazi et al (Shirazi, 2000) at Erosion-corrosion Research Center at the University of Tulsa used a multi phase (gas-solid-liquid) flow-loop to evaluate the sand monitors and the erosion-corrosion mechanisms. The major components of the flow-loop were two compressors, diaphragm pump, large separator tank, several heat exchangers, a scrubber and a cyclone separator. The flow-loop is capable of delivering a superficial liquid velocity of up to 3.4m/s while using the sand injection nozzle and superficial gas velocity up to 30m/s in a 25mm test section.

Another well known accelerated test called direct impingement jet loop to simulate the wear rate in pumps, turbine blades, other rotating equipments, bends and pipelines were done by Chiovelli et al at the Syncrude Research centre, SINTEF corrosion center, Neville et al at Heriot-Watt university (Neville, 1997), Hutchings et al at University of Cambridge, Matsumura et al, Meyer et al (Mayer, 1995) and many others.

Neville et al used cast iron and austenitic stainless steel (both are candidate material in pump components), high alloy stainless steel, titanium and its alloys, drill bit materials like Co-based X-40 alloy and austenitic cast iron. Weight loss measurement and standard electrochemical techniques were used to determine the erosion-corrosion effect with twelve impinging jets in the test rig. They also studied the behavior of high velocity oxy-fuel process thermally sprayed cermet coating on stainless steel in saline solution in the presence of solid up to 30% at 17m/s (Neville, 1999). Meyer et al used various impingement angles from 40^{o} to 90^{o} and the flow velocity up to 30m/s for an average of 25 hours with caustic solution

A lab scale rotating cylinder system was used by several researchers including Luo et al (Luo, 2001) and Edward et al (Edward, 1975). Luo et al used Teflon mounted on the stainless steel shaft cylindrical specimen holder. The specimen or the working electrode was 8mm long and 12 mm in outer diameter and was mounted on the middle section of the cylinder and electrical contact was made via carbon contact brushes connected to the rotating shaft at 50 - 10,000rpm. Electrochemical measurements and SEM analysis were

used to analyze the eroded surface. In another study, Bonnel et al (Bonnel, 1983) used the same rotating electrode with carbon steel API type N80 cylindrical working electrode and the exposed cross section of 1 cm^2. However Efird (Efird, 2000) showed that the corrosion rates in rotating cylinder tests were significantly lower than in the pipe flow and jet impingement test and explained the differences by the concept of steady state mass transfer versus distributed mass transfer.

Atomic Energy of Canada Limited (AECL) designed and developed two types of wear simulators called ERABLE and SYRACUSE and French Atomic Energy performed numerous tests using AECL's ERABLE wear simulator (Lina , 2001). This consists of autoclave, a tube wear specimen, tube support specimen holder and high temperature force transducers and high temperature displacement transducers. Several factors were studied using this instrument including the impact of temperature, coatings, surface treatments, experimental parameters such as type of motion, load, contact pressure, test duration etc.

2.6 Erosion-corrosion model predictions

The modeling of erosion-corrosion in complex turbulent two phase flow requires the ability to determine the flow field, erosion and local wall mass transfer rates of corrosion reactants and products.

2.6.1 Flow models

Recent studies focus on the use of commercially available computational fluid dynamics (CFD) code for the erosion-corrosion prediction. This is a three dimensional flow field solver that also contains the Lagrangian particle tracking model used in several erosion-corrosion studies. This prediction procedure gives better understanding the effects of various parameters on erosion-corrosion, such as inlet conditions, fluid properties, flow rate, particle size and concentration, and geometry. There are two widely adopted numerical ways to handle dispersed two-phase flow.

- The Eulerian-Lagrangian approach and

- Eulerian-Eulerian approach.

Wilson proposed a model for higher concentration slurry flow and is based on the sliding bed theory (King 1991). It equates the driving force on the surface of the sliding bed of material to the retarding forces caused by friction between the bed and the pipe wall. Modified two layer model of Wilson (Shook 2000-a) sometimes called 'Saskatchewan Research Council' (SRC) model is worth considering for settling oilsand slurries at high concentration with particle diameter smaller than 500μ. In the turbulent region the effective viscosity of the slurry can be correlated to solid concentration and carrier fluid viscosity as follows: (Shook, 2000-a)

$$\frac{\mu}{\mu_L} = 1 + 2.5C + 10C^2 + 0.0019Exp(20C) \qquad 5.19$$

Where C is the solid volume fraction. Based on this wall shear stress and particle velocity v_p can be calculated.

2.6.2 Erosion models

Iain Finnie's (Finnie, 1958) pioneering effort in erosion developed an analytical model to predict erosion rates using the equation of motion of the particles based on the assumption that the mechanism of erosion was micro machining. The model essentially computes the volume of the crater generated in the eroding material when it is impacted by a hard angular particle at a given velocity and angle of incidence, and further assumes that this crater volume or a potion of it removed causing weight loss. The cutting model is strictly valid for erosion at oblique impact angles and only in the case of annealed pure metals and not in alloys. In addition, the use of scanning electron microscopy (SEM) to observe eroded surfaces has established that erosion process in metal is primarily a sequential extrusion, forging and fracture phenomena. This is not the primary mechanism by which ductile structural materials erode at high impact angles.

Modifications were made to Finnie's basic thesis on the cutting mechanism to account for other observed type of plastic deformation and for aspects of micro-cutting model in order to metals that were necessary to bring resulting calculation more in line with measured erosion losses. In 1963 Bitter included deformation wear and modified Finnie's

model. While Bitter's model of erosion is one of the most complete, the number of material-dependent constants makes it nearly impossible to use in most practical situations (Nesic, 2001).

As the results of poor performance in prediction of erosion, Nesic and Bergevin (Nesic, 2001) proposed a modification to Finnie's model by including Bitter's assumption of a critical velocity for plastic deformation (V_{cr}). This critical velocity is then used in place of impact velocity and yields the following equations.

$$V_p \sin\alpha = V_p \sin\alpha - V_{cr} \qquad 2.13$$

And the volume removed by an impact Q for $\alpha < 18.5^o$ becomes

$$Q = m_p(V_p \sin\alpha - V_{cr})\{ V_p \cos\alpha - 3/2(V_p \sin\alpha - V_{cr}) \}/2p \qquad 2.14$$

And for $\alpha > 18.5^o$

$$Q = m_p(V_p \sin\alpha - V_{cr})^2 \cos^2\alpha / \sin^2\alpha \qquad 2.15$$

The parameters needed in the above equation such as impact angle, impact velocities, impact frequencies etc can be directly obtained from particle trajectory calculation. Critical velocities for number of metals have been empirically determined by Bitter and for stainless steel, the critical velocity = 0.668m/s. This value was used by Nesic (Nesic, 2001) to accurately predict erosion of stainless steel by sand particles.

Sundararajan et al (Sundararajan, 1991) proposed a comprehensive analytical model based on critical strain criterion for solid particle erosion. The model combined the concept of localization of plastic deformation leading to lip formation and generalized the energy absorption relations valid for all impact angles and all shapes of eroding particles. Subsequently he modified his model and spilt it into two components. One for erosion at normal impact angle and other for oblique impact angles

Salama's (Shirazi, 2000) empirical model originally intended for sand in a single phase carrier fluid was extended by Shirazi et al (Shirazi, 2000) to multiphase flow by adding terms that account for mixture density and velocity. This revised model applies geometry

dependent constant that are obtained empirically and used in elbows and bends as follows.

$$E.R = \frac{1}{S_m}\frac{WV_m^2 d_p}{D^2 2\rho_m} \qquad 2.16$$

Where:

E.R = erosion penetration rate, mm/year

W = sand production rate, kg/day

V_m = fluid mixture velocity, m/s

d_p = sand size, micron

D = pipe diameter, mm

ρ_m = fluid mixture density, kg/m3

S_m = a geometry dependent constant specified by Salama.

2.6.3 Corrosion model

One model that assumes corrosion rate under two phase flow conditions is oxygen mass transfer control and it is a reasonably good assumption for slurry pipe flow. Oxygen concentration distribution across the laminar boundary layer can be obtained from LRN K-ε model and then oxygen mass transfer flux to the solid wall can be determined by using Fick's first law and hence the local corrosion can be calculated based on the local reactions.

$$Jo_2 = -D\frac{d(\rho m)}{dy} \qquad 2.17$$

Where:

D = diffusion coefficient, m^2/s

m = mass fraction of dissolved oxygen, kg/kg

ρ = density, kg/m^3

The diffusion of oxygen is considered as molecular diffusion and turbulent diffusion by Nesic (Postlethwaite, 1991-a). In simple flow geometries, mass transfer coefficient were

correlated through Schmidt number, Reynolds number and Sherwood number by Berger et al (Berger, 1977), Chilton-Colburn (Poulson, 1982), for fully developed pipe flow Luis Efrain (Luis, 1984) in steam extraction lines of power stations. But none of these clearly demonstrate velocity effect on the passive layer, which changes significantly at low temperatures. Once mass transfer coefficient (k_m) is known, the corrosion rate can be determined by the following formula (Nesic, 2001).

$$C.R = \frac{2k_m C_{bO_2} M_{Fe} Fe}{\rho_{Fe}} \qquad 2.18$$

Where:

M_{Fe} = molar mass of Fe

ρ_{Fe} = density of Fe

C_{bO2} = bulk concentration of oxygen

k_m = wall mass transfer coefficient

Predicting the velocity sensitive corrosion in the field through laboratory simulation is an ongoing interest and studied by Silverman et al (Silverman, 1999), Nesic et al (Nesic, 1997, 2001-b) and many others. Rotating cylinder was used to simulate the field geometries due to simplicity, uniform current distribution and easy application of hydrodynamic principals.

2.7 Past proposed solutions

2.7.1 Cathodic protection

Cathodic protection is the reduction of corrosion by shifting the corrosion potential of the corroding material towards a less oxidizing potential by applying an external electromotive force (current). Cathodic protection can be used to reduce corrosion and synergistic attack in slurry erosion-corrosion. However it has not found widespread application in internal pipeline protection.

2.7.2 Inhibition

Organic corrosion inhibitor is the most effective means of protecting the severe internal corrosion of carbon steel pipelines in oil product transportation. Chromate inhibitors were used for carbon steel slurry pipelines (Postlethwaite, 1986) and molybdate inhibitors for coal water slurry lines (Sastri 1983, Corradetti, 1991) by Energy and Mines Resources Canada and monoethylene glycol, diethylene glycol and methanol were used for gas pipe lines. All these results show a good reduction on corrosion, wear rate and total metal loss. Inhibitors work only when they can reach the steel surface. Sand deposits prevent such contact and a minimum velocity is also important in corrosion inhibition. Postlethwaite (1986) suggested inhibitor and/or de-aeration, resulting in a smooth rust and scale free pipe, would control the erosion-corrosion.

2.8 Summary of literature review

The literature review shows the erosion-corrosion effect by various parameters including temperature, sand concentration, velocity etc. Several models were developed to predict the erosion-corrosion in oil, gas and mining transportation and exploration lines. Synergistic effect was predicted as the percentage of erosion and laboratory scale studies were completed to estimate and simulate the flow-induced-corrosion using rotating cylinder electrode

However difficulties were faced in the past in measuring the flow-assisted-corrosion using electrochemical measurement and rotating cylinders to simulate the field conditions. Furthermore, measuring and separating the passive layer removed by erosion and the increased corrosion due these effects are still not clear. Synergistic mechanism and the different constituent causes the synergistic effect are not well defined in slurry transportation. Limited literature was found in the oil-sand erosion-corrosion and it may due to the local nature of oil-sand reserves mainly in Alberta.

Literature review also shows that the erosion-corrosion can be controlled either by modifying the slurry or by modifying the pipeline. For short length pipes, the use of

protective lining, inhibitors or external metal allowance could be feasible; however the economic considerations influence the above control methods in many oilsand slurry transportation lines.

Therefore the literature on oilsand erosion-corrosion and the problems faced in plant studies shows the need for a good experimental setup to simulate the actual oilsand slurry flow. This will distinguish the enormous erosion-corrosion effects, produce good experimental data and will serve as the foundation to understand the problem; viz., to find out the actual mechanism and build a mathematical model to predict the erosion-corrosion. Finally in this work we propose an innovative approach to mitigate the erosion-corrosion.

3. Materials and Methods

This chapter discusses the main features of the design, test methods and procedures used to simulate the slurry flow. Operation of the loop, sample calculations, accuracy of the measurements, calibrations and the difficulties faced in these areas are also discussed in this chapter.

3.1 Slurry flow-loop

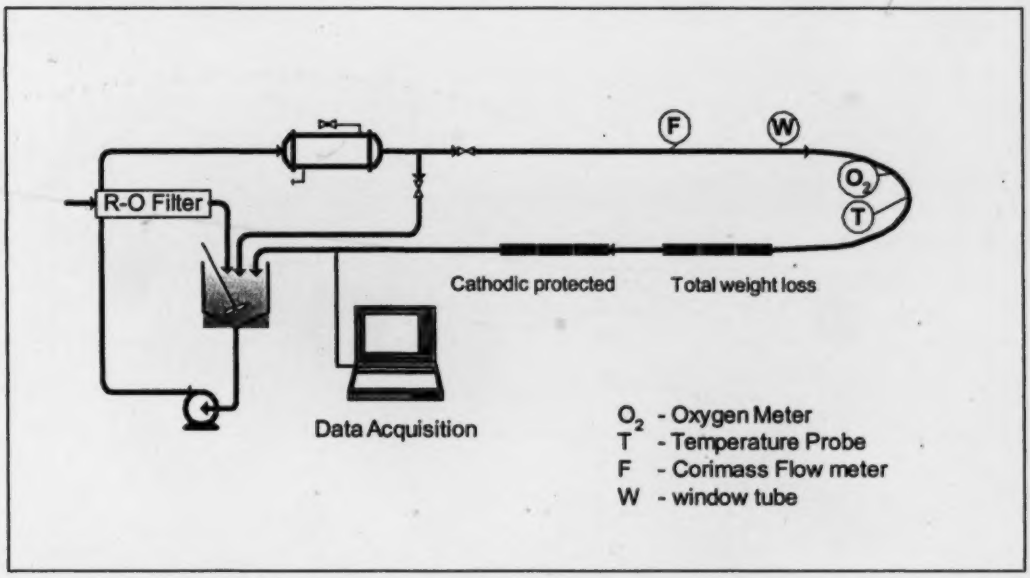

Figure 3.1 : Slurry flow-loop to simulate the oil-sand transport line

The erosion-corrosion slurry flow-loop consists of a reciprocating cavity pump, heat exchanger, a mass flow meter, specimen holder, sensors and data acquisition system as shown in the Figure 3.1. Building hot water was used to control and achieve the slurry temperature by passing through the stainless steel heat exchanger. Initially, the city of Edmonton water was used to make the slurry with the total hardness of 162ppm of $CaCO_3$ (Epcor, March 2003). Minute amount of deposits on the cathodically protected test pieces were noticed due to the high hardness of the supply water especially during the wintertime. This was verified by the XRD analysis of the deposited powder that mainly consists of calcium components as shown in the Figure 3.2. This is somewhat

similar to the steel piles in the jetties and offshore platform, where deposits like barnacle and seashells were found after few years of cathodic protection. Therefore all the tests were decided to be carried out with purified water by combined mechanical filtration and reserve osmosis filtration as shown in Figure 3.3. The reverse osmosis system consists of thin film composite membrane, sediment filter, activated pre-carbon filter and post-carbon filter and its remove almost 93 -98% of calcium and 90 -95% of chloride. A constant slurry concentration was maintained by incorporating a mixer in the circulation tank and monitored by Krohne corimass G+ MFM 485 mass flow meter throughout the test. Even though ASTM D888-66 recommends two different analytical methods to accurately test dissolved oxygen in water, Extech instruments Model 407510 dissolved oxygen meter was used to monitor the oxygen concentration in the flow-loop due to short measurement time and easy handling.

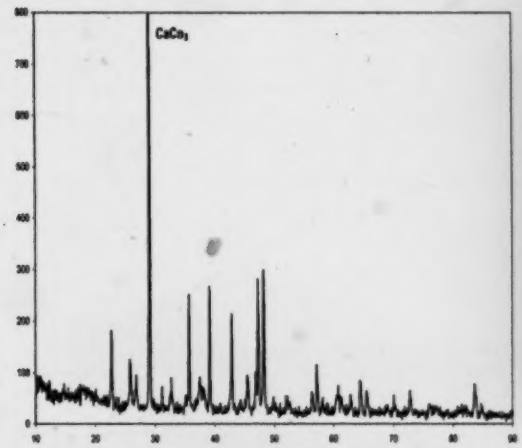

Figure 3.2 : XRD Analysis of C.P deposits

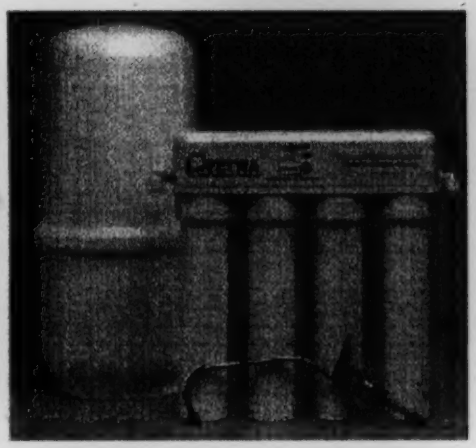

Figure 3.3 : Reverse osmosis filter unit (Petwa)

Three test pieces were used in all the tests to make sure the repetition of the test results. Carbide papers were used to clean the internal surfaces of the test pieces. Electrical isolation was made for all test pieces including cathodically protected test pieces by placing non-conductive plastic bushes in between the samples. The weight loss rates of the carbon steel pipe at a negative potential of 800 mV with respect to saturated calomel

electrode (SCE) by cathodic protection is considered as pure erosion. The weight loss rates at the test pieces without cathodic protection are considered as total erosion-corrosion. All these tests were carried out for five to six hours and the parameters were kept well with in the limits and acquired using a National Instrument's Lab View® data acquisition system. The average values from the acquired data were used in this presentation and calculations.

The erosion-corrosion tests were performed for velocities of 1.5, 2.0, 2.5 and 3 m/s with sand concentration ranging from 2 to 12 % in 850 ppm NaCl solution at 22°C, 32°C and 42°C. Two optimum velocities of 2 and 2.5 m/s were selected to run the tests at 42°C due to difficulty in maintaining the temperature without proper heating and control arrangements. After the test, corrosion products and foreign matter from the surface of exposed coupons were removed by inhibited acid and washed and dried. Initial and final weights of each sample were carefully measured using Scientec SA-510 analytical balance with the readability of 0.1mg.

3.1.1 Test piece holder design

To arrive at the final flow-loop design, we considered many factures such as the cost, space availability and actual plant situations. Simulating the fully developed slurry flow and the design of the test piece holder was one of challenge faced in this research. To simulate steady fully developed flow, upstream and down stream are allowed one meter and ½ meter long pipe respectively. Test specimens were in the form of 76 mm long by 26 mm diameter standard A106 carbon steel pipe and the chemistry of the A106 carbon steel is similar to the field oilsand slurry line. The length of the test specimens was chosen from the maximum available analytical balance capacity and the duration of the test was decided to reduce the measurement errors.

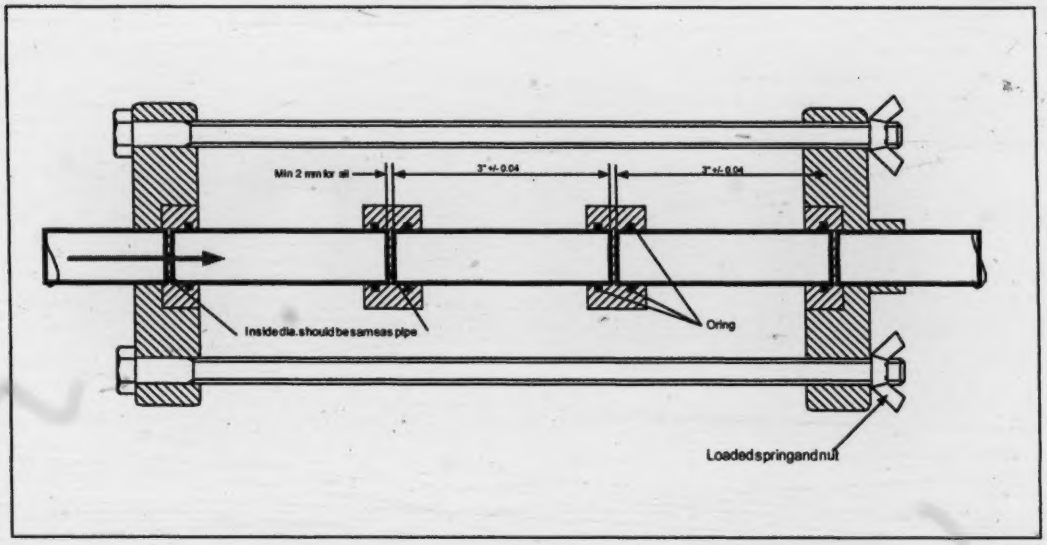

Figure 3.4 : Test piece holder design for flow-loop weight loss measurements

Cathodic protection was maintained by using a one-inch long pipe identical to the test piece on both ends of the test piece as anode without disturbing the flow as shown in the Figure 3.5. The cathodic protection potential was maintained as per the standard (NACE, BS7361) and very sharp attenuation or drop in voltage was observed in the short length of the test piece.

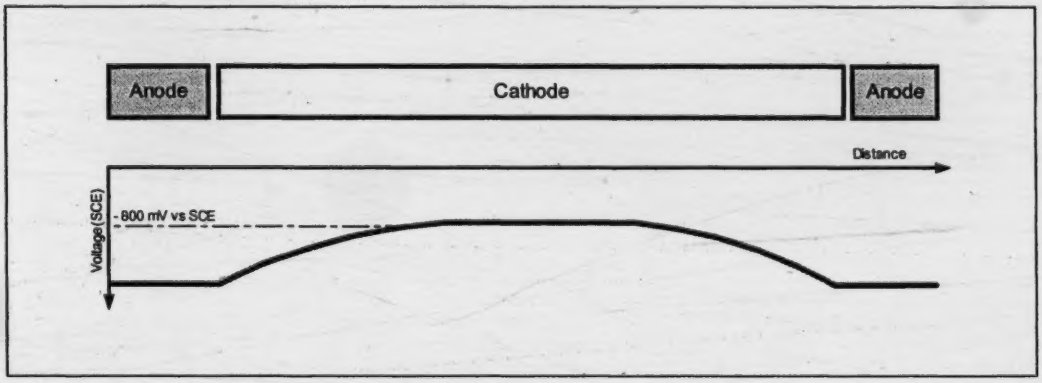

Figure 3.5 : Cathodic protection criteria for erosion measurements

3.1.2 Specimen cleaning and weighing

First the internal surface of the test specimen was abraded manually with wet 400 and 600 grid papers and washed with de-mineralized water and ethanol. Then it was blown

with filtered dry air and kept in a nitrogen-blanketed desiccator's vessel for approximately 12 hours and its initial weight was recorded

After the test, the internal surface of the test pieces were chemically cleaned with inhibited acid, washed with clean de-mineralized water and acetone and dried for 12 hours. Then the final weight of the sample was measured with an accuracy of 0.1mg. The inhibited acid was made out of 500 ml hydrochloric acid (HCl, specific gravity of 1.19), 3.5 gram hexamethylene tetramine and the balance regent water to make 1000ml as recommended by ASTM G1-90 (1999)

3.2 Test material

The material inspection certificate supplied by *Benteller* pipe manufacturer for standard SMLT A/SA106 –B plain end pipe and corresponds to the flow-loop specimen heat number is shown in the Table 3.1. The pipe was supplied by Comco Pipe and Supply Company in Edmonton.

Table 3.1: Chemical composition of A/SA106-B grade line pipe steel Heat No: 110552

Components	weight %	Components	weight %
C	0.140	Ni	0.05
Si	0.200	Cu	0.09
Mn	0.85	B	0.0001
P	0.005	Nb	0.002
S	0.003	Ti	0.002
Cr	0.09	V	0.001
Mo	0.01		

3.3 Slurry simulation

AFS 50/70 silica sand with the grain size of 212 – 300μm and the specific gravity of 2.65 supplied by *US Silica* was used to make the slurry. The slurry density was adjusted by adding sand to the mixing tank. The main problem encountered in the mixing tank was

related to the accumulation of sand at the tank bottom. This caused unsteady slurry density in the flow-loop and noticed from the mass flow meter. This problem was overcome by raising the outlet of the tank (inlet to the pump) few inches away from the tank bottom.

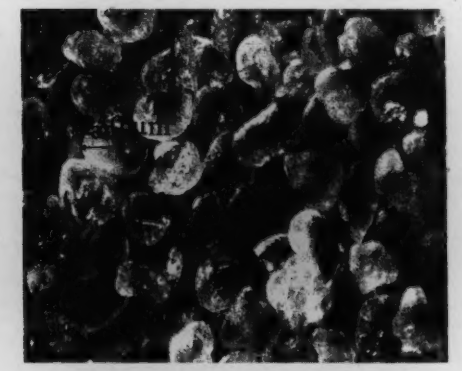

Figure 3.6 : Micrograph of silica sand

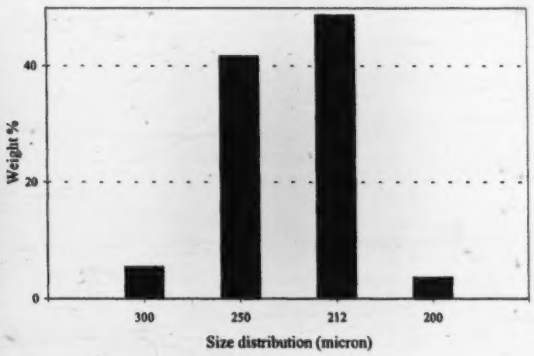

Figure 3.7 : Sand distribution

Figure 3.6 shows the irregularity and distribution of the sand in an as received condition. In order to avoid sand particle size and shape degradation during the tests, each slurry batch was used only for a relatively short period of time (6hrs). Indeed several particle size and microscopic analyses indicated that the effect of attrition on the size distribution was not significant.

3.4 Corrosion and synergistic effect measurements

Corrosion current can be determined by extrapolating the anodic and cathodic line from the Tafel plot as shown in the Figure 3.8. The theoretical current for anodic and cathodic reactions is shown as straight lines and the value of either the anodic or cathodic line at corrosion potential (E_{corr}) is called the corrosion current (I_{corr})

The curved line is the total current or the sum of the anodic and cathodic currents and is measured by sweeping the potential of the test specimen, normally from -250 to +250mv using a potentiostat. The sharp point (E_{corr}) in the curve is the point where the current

changes sign as the reaction changes from anodic to cathodic. This disturbs the corrosion current measurement directly at this point and usually extrapolation is used to estimate the corrosion current. The recent electrochemical instruments automatically convert the corrosion current into corrosion rate in mm/y or mpy. In real systems the corrosion current depends on many variables including the metal, solution composition, temperature, solution movement, metal history, and many others.

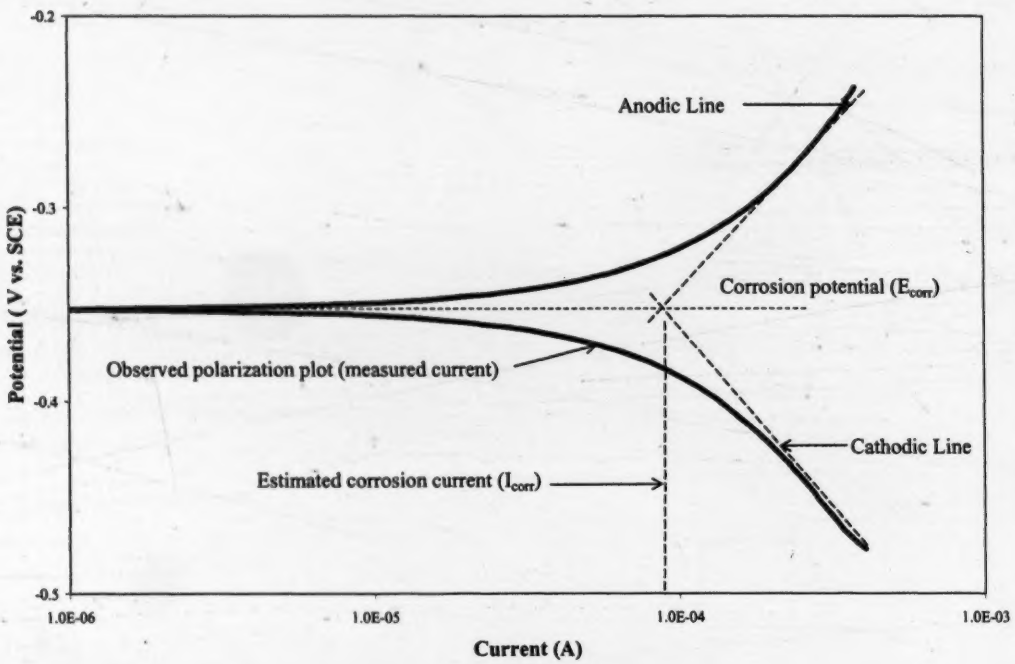

Figure 3.8 : Tafel polarization diagram and the corrosion current extrapolation

Weight loss measurements were used to measure the corrosion rate. The flow-loop was cleaned and run several hours to remove all sand before the corrosion measurement. All the weight loss measurements were made with three test specimens for 6 hour test duration. Corrosion measurements by online flow-loop electrochemical Tafel tests were also carried out for comparison purpose with the weight loss as in Figure 3.9.

The flow-loop electrochemical analyses were performed with Gamry Electrochemical measuring system. Platinum (Pt) wire was glued on to the pipe wall without disturbing

the flow to serve as the reference electrode and other pipe pieces were used as working and counter electrode as shown in the Figure 3.9. The measured potentials were re-scaled to standard saturated calomel electrode (SCE) by comparing the open circuit potential of the test piece with respect to platinum electrode and SCE in the same environment as shown in Figure 3.10. Electrochemical measurements were made without sand and with 6% sand at a scan rate of 0.5 mv/sec. Measurements in other sand concentrations were extracted from this for the calculations.

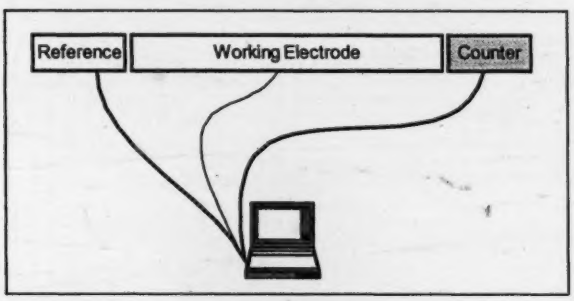

Figure 3.9 : On-line corrosion measurements

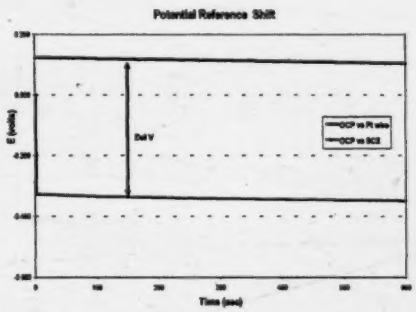

Figure 3.10 : Open circuit potential

3.5 Mass transfer simulation

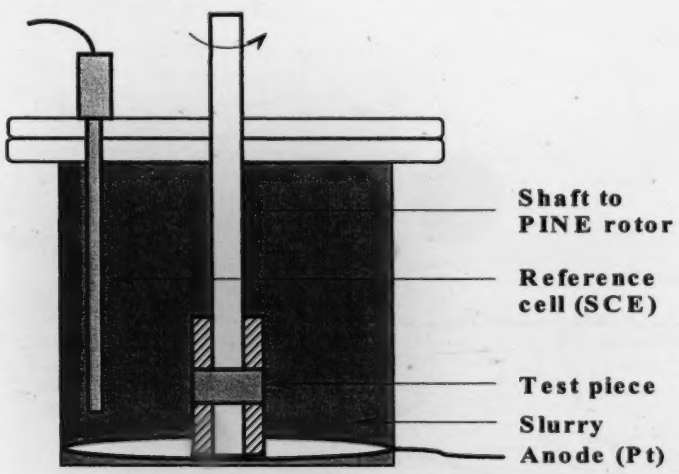

Figure 3.11 : The rotating cylinder electrode to measure the oxygen diffusion rate

The oxygen transfer rate through the mass transfer boundary layer in the pipeline is simulated through the rotating cylinder electrode as shown on Figure 3.11. The electrode

is in the form of 5.7mm long by 33 mm diameter standard ASTM A106 GrB carbon steel taken from the same test piece material. Carbide papers of 400 and 600grid were used to clean and polish the surfaces of the electrode. The limiting current tests were performed with Gamry Electrochemical system for velocities ranging from ~0 to 4.8 m/s (rotating speed from 0 – 4000 rpm) with 850 ppm NaCl at ambient temperature as of the flow-loop. The limiting current is calculated based on the maximum current density that can be used to obtain the desired electrode reaction without undue interference such as from polarization and assumed at negative 950 volt with respect to SCE. The boundary layer velocity at the surface of the test piece relative to the fluid was assumed to be zero (no slip). The same was normally assumed in incompressible pipe flows.

3.6 Calibrations

Calibration provides confidence in measurement and assurance that an instrument has the accuracy required to maintain a product or process with in the specification. In general, flow measuring devices were calibrated by three methods as described elsewhere (Spitzer, 1991):

(1) A wet calibration using actual fluid flow
(2) A dry calibration using flow simulation by electronic or mechanical means
(3) A measurement check of physical dimensions and use of empirical tables relating flow rate to those dimensions

Flow meter was calibrated for flow rate and density as per the manufacturer's instruction. Initially the flow rate was compared with the volumetric measurement using 200 liter collection tank. Even though the measurements were carefully taken, the calibration is only accurate as the standard to which the meter is being compared. Therefore batch calibration were completed using city water, collection tank and a weighing machine to check, compare and confirm the flow meter readings. The calibration curve in Figure 3.12 shows that the meter readings were very much close to the calibrated values. As we used the stop watch, manually transfer the water and used scale (250 lbs) with the smallest measurement of 1oz, the small variation between the meter reading and the

measured value is considered from this measurement error. Therefore factory calibrated flow meter readings were assumed to be correct and used in all calculations.

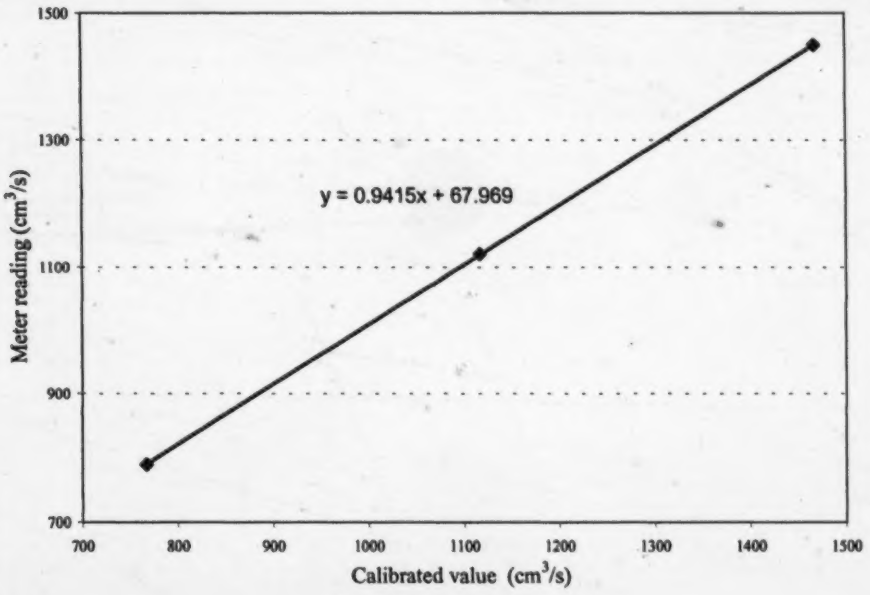

Figure 3.12 : Corimass meter calibration for flow rate

Slurry concentration was calculated from the density measurements and compared with the volumetric density measurements using measuring cylinder and the electronic balance. The density was calculated by dividing the measured weight by measured volume. Whenever much deviation were noticed from the volumetric calibration, the mass flow meter was re-calibrated for density measurements. Oxygen meter was calibrated from time to time as per the manufacturer's instructions

3.7 Assumptions and validations

- The weight loss rates of a cleaned test specimen at a negative potential of 800 mV with respect to saturated calomel electrode (SCE) by cathodic protection is considered as erosion. However if this represents the actual erosion in the plant situation is still not clear, due to the sand impinging directly on oxide layer rather

than the cleaned bare metal surface. Oxide layer cannot be ignored and pure erosion reported here may be over estimated than actual plant conditions.

- Bushes and end connections were machined to the same internal diameter as of the test piece and the flow is assumed to be fully developed near the test piece (no disturbance)
- Sand particle shape and size remain same with in the test period and this was confirmed with the stereo microscope.
- One meter upstream and ½ meter down stream will provide fully developed flow at the test piece.
- Erosion-corrosion rate, determined with typical test piece is an average value over the entire test period of five to six hours. Changes in the test conditions were kept as minimum as possible by design, flow control and surface preparation.
- Oxygen diffusion controls the corrosion process in oilsand slurry flow.

3.8 Flow-loop operating procedure

Startup, shutdown and emergency shutdown procedures are attached in Appendix-I for easy reference and for future use.

3.9 Calculations

Generally corrosion rates are interpreted in imperial units like mils per year (mpy) in North America and all the test results in this study were converted to this unit. However these can easily converted to SI units (mm/a) by multiplying a conversion factor (0.0254).

3.9.1 Corrosion rate

The formula used to convert the weight loss measurement to estimated erosion-corrosion rate is given below and is based on NACE standard RP0775-87.

$$P = \frac{W * 365 * 1000}{A * T * D * 24} \qquad 3.1$$

Where:

P = average penetration rate in mils per year, mpy

W = weight loss in grams, g

A = initial exposed surface area of the test piece, square inch

T = exposure time, hrs

D = density of the test piece material in grams per cubic meter, g/cm3

3.9.2 Density

Slurry concentration by weight percentage can be derived from the slurry density as

$$\text{Slurry density by weight} = D_s(X/100) + D_w(1 - X/100) \qquad 3.2$$

Where:

X = slurry concentration, wt %

D_s = dry bulk density of Sand, 2650 kg/m^3

D_w = density of water, kg/m^3

Weight percent conversions from slurry density at different temperatures were shown in Figure 3.13.

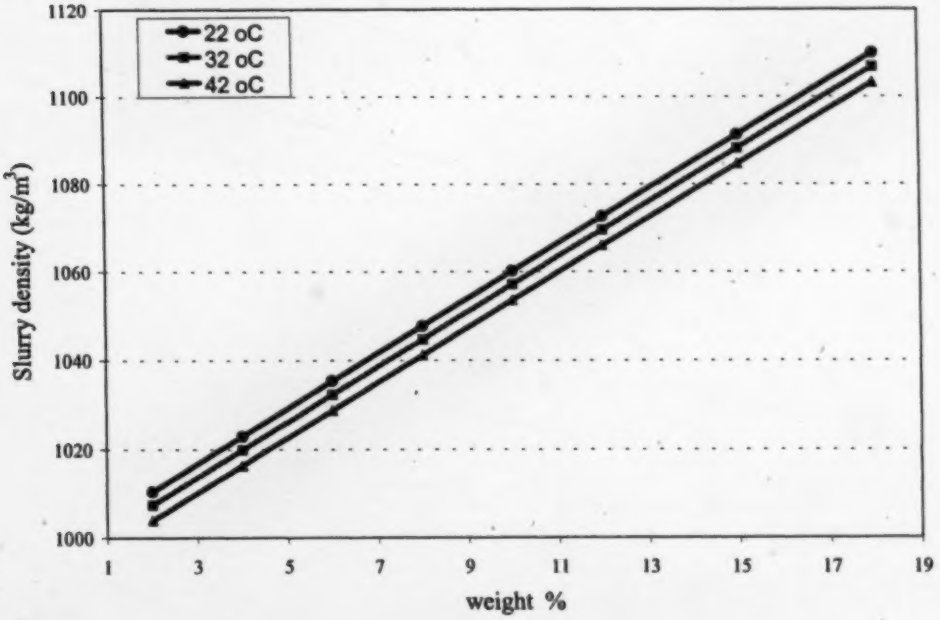

Figure 3.13 : Slurry density to weight percentage conversion diagram

3.9.3 Measurement errors

The following errors were determined by tests and adjusted from the test results.

	Source of Error	Variation	Error
1	Analytical balance	Manufacturers allowance	± 1 mg
2	Test piece outside corrosion	As per tests	+ 4 ± 1 mg
3	Cleaning loss	As per ASTM	+2 ± 0 mg
Total error			+6 ± 2 mg

4. Results and discussion

The results obtained from the flow-loop and the electrochemical measurements are presented in this chapter. Some of the results were compared with other techniques and similar studies published in the past. All the results presented here are for the carbon steel pipe material, ASTM-SA106GrB. The latter part of this section deals with the statistical and error analyses.

4.1 Oxygen diffusion

Limiting current is one of the standard methods to measure the mass transfer coefficient and is used in this study to calculate the oxygen transfer rate through the boundary layer. There are several references which provide such correlations in the previous corrosion studies (Efrid 2000, Postlethwaite 1986, Nesic, 1997).

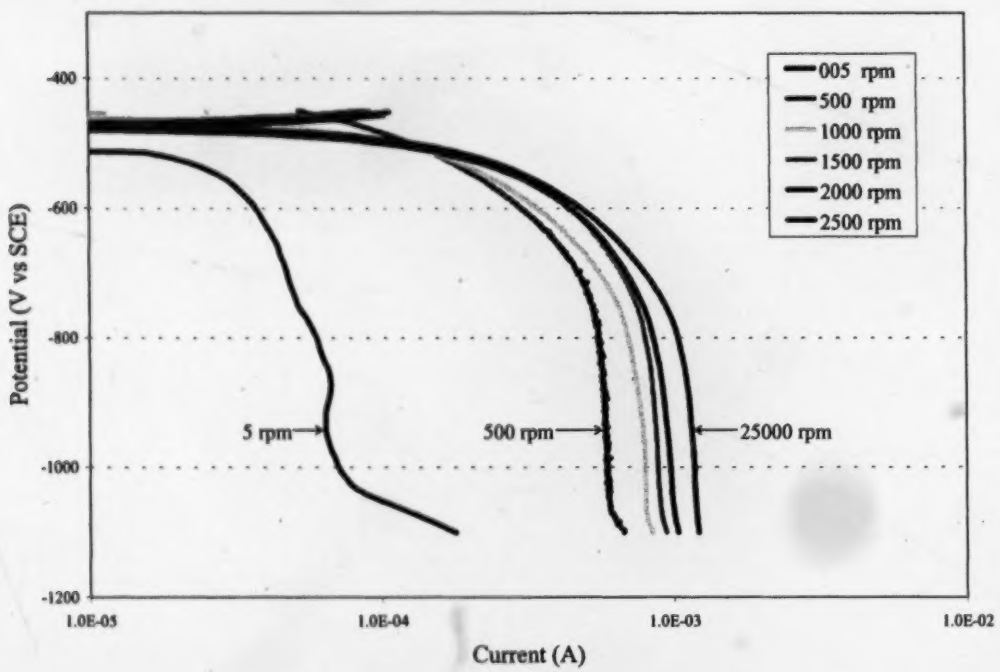

Figure 4.1 : Limiting current test with rotating cylinder electrode

The Figure 4.1 shows the limiting current test with a rotating cylinder at different rotational speeds at room temperature. The limiting current is increases with the rotational speed and shows that the diffusion current which is proportional to the oxygen diffusion rate is significantly increase initially up to 500 rpm and then slightly increase up to 2500rpm. This is because the flow regime is in turbulent region from 500 rpm to 2500 rpm and the velocity effect on the turbulent diffusion layer thickness is small compare to velocity effect on the laminar diffusion layer.

4.2 Oxygen concentration

The saturated amount of dissolved oxygen in the flow-loop and its variations within the test duration was one of the concerns in this study. Filtering the water using reverse osmosis unit for about 18 hours was part of the standard start-up procedure to fill the tank; and thus there is reason to believe that the initial oxygen conditions were saturated for all tests at the test temperature. Oxygen measurement using Extech dissolved oxygen meter and the data from the literature confirm this. Figure 4.2 shows the oxygen concentration based on NACE RP-02-78 (1978) and the measured value using Extech dissolved oxygen meter with an accuracy of ±0.4 ppm.

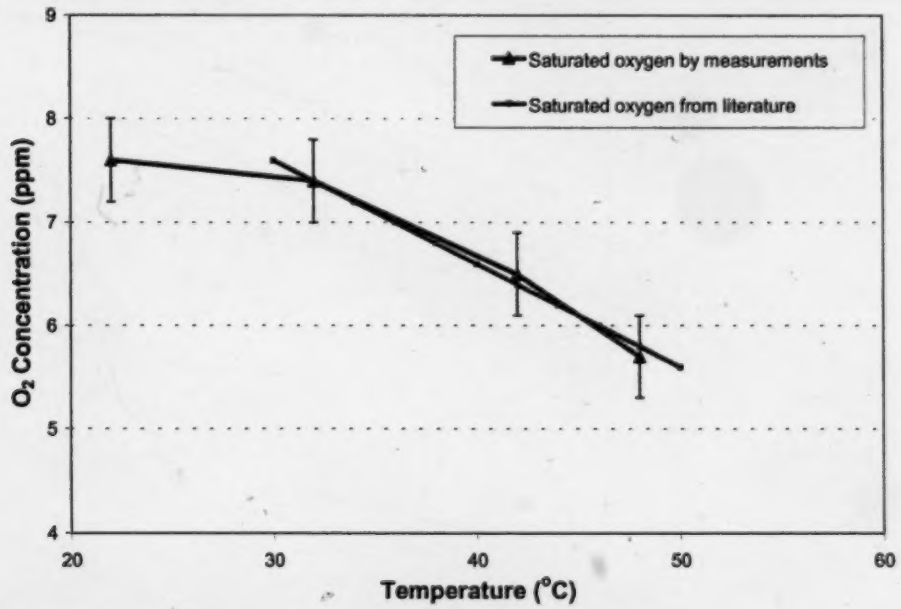

Figure 4.2 : Saturated oxygen concentration in the flow-loop

Figure 4.3 shows the initial, final and average oxygen concentration at three different temperatures. The initial and final points in this figure were the average over several test result. The final oxygen concentration was taken after the six hour test and slight deviations were noticed when the sand concentration was high. This may due to the stirrer's mixing efficiency reduced with the sand load and thereby reduce the oxygen level. Oxygen was removed during the test due to corrosion of the loop at all there temperatures and after 6 hrs test the final oxygen concentration was around 2 ppm lower than the initial concentration.

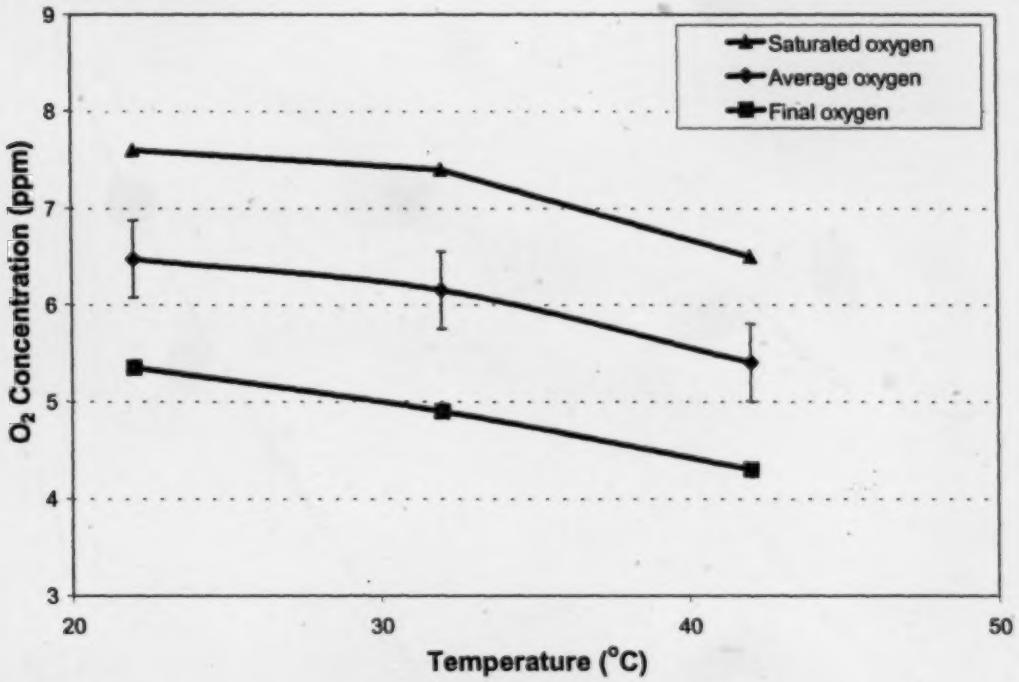

Figure 4.3 : Slurry oxygen concentration change with in a test in the flow-loop

4.3 Corrosion and Synergistic effect

Corrosion measurements by weight loss and on line electrochemical measurements as in Figure 4.4 show that the weight loss measurements were matched to electrochemical measurements at stagnant (non-flow) conditions however significant deviations occur at flowing conditions. Electrochemical measurements are instantaneous measurements,

measuring the iron dissolution or general corrosion rate. On the other hand weight loss measurements are the average measurements over the test duration and good for both reaction and diffusion control process. Amarnath (Amaranth, 2002) and Lu (Lu, 2004) reported that electrochemical measurements deviate much from weight loss measurement in flowing condition. Amarnath used weight loss measurements to calculate the corrosion rate. Efird (Efird, 2000) argues that the results from both tests are right, but they are just measuring different aspects. Weight loss measurements include flow effect such as increased oxygen diffusion rate; oxide diffusion rate from passive layer to bulk of the solution; sand impingement on passive layer etc; but electrochemical measurements do not. The difference may be considered as flow assisted corrosion. This can be seen from the Figure 4.4 and the difference in electrochemical measurement and weight loss measurements can be considered due to flow effects and mainly depend on velocity. Therefore weight loss measurements were used in this study to calculate corrosion rate at no sand in the flow-loop.

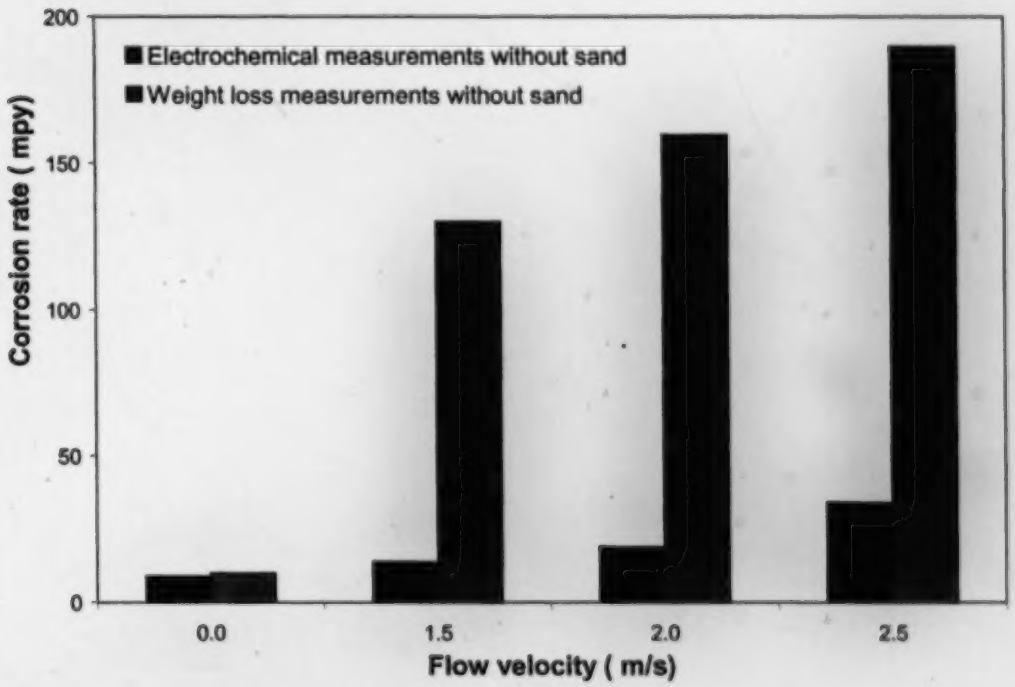

Figure 4.4 : Corrosion measurement at 22°C (Weight loss vs. Electrochemical)

It was also noticed that an equilibrium corrosion thickness was maintained at a particular velocity as shown in the micrograph Figure 4.5. This thickness depends on flow velocity. The thickness was measured using the optical microscope and an average of 50μ corrosion thickness was measured at 2.5m/s without sand after 22 hours test. When the sand was introduced (6% by weight) at the same flow conditions the corrosion products were removed substantially and the thickness was measured below 10μ range. This may be the reason why the electrochemical measurement in Figure 4.6 shows that the corrosion potential (OCP) decrease and corrosion rate increases with introduction of sand.

Figure 4.5 : Corrosion thickness at 2.5 m/s and 32°C after 22 hrs without sand

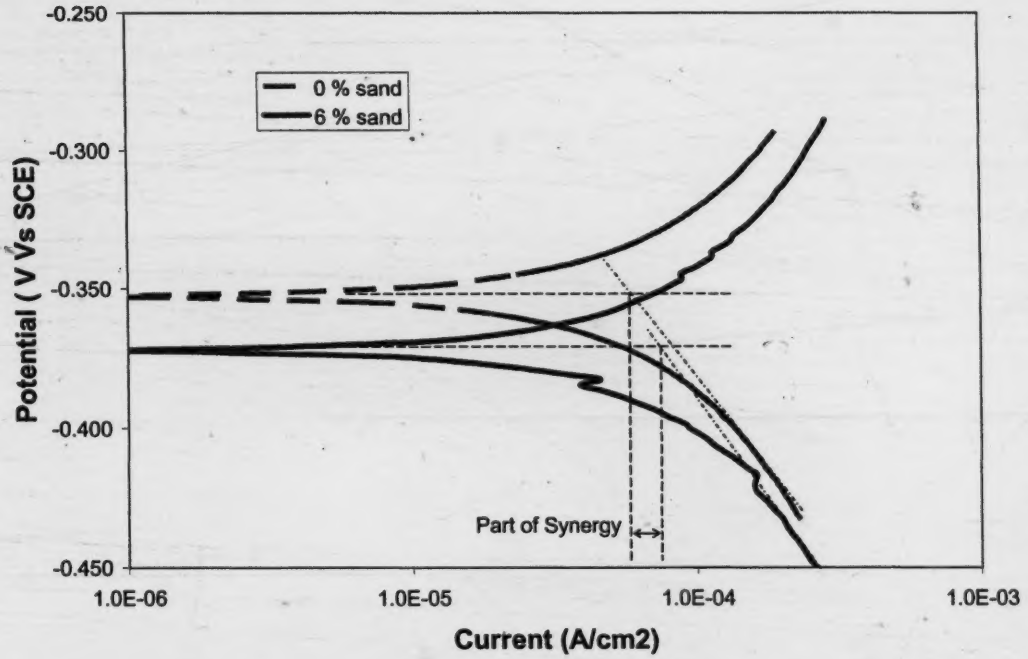

Figure 4.6 : Electrochemical measurement at 32°C and 1.5 m/s (With and without sand)

This Tafel plot difference with and without sand can be considered as the corrosion increase due to passive layer erosion and base metal erosion and considered as the fraction of the synergistic effect (defined in Chapter 1.2). It is also known that electrochemical Tafel plots are used to measure the general corrosion rate and not the pitting corrosion. Therefore the third component of synergistic effect called micro-stress-corrosion is a form of micro pit, a time dependent process and does not affect the Tafel measurements. Thus the synergistic effect due to passive layer erosion and base metal erosion can be calculated as follows.

$$[\bullet S.R_{Tafel}]_{v\ m/s,\ x\%\ sand} = [C.R]_{v\ m/s,\ x\%\ sand} - [C.R]_{v\ m/s,\ 0\%\ sand} \qquad 4.1$$

Where:

C.R is corrosion rate measured from the Tafel extrapolations.

$[\bullet S.R_{Tafel}]$ is the difference between the electrochemical measurements at 0% and x% sand at same flow condition. This considered as synergistic effect came from the increased corrosion due to oxide layer erosion and base metal erosion.

However this hypothesis needs to be verified and checked with other condition and therefore included in the future studies.

4.4 Erosion-Corrosion

The temperature, flow rate and the mean velocity presented here were averages over the test duration calculated from the acquired data. Mean velocities were calculated from the flow rate, accounted for the area available for the flow.

4.1.1 Effect of sand concentration

The erosion and erosion-corrosion with sand concentration at different velocities for six hours of exposure time are shown in Figure 4.7. Sand concentration increases erosion, corrosion and erosion-corrosion; however its influence is much higher on corrosion and synergistic effect than on erosion. Within small variations, the erosion rate increase linearly with sand concentration.

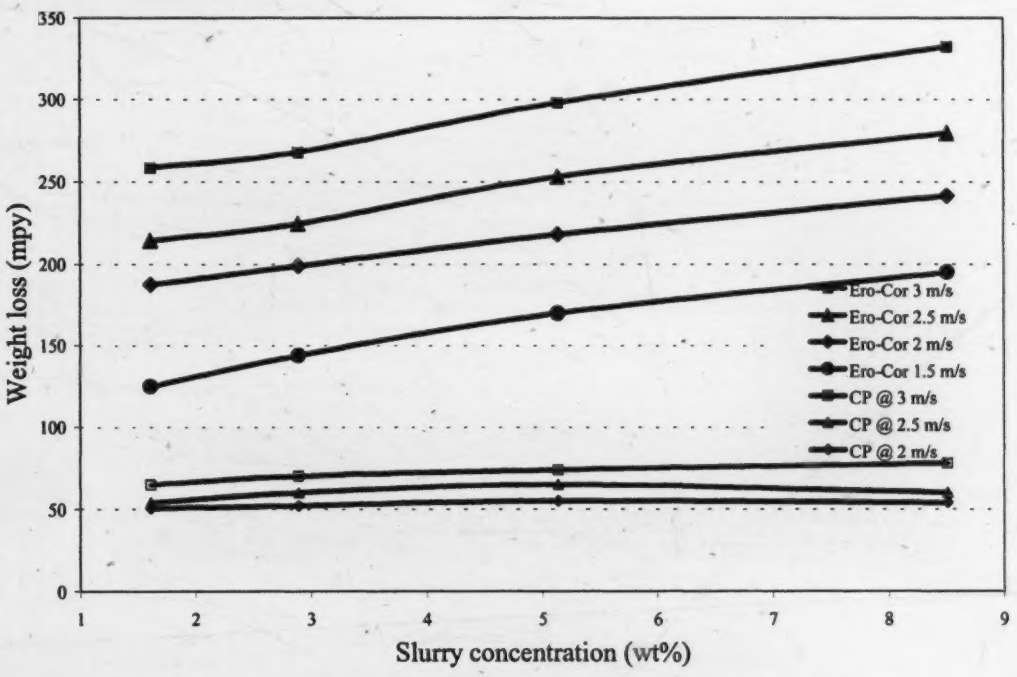

Figure 4.7 : Effect of sand concentration at different velocities at 22°C

Comparable trends were observed when the matching tests were conducted at higher temperatures of 32°C and 42°C as shown in Figure 4.8 and Figure 4.9. Only two optimum velocities were selected to run the tests at 42°C as mention in the previous chapter. These three figures also show that the erosion-corrosion, corrosion and erosion are enhanced by sand concentration, flow rate and temperature.

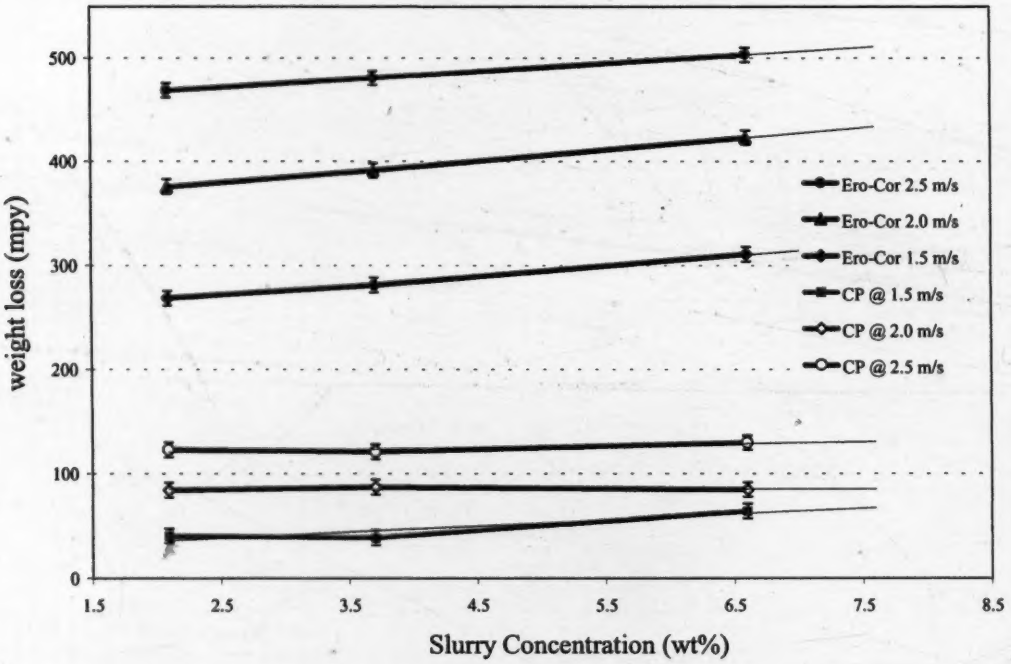

Figure 4.8 : Effect of sand concentration at different velocities at 32°C

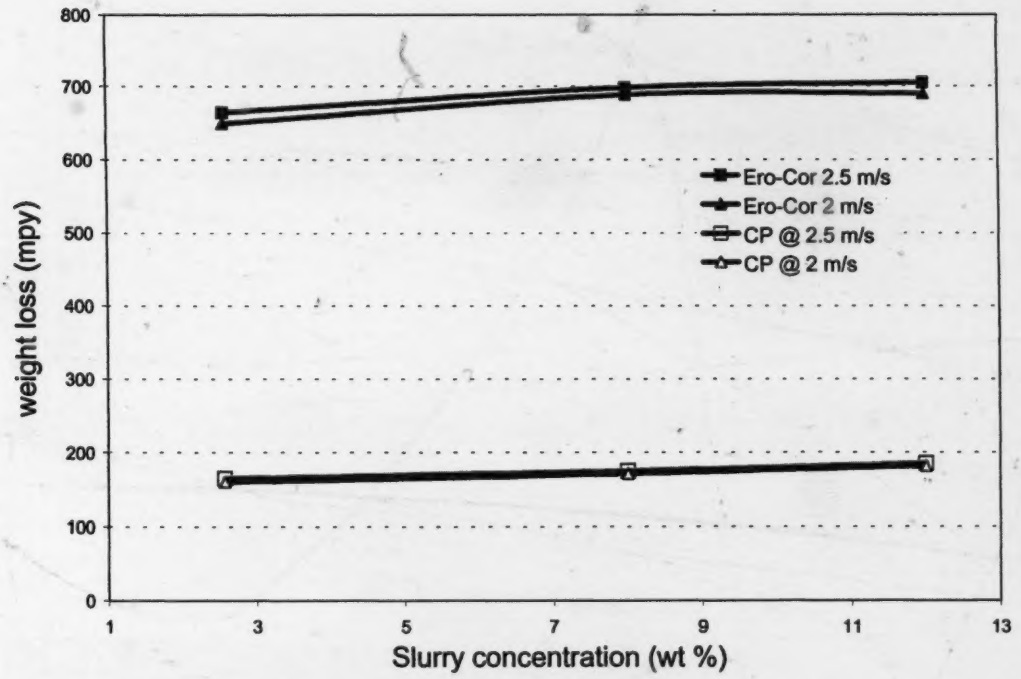

Figure 4.9 : Effect of sand concentration at different velocities at 42°C

It is also useful to note from Figures 4.7, 4.8 and 4.9 that, when the temperature is low, erosion becomes more independent of sand concentration. However it increases with sand at higher temperature. This may due to particles impact velocity changes owing to viscosity change in a power law fashion with temperature (0.98cP to 0.62cP from 22°C to 42 °C, McCabe, 1993).

At a base flow rate of 2 m/s as in Figure 4.10, the change in sand concentration does not have much effect on erosion however it increases the oxygen mass transfer rate and increases synergistic effect. Corrosion is defined as the weight loss due to flow without sand in aerated saline water (Chapter 1.2) and therefore the introduction of sand, does not affect the corrosion.

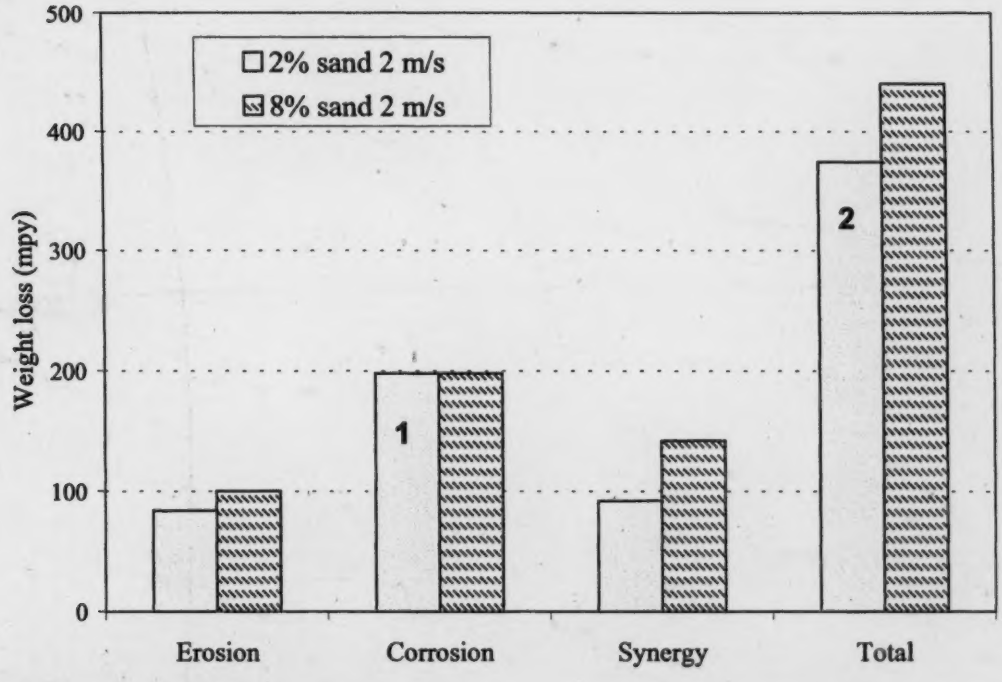

Figure 4.10 : Effect of slurry concentration on erosion, corrosion, synergistic effect at a base flow rate of 2 m/s and 32°C

This figure also shows that the total material loss is almost double compared to corrosion even for sand concentration low as 2%. As the corrosion is defined as the material loss without sand, this figure support and demonstrate the completely different problem (not related to this study) faced in oil extraction and transportation lines in Alberta, where severe damage occurs near the 6 o' clock position as in Figure 1.1a (Chapter 1). The oil extraction process from the oil wells brings a minute amount of sand with the oil water emulsion. When the flow rate is low, as the case in oil exploration, the minute amount of sand were carried along the bottom of the pipe and is enough to increase the local sand concentration to a substantial level near the 6 o' clock position in horizontal pipeline. This in turn causes pronounced damage at 6 o'clock position (almost double compared to rest of the pipe peripheral area) in oil exploration and transportation lines. In other words the whole peripheral area of the pipe damage by corrosion(1) if there is no sand and if there is a small amount of sand, 6 o'clock position damage at total erosion-corrosion rate (2) compared to rest of the peripheral area at corrosion rate (1).

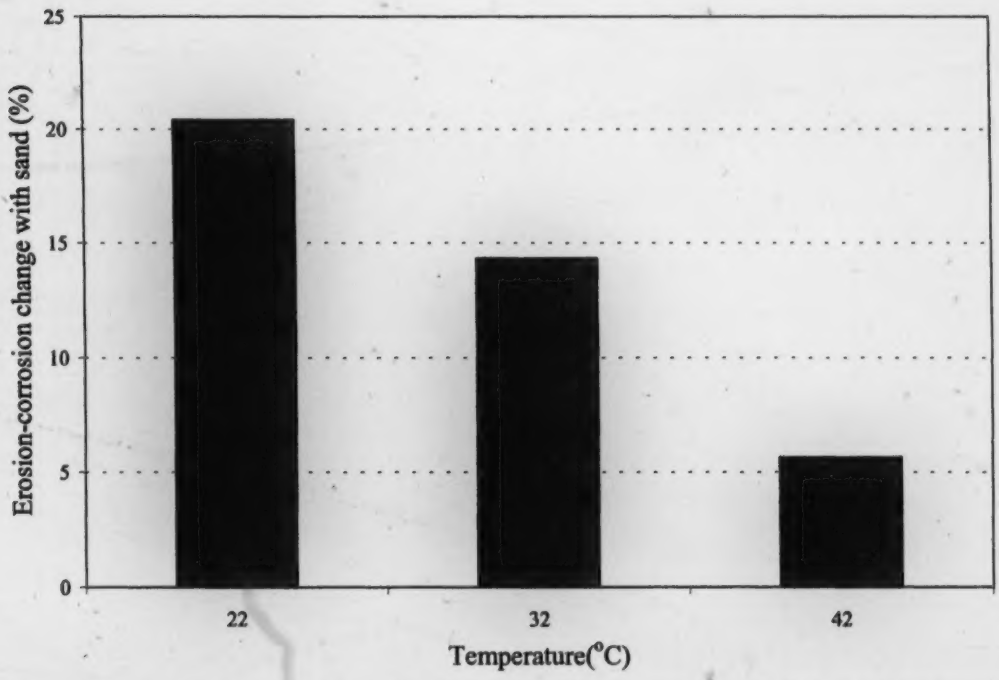

Figure 4.11 : Ave. erosion-corrosion change with temperature @ 5% sand increment base 2 m/s and 3% sand

When the percentage change of erosion-corrosion is calculated based on the equation 4.2, every 5% increase in sand decrease the percentage change in erosion-corrosion considerably as shown in Figure 4.11. This shows that controlling the amount of sand at higher temperature above 40°C will have less effect on controlling erosion-corrosion.

$$\text{Percentage change in E-C} = \left[\frac{\Delta_{E\text{-}C}}{\text{E-C}_{2\text{ m/s}}}\right]_{(T)} 100 \qquad 4.2$$

Where:

$\Delta_{E\text{-}C}$ = change in erosion-corrosion from 3% sand to 8% sand at 2m/s

$\text{E-C}_{2m/s}$ = Erosion-corrosion at 2 m/s and 3 % sand

There is a pronounced variation of metal loss around the periphery of the pipe in slurry transportation noticed in this study as well as documented by many others (Roco, 1988). The maximum damage occurs at 6 o'clock positions and the minimum at 12 o'clock positions respectively. The sand flow observed through the inspection glass in the flow-

loop and the visual inspection of the test specimen further confirms this. However it appears to be longer duration (more than 250 hrs at 6% sand) of test needed to get a measurable thickness difference from the flow-loop of this study.

4.1.2 Effect of slurry velocity

The erosion, corrosion, synergistic effect and the total erosion-corrosion at 32°C with three different velocities are shown on Figure 4.12. This shows the weight loss due to corrosion and synergism is substantial compared to erosion and increase with the velocity. This was observed at all three temperatures. Increase in slurry velocity increases all three components due to increase in inertia, impacts, turbulence and smaller oxide layer and mass transfer boundary layer etc. This figure also shows that the velocity effect on synergy is much higher than corrosion or erosion. Electrochemical tests with rotating cylinder at different velocities, shown in Figure 4.1, confirm the increase in mass transfer rate with velocity and this in turn increase the corrosion and synergistic effect. This supports the idea that corrosion is mass a transfer controlled process. In other words corrosion and synergistic effect will remain the same with increase in velocity if it is reaction controlled. The same was supported by many researchers in slurry erosion-corrosion (Luo 2000, Postlethwaite 1986, Melchers, 2003)

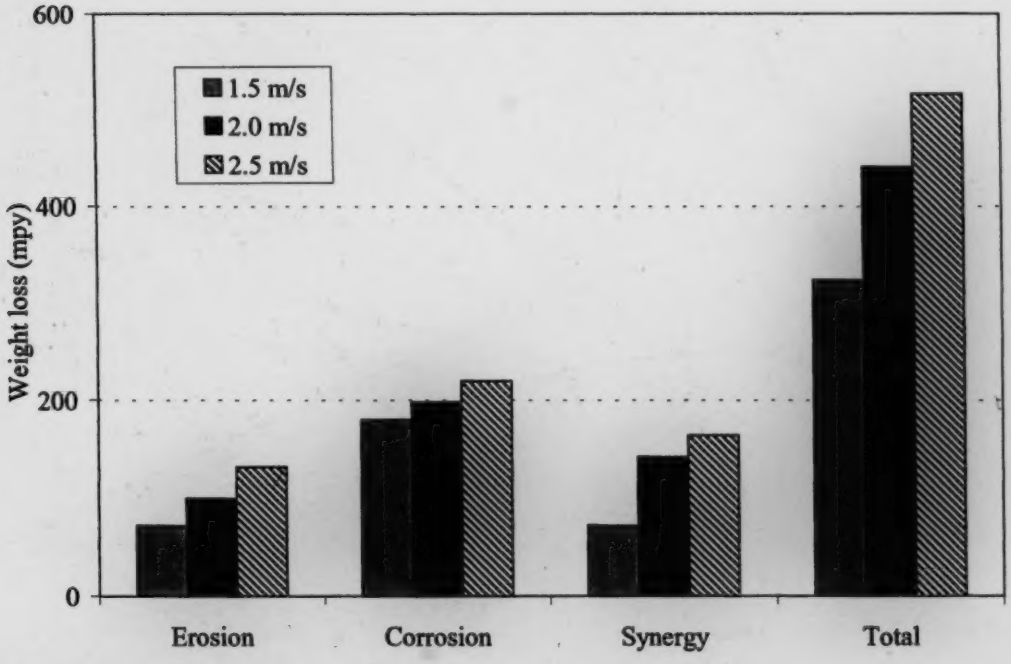

Figure 4.12 : Effect of slurry velocity on erosion, corrosion and synergy at 32°C with 8% sand concentration

Even though the total erosion-corrosion increases with temperature, the increment of 0.5m/s in velocity decreases the change in erosion-corrosion at 42°C as shown in Figure 4.13. The percentage change of erosion-corrosion with change in velocity is calculated based on the following formula. This figure also shows that controlling the flow velocity at higher temperature above 40°C will have less effect on controlling erosion-corrosion.

$$\text{Percentage change in E-C} = \left[\frac{\Delta_{E\text{-}C}}{\text{E-C}_{3\,\%\,\text{sand}}}\right]_{\{T\}} 100 \qquad 4.3$$

Where:

$\Delta_{E\text{-}C}$ = change in erosion-corrosion from 2m/s to 2.5 m/s at 3% sand

$\text{E-C}_{2m/s}$ = Erosion-corrosion at 2 m/s and 3 % sand

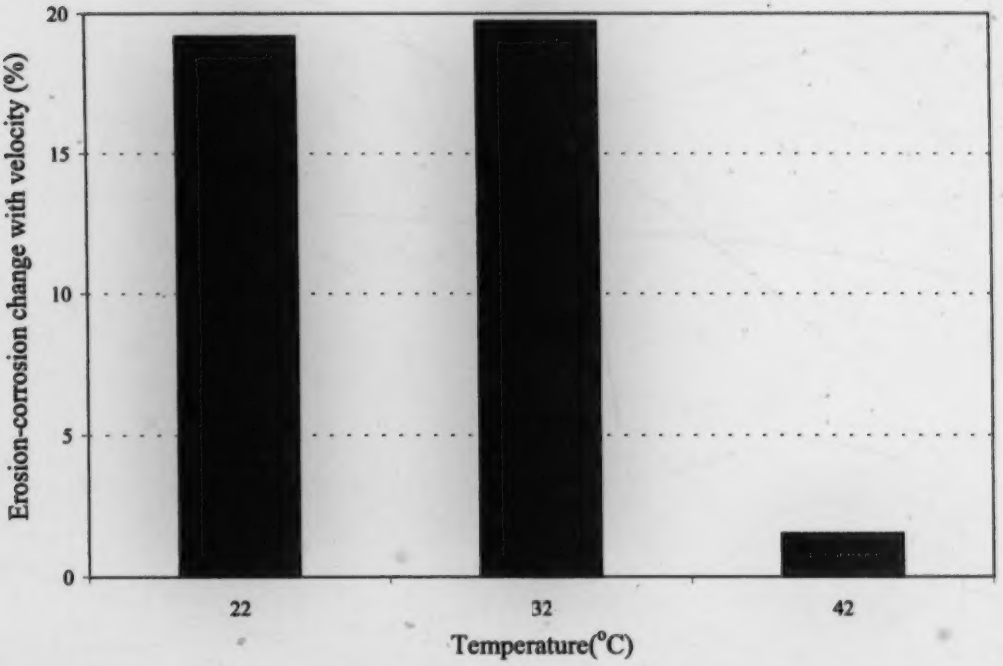

Figure 4.13 : Erosion-corrosion change with temperature @ 0.5 m/s velocity increment

4.1.3 Effect of temperature

The components of the erosion-corrosion at 2 m/s with 8% sand concentration for three different temperatures are shown on Figure 4.14. This shows that the weight loss due to corrosion and synergism is higher than erosion and increases with temperature. The same was observed at other velocities too. This figure also shows that the temperature effect on synergy is much higher than corrosion or erosion.

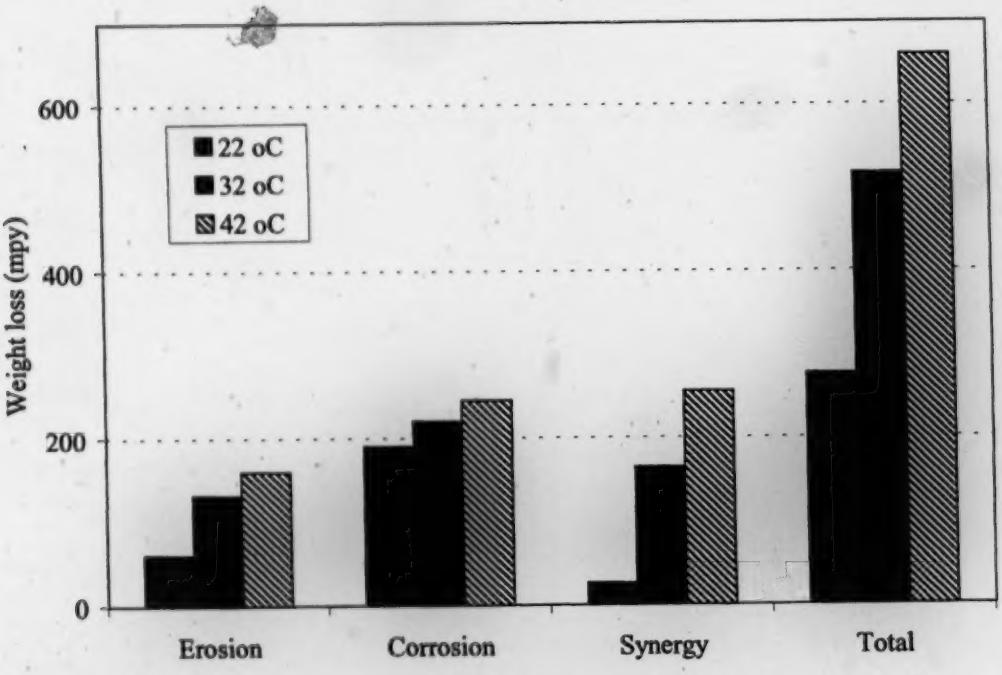

Figure 4.14 : Effect of temperature on erosion, corrosion and synergy at 2 m/s with 8% sand

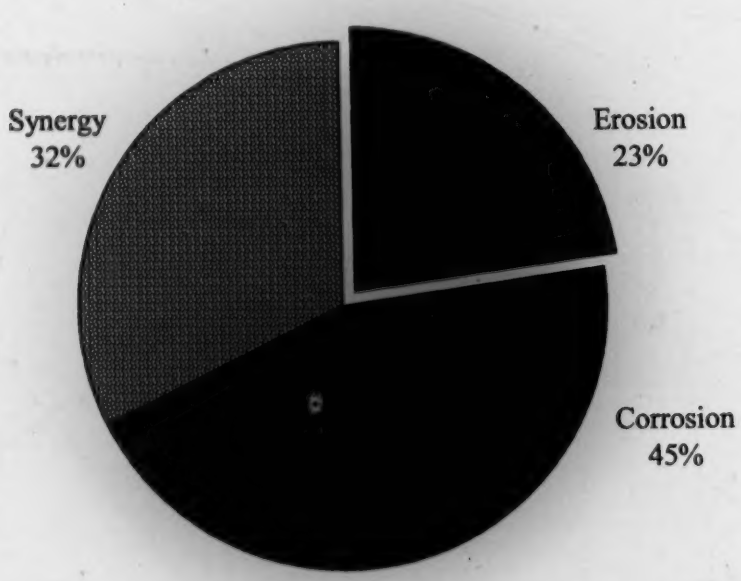

Figure 4.15 : Contribution of erosion, corrosion and synergism (2m/s, 8% sand 32 °C)

Within these test conditions corrosion and synergistic effect contributes almost 75% of the total erosion-corrosion as shown in the pie chart, Figure 4.15. This pie chart is at 2 m/s flow rate and 32°C temperature with 8% slurry concentration.

The shaded area in Figure 4.16 shows that the corrosion and synergistic effect (C+S) is more dependent on temperature than sand concentration. The same pattern was observed with other velocities too. Increased diffusion rate due to increase in temperature is the main reason for this effect. This confirms the hypothesis documented in the past where diffusion coefficient D has a pre-exponential function of temperature. This correlation and the results in Figure 4.16 confirm that the temperature plays a big role in erosion-corrosion. From room temperature to 42°C, within a temperature increment of 20°C, the total erosion-corrosion change more than three times from it original value. It is also observed from this figure that the rate of change of erosion increase with temperature.

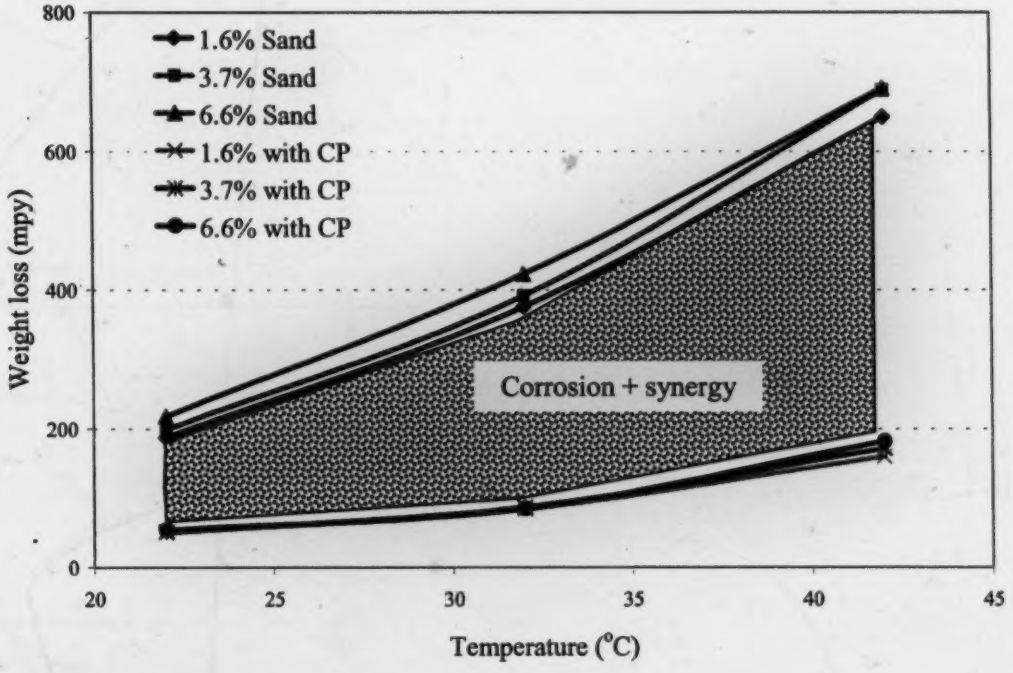

Figure 4.16 : Temperature on erosion-corrosion at 2 m/s.

In summary, these figures demonstrate that temperature has a much stringer influence than velocity or sand concentration on erosion-corrosion. The velocity, temperature and sand concentration affect more on synergy than corrosion or erosion. Also the temperature effect on synergy is much higher than corrosion or erosion and is high at 42°C. This is believed to be the following: *Increase in velocity or sand concentration increase the mass transfer and decreases oxide layer due to high turbulence, whereas increase in temperature decrease the saturated oxygen concentration in the bulk of the slurry but increases exponentially the oxygen diffusion rate and the latter leads the whole erosion-corrosion process at high temperatures (30 - 42°C).*

4.5 Comparison with previous studies

The table 5.1 lists the results of several studies in slurry erosion-corrosion. Though the slurry chemistry, test specimen material and configurations were different, the results of this study are close agreement with other researchers' results.

Table 4.1: Results from the previous studies

Research	Conditions	Erosion-corrosion
This Study 2003	850ppm NaCl 22 – 42°C, 0 – 3 m/s, 50-70 mesh sand up to 12% by weight	5 – 18 mm/y (200 -700 mpy
Amarnath et al, 2002	3.5% NaCl 25°C, API X52 material using rotating cylinder, disk, flat plate, parallel disk, 0 – 5 m/s	3.6 – 6.4 mm/y (146 256 mpy)
Goosen et al, 1999	50 -90mm mild steel pipe 2 - 5m/s bottom ash slurry flow	1 – 7 mm/y
Shadly J.R, 1995	ELBOW, CO2 environment, carbon steel 1 – 5 m/s sand 90 – 125 um	1- 37 mm/y
Efird et al, 1993	½ and 1" pipe and Jet, wall shear stress from 1 - 1000N/m^2	5 – 17mm/y (200 – 700 mpy)
Nesic and Postlethwaite 1991-a	2% slurry, disturbed flow conditions 20 – 40 mm pipe expansion	18 – 30mm/y (720 – 1200 mpy)
Postlethwaite et al, 1986	83 mm pipe in 3%NaCl at 20% silica sand 30- 50 mesh 2 – 6 m/s	6 – 25 mm/y (240 – 1000 mpy)
Luis Efrain, MIT PhD Thesis 1984	Low carbon steel, 120 - 180 °C 3m/s pH 5.6 Steam extraction line very low oxygen (ppb)	1-9 ug/cm^2/h – low O_2

4.6 Morphology

Due to the curved nature of the specimen and varying focus, the optical microscope images were not clear and therefore some specimen were analyzed by stereo microscope and some by SEM. The porous corrosion product formed along the flow direction at 2.5 m/s is shown in Figure 4.17. The dried product on the top of the surface is reddish brown in color and believed to be Fe_2O_3.

In case of flow without sand, the visual observation of the corrosion products were all reddish brown Fe_2O_3, however with sand, both blackish brown Fe_3O_4 and reddish brown Fe_2O_3 were noticed as shown in Figure 4.17 and Figure 4.18 respectively. Figure 4.18 shows that more active surfaces were formed during slurry erosion and diffused oxygen at the metal surface was not enough to convert all active iron (Fe^{2+}) into higher oxidation products (Fe^{3+}) like Fe_2O_3 and some of the Fe^{2+} converted to lower oxidation ($Fe^{2.66+}$) and formed blackish brown Fe_3O_4.This is another visible evidence for mass transfer controlled corrosion process.

Figure 4.17 : Micrograph of the corrosion at 2.5 m/s and 32°C after 22 hrs

Figure 4.18 : Erosion-corrosion after 30 hrs (color photo attached in Appendix II)

Figure 4.19 : Flow path and micro-pits at the clean surface (after 30 hrs)

Figure 4.20 : Erosion-corrosion surface profile along the circumference.

The Figure 4.19 shows the erosion-corrosion surface after 70 hrs with 6% sand at 2m/s. It is not clear why the micrograph Figures 4.19 and 4.20 show alternative layers of undamaged ridges and damage grooves in the direction of flow. Most of the groves were more in the range of 350μ, higher than the average diameter of sand; this shows that some of the sand was carried along the groves. The same was observed with smaller size ridges and more uniform in the flow direction even after 70 hours of operation at high velocity of 3.5 m/s with ~6%. This may be due to flow, particle interaction, pipe material effect such as 'roll banding' or combination of all.

Further more erosion-corrosion often develops in the form of pits in micro level and increased surface roughness as noticed in the Figure 4.19. The same was reported by Luo & Lu in carbon steel, He (2002) and Burstein (2000) in stainless steel and this supports the proposed synergistic mechanism, `micro-*stress-corrosion*` in the next section

The micrographs Figures 4.19 and 4.20 also show that the increased surface roughness by forming groves and ridges along the flow direction increases the exposed surface area for corrosion attack, even though the apparent diameter of the pipe remains same. In other words the apparent exposed surface area used in corrosion calculations are much smaller than actual exposed surface area. This means the apparent corrosion rates used in this

study are higher than the actual corrosion rates calculated from the apparent surface area. This is somewhat analogous to the engineering stress vs. true stress in tensile test measurement. This increased surface area increases the quantity (total flux) of oxygen transferred to the surface even though the mass transfer rate remains constant. As the corrosion is mass transfer controlled, increasing the amount of oxygen transferred to the surface increases the corrosion. Hence the previously reported hypothesis: *'the role of erosion is to prevent the formation of rust film, not to erode the corrosion roughened surface'* (Postlethwaite 1986) requires a revision. This hypothesis is modified and integrated with the above findings as follows; *within the standard pipe flow velocity of 0 – 3m/s, the role of erosion is to reduce the formation of rust film and increase the exposed surface area for corrosion attack by the forming groves along the flow direction.*

Figure 4.21 : Erosion-corrosion surface roughness along the flow direction

It is also noticed from the above Figures 4.20 and 4.21 that the surface roughness along the flow direction is much smaller compared to the roughness along the circumference (peripheral). In other words the peaks along the circumferential direction are 5 – 7 times higher than the peaks along the flow direction. Therefore the influence of surface roughness is more on increasing the total drag force on the fluid (wall shear stress * circumference) and thereby reducing the flow than directly disrupting the slurry flow. This intern increases the pumping requirements.

Figure 4.22 : (a,b) SEM images of erosion at along the circumference

The SEM analysis of the erosion in Figure 4.22 (a,b) shows the erosion groves along the flow direction.

Figure 4.23 : SEM image of erosion ploughing scars on the flow-loop specimen

There was no-distinctive scar pattern due to sand impact as expected and observed in the rotating cylinder tests (Lu 2003), with Jet impingement test (Neville, 2003) and single particle impact on Aluminum (Levy, 1995). Few ploughing scars along the flow direction as in Figure 4.23 were observed in several SEM analyses, however these scars were isolated cases and do not represent the whole examined surface. This casts the doubt on these ploughing scars. Are these isolated marks damage due to the chemical cleaning or

corroded immediately after being removed from the flow-loop or caused by few heavy sand in the slurry, is not clear at this stage and needs further investigation.

The most awful effect of the erosion-corrosion was noticed at the flow-loop slurry pump rotor (impellor). The Figure 4.24 shows the new rotor and used rotor after six months of operation at 2-12 % slurry concentration. The hard phase chromium coating was removed and the entire surface contact with the stator, almost 50 % of the total surface was removed. The pumping efficiency was reduced almost by 60%.

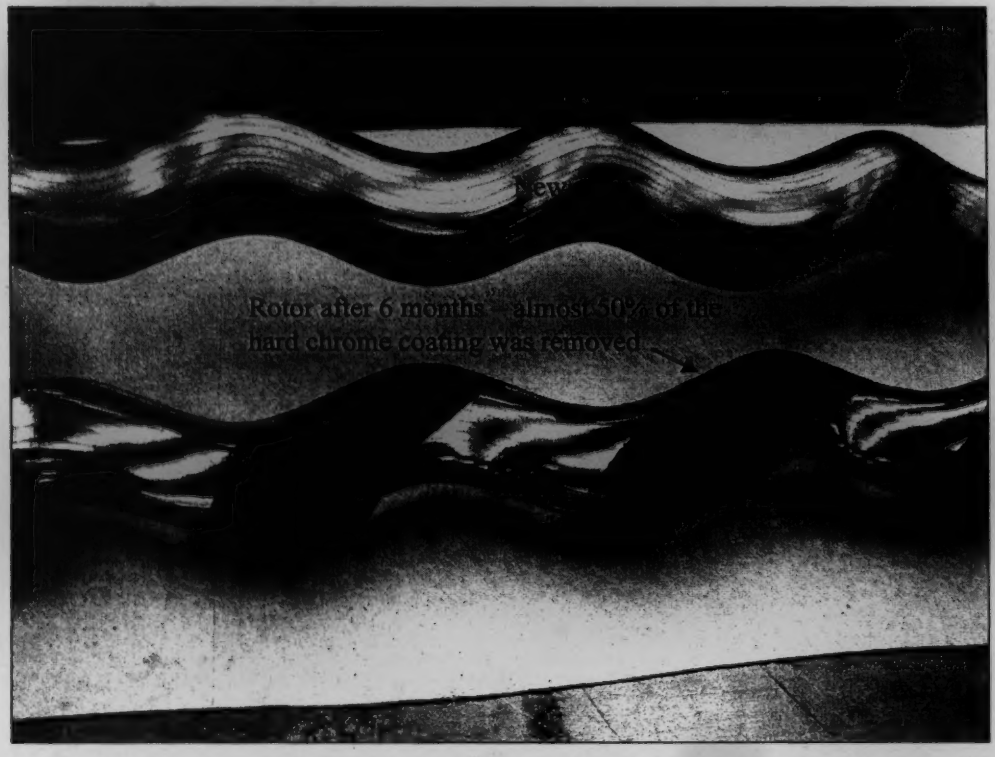

Figure 4.24 : Flow-loop reciprocating pump rotor (color photo attached in Appendix II)

4.7 Accuracy of the measurements

Figure 4.25 shows the temperature variations within a test completed on 5 and 6 May 2003 and Figure 4.26 shows the mean temperature and the deviation from the mean.

Figure 4.27 sows the flow rate variations with in a test completed on 23 and 24 April 2003 and Figure 4.28 shows the mean temperature and the deviation from the mean for all the tests. Both the temperature and velocity variations were kept well within the limits as compared to similar experiments published in the past (Amarnath, 2002))

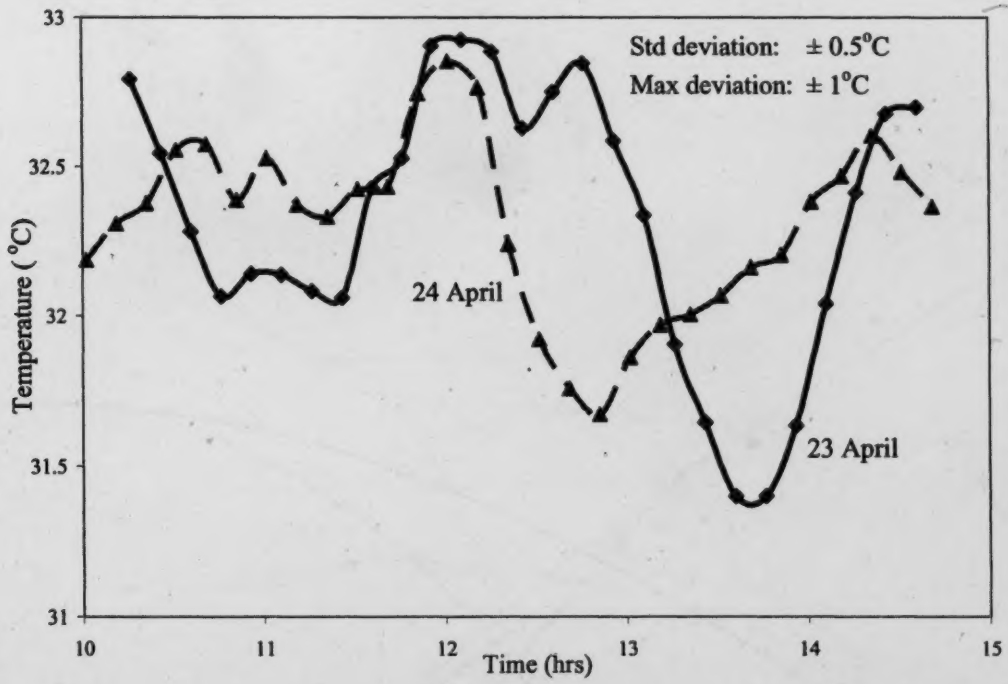

Figure 4.25 : Temperature variation in the erosion-corrosion test at the flow-loop

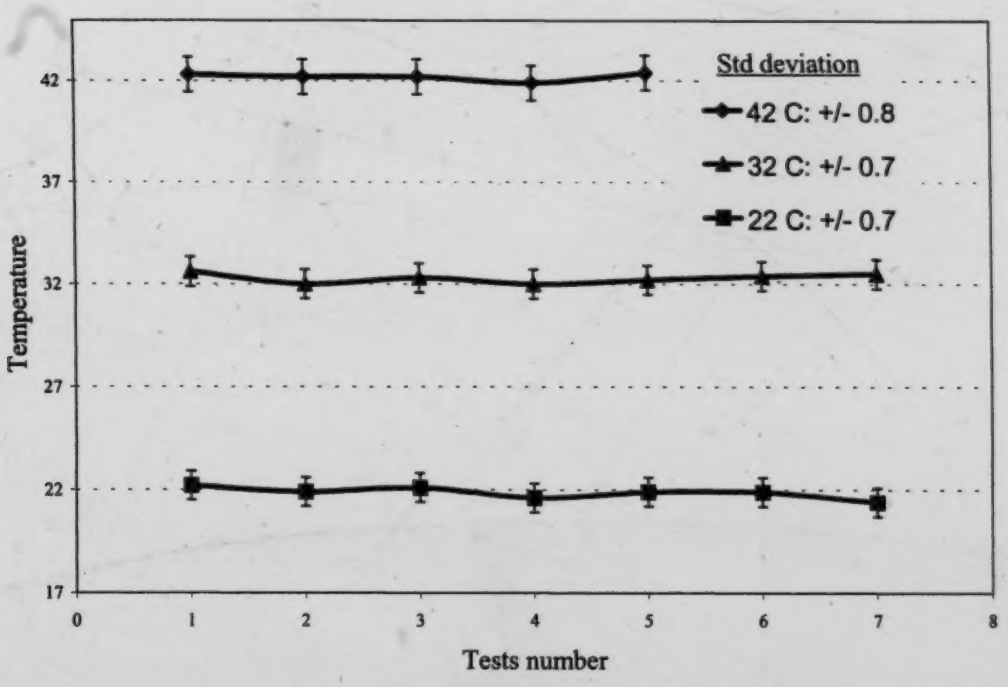

Figure 4.26 : Temperature deviations in the erosion-corrosion test at the flow-loop

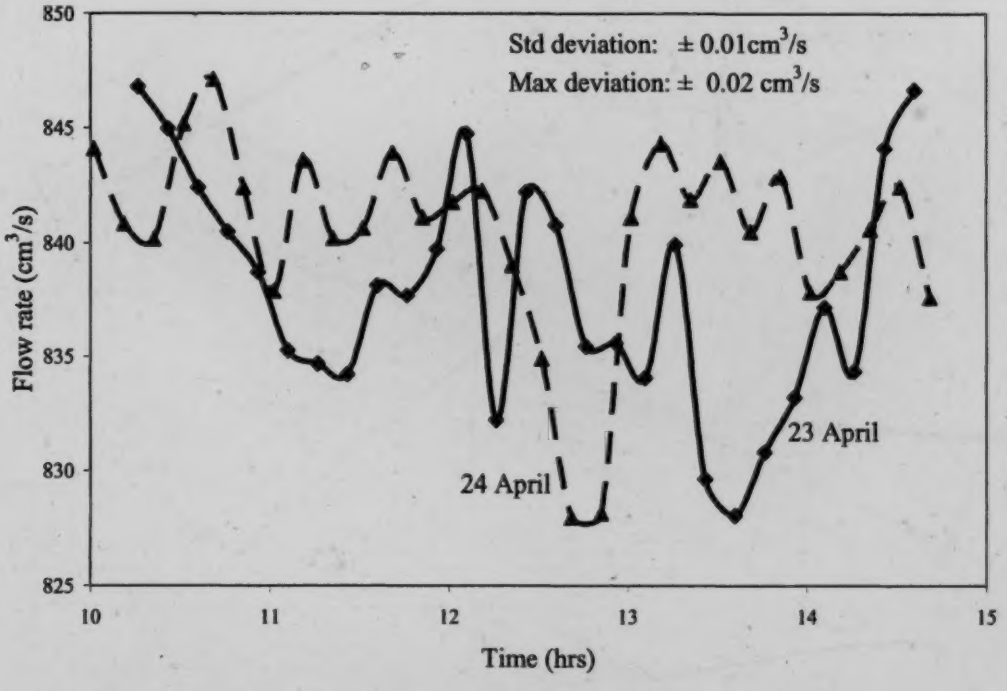

Figure 4.27: Velocity variation in the erosion-corrosion test at the flow-loop

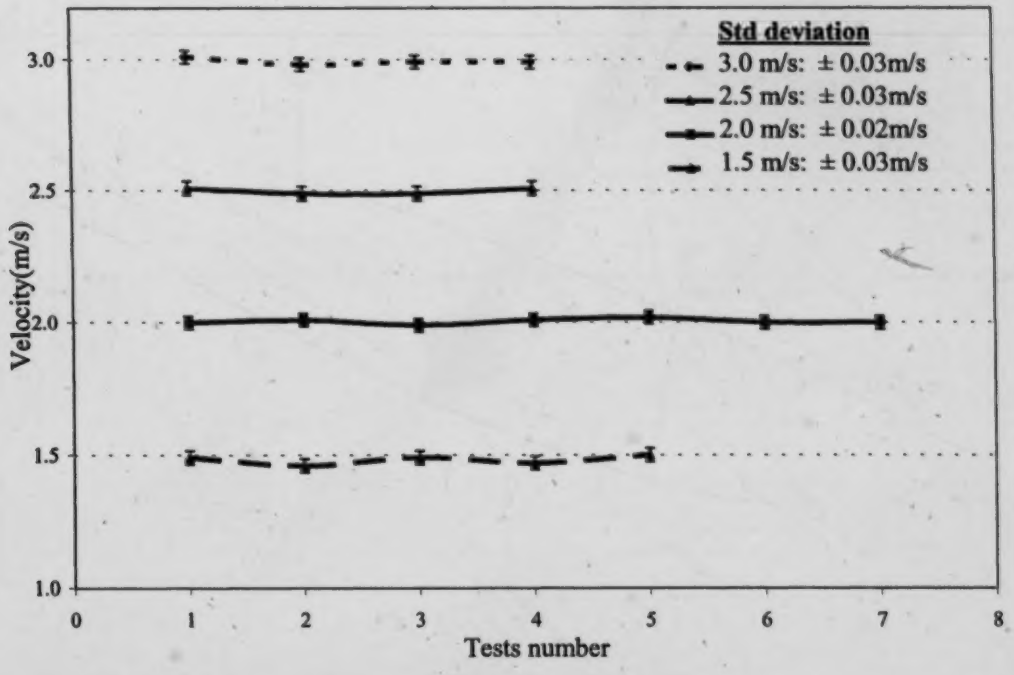

Figure 4.28 : Velocity deviations in the erosion-corrosion test at the flow-loop

5. Mechanism and modeling

This chapter largely explains the synergistic effect mechanism, along with flow assisted corrosion mechanism, a simulation method to predict the flow assisted corrosion and a modification to single particle erosion model to fulfill the pipe slurry flow conditions.

5.1 Corrosion

5.1.1 Mechanism

Corrosion reactions are oxidation-reduction reactions and reduction portion of the reaction depend on oxygen transfer rate, drives the whole corrosion process. As described in the literature survey the overall reaction is

$$2Fe + 3H_2O + 1½\ O_2 \leftrightarrow 2Fe(OH)_3 \qquad 5.1$$

In neutral or alkaline solution the individual reactions are:

$$Fe \leftrightarrow Fe^{+2} + 2e^- \text{ Step one (Oxidation reaction) Rapid reaction} \qquad 5.2$$

$$Fe^{2+} \leftrightarrow Fe^{+3} + e^- \text{ Step two (Oxidation reaction)} \qquad 5.3$$

$$Fe \leftrightarrow Fe^{3+} + 3e^- \text{ Oxidation reaction} \qquad 5.4$$

$$O_2 + 2H_2O + 4e^- \leftrightarrow 4OH^- \text{ Reduction reaction} - \textit{O}_2 \textit{ transfer control} \qquad 5.5$$

The oxygen attacks the metal surface, releasing ferrous and hydroxyl ions into the surrounding boundary layer. A secondary reaction then takes place; further oxidizing the ferrous ion to the ferric ion and forms an insoluble precipitate of iron hydroxide and tends to stick onto the pipe wall. The initial stages of the reaction occur fairly rapidly. As ferrous and hydroxide ions build up near the surface, the reactions begin to slow down and eventually to an equilibrium rate governed by the rate at which oxygen diffuses through the rust and the diffusion boundary layer.

In flow or slurry flow condition some of this oxide layers were removed and carried away with the bulk of the flow due to turbulence and sand impingement. It can be assumed that at a particular flow condition, temperature and slurry concentration, the oxide production rate (oxygen transfer rate) and the oxide removal rate is in equilibrium and the equilibrium thickness of oxide layer remains same. This happens in the flow-loop and the equilibrium thickness can be measured as explained in the previous chapter Figure 4.5.

The equilibrium process can be represented as in the following schematic diagram Figure 5.1 (modified from Melchers 2003 and Heitz 1991).

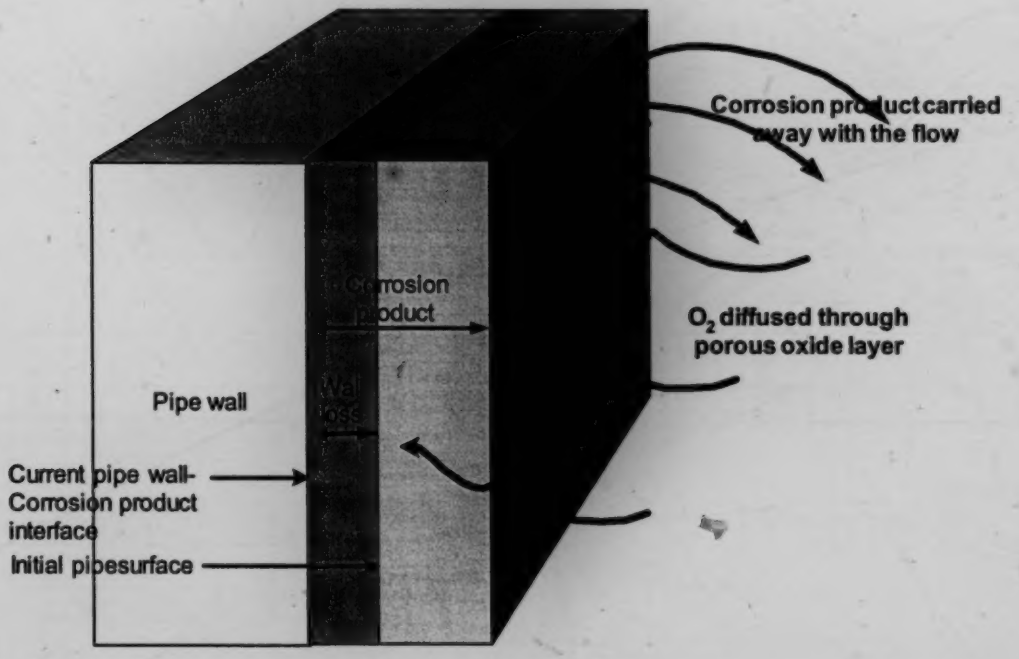

Figure 5.1 : Schematic representation of the equilibrium corrosion process

5.1.2 Diffusion rate (k_d)

Corrosion rate is equal to the limiting current if all the oxygen diffused through the mass transfer boundary layer and reacted with the ferrous ions at the metal surface and converted into $Fe(OH)_2$, providing that there is no other resistance to oxygen diffusion like oxide or passive layer etc. If there is an oxide layer and some of the oxygen consumed during the diffusion process to convert $Fe(OH)_2$ into other stable products, then the corrosion rate would be less than the limiting rate. In fact it has been well documented that the latter occurs in actual corrosion process and the disagreement between many researchers in the past was the ratio between corrosion current and the limiting current.

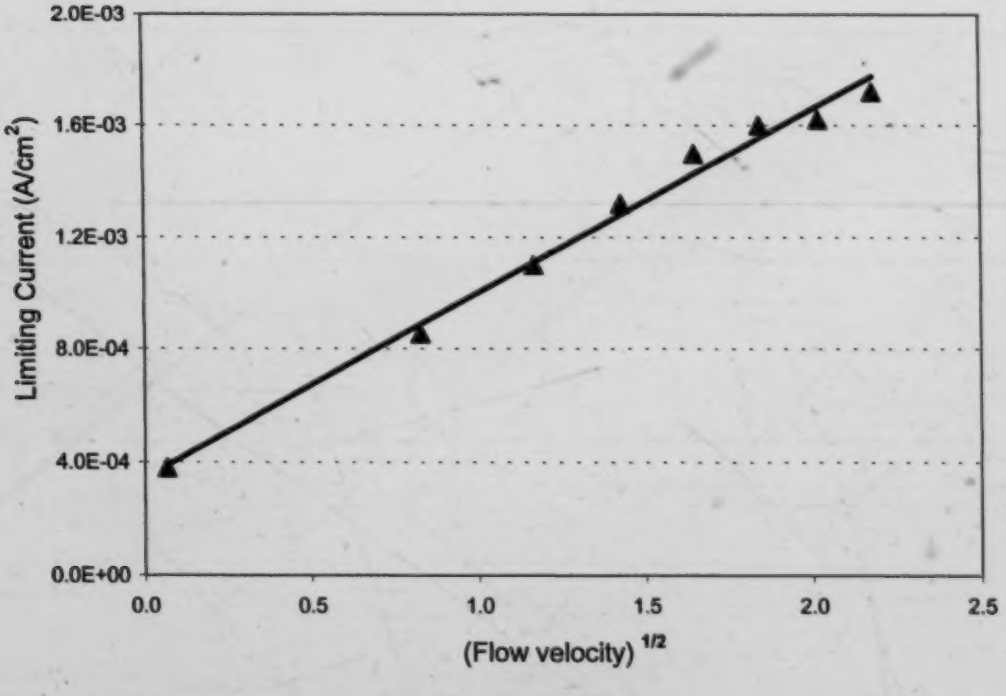

Figure 5.2 : Limiting current test with rotating cylinder electrode

The straight-line relationship between the limiting current and the square root of angular velocity in Figure 5.2 confirms the hydrodynamics of the rotating cylinder and thus the hydrodynamic equations developed in the past for this can be used without further arguments.

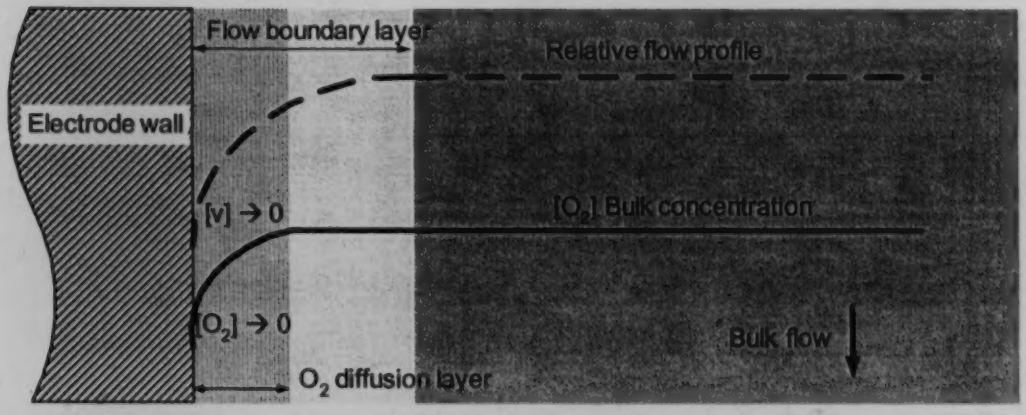

Figure 5.3 : Schematic O_2 diffusion and flow profile in rotating cylinder

The oxygen diffusion through the mass transfer boundary layer and the velocity profile in a rotating cylinder can be illustrated as in Figure 5.3. The electrode surface was polished prior to each test and therefore it was assumed that there was no buildup of oxide layer during the short cathodic polarization test. All the oxygen that diffused to cathode surface is assumed to be consumed and converted to $(OH)^-$.

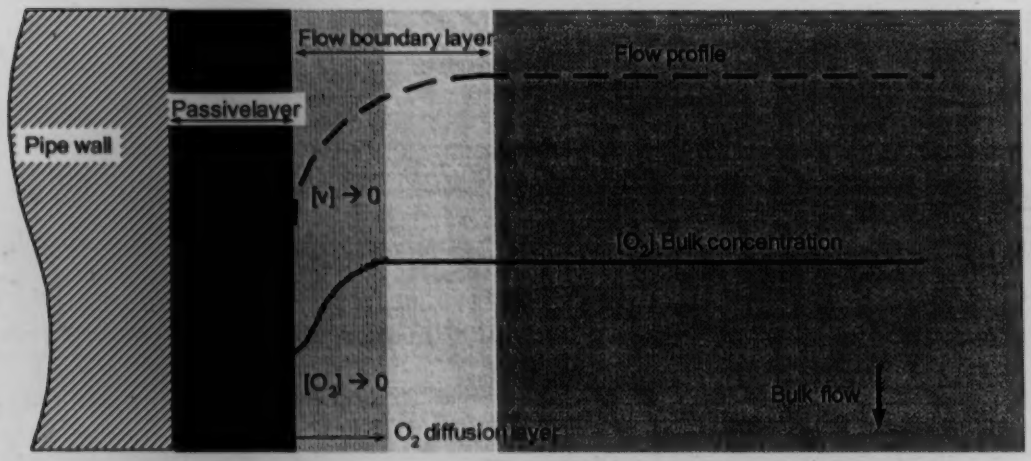

Figure 5.4 : Schematic O_2 diffusion, flow profile and oxide layer near pipe wall (color photo attached in Appendix II)

The oxygen diffusion in the actual pipeline carrying aerated slurry can be schematically illustrated as in Figure 5.4. It shows the mass transfer boundary layer, oxide layer and the velocity profile. Compared to the rotating cylinder, the oxygen diffusion is further reduced by porous oxide layer in pipe lines.

Postlethwaite (Postlethwaite, 1987) assumed that all the chemical oxidation reaction occurs at the surface within the mass transfer boundary layer and from the chemical equilibrium, he proposed that the corrosion current equal to ⅔of the limiting current. In real circumstances in pipe flows however not all the reactions take place at the surface and there is a substantial thickness of oxide layer as described in the previous chapter (Figure 4.5) and does not follow this prediction.

In another study Efird (Efird, 1998) correlates the mass transfer coefficient with limiting current through wall shear stress. He assumed that wall shear stress τ_w is proportional to

the square of limiting current (i_{limit}^2). Melchers (Melchers, 2003) defined two coefficient and used mathematical model to simulate the sea water corrosion of mild steel and correlated through the field data.

To investigate further the relation between the corrosion current, the limiting current results and weight loss measurements from the flow-loop were plotted against the mean flow velocity as in Figure 5.5.

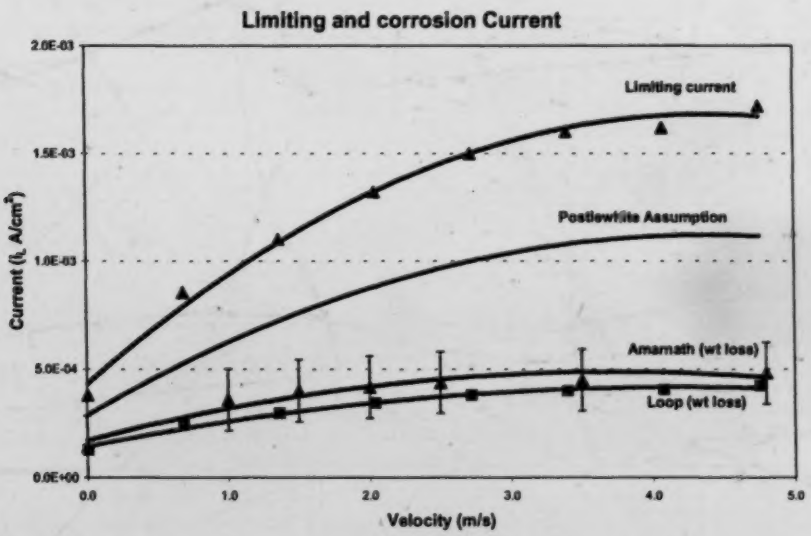

Figure 5.5 : Limiting current and corrosion current with velocity

The top line represents the limiting current measured with the rotating cylinder electrode and the second line is based on the assumption (Postlethwaite, 1986) that corrosion current equal to ⅔of the limiting current.

The third line is the Amarnath et al published results (Amarnath, 2002). They used weight loss measurement to calculate the corrosion rate and confirmed their results with rotating disk, parallel disk, flat plate and rotating cylinder at 25°C in 3.5% NaCl solution for API X52 grade steel. The error bar shows the range for diverse rotor arrangements. The bottom line in Figure 5.5 shows the corrosion current calculated back from the flow-loop weight loss measurements of this study using Faraday's formula (Chapter 2.2). The

flow-loop measurements were very much agreement with the published corrosion measurements from Amarnath et al.

Once the correct hydrodynamics is established in the rotating cylinder as in Figure 5.2, the actual limiting current (i_{lim}) can be empirically correlated through limiting current at room temperature as follows.

$$i_{\lim} = i_{\lim_o} + Av^{1/2} \qquad 5.6$$

Where:

A	=	empirical constant
i_{lim_0}	=	limiting current at zero rotational speed
v	=	flow velocity

The same was reported as $i_{lim} = \alpha + \beta.v^{½}$ by Poulson (Poulson, 1982) where he describes α as a constant representing the natural convection and by Efrid (Efrid 1998). He proposes τ_w proportional to (i_{lim}^2).

This will be continued in the future and the works that are completed during this period is presented in the future works.

5.2 Erosion

Three different mechanisms proposed by Finnie's cutting wear, Bitter (1964)'s deformation wear and Levy's platelets wear were studied in the context of slurry pipelines. The test results at 8% sand show that the erosion represents a relatively small portion around 25% of the total material loss in the flow-loop. CFD simulation shows that the angle of impact of sand particle relative to pipe wall is small and in the range of 4^O - 11^O as shown in Figure 5.6 (Wang, 2003). Cutting wear is due to shear force acting parallel to the surface and energy required is much lower compared to deformation wear. Therefore the erosion mechanism in pipelines carrying high concentration slurry within

the standard pipe flow range can be assumed to follow the Finnie's cutting mechanism closely, than others.

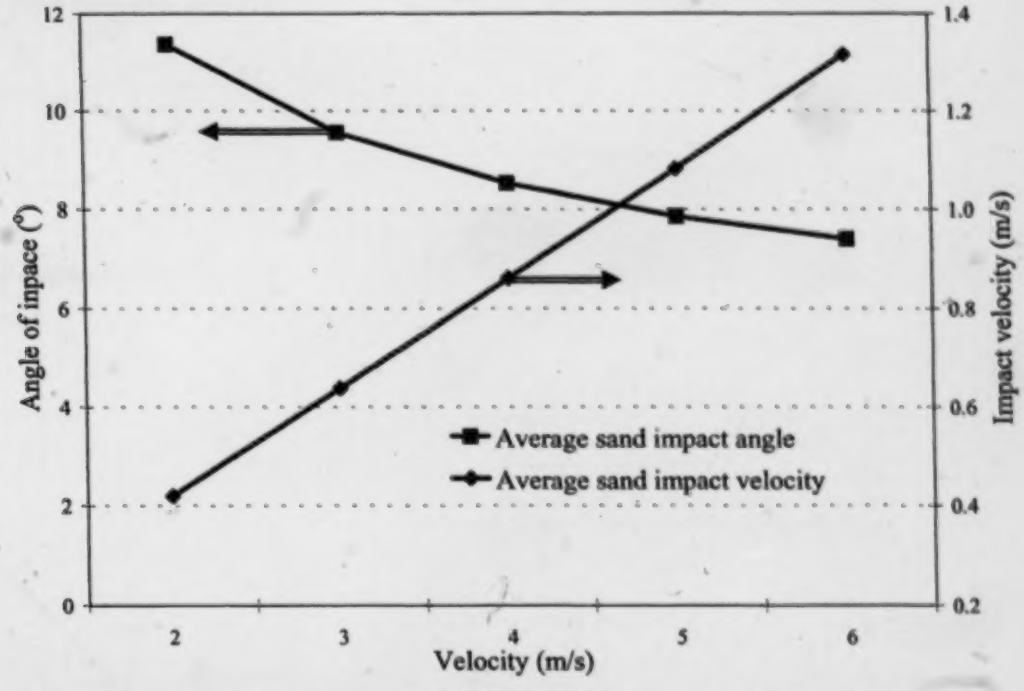

Figure 5.6 : Sand impact velocity (v_p) and angle with the mean velocity (Wang, 2003)

Erosion modeling revolves around the sequence of events, than a single event that occurs when the surface is struck by successive small solid particles. Single particle erosion rate can be model through modified Finnie's equation (Nesic, 2001). This model has two parts, one for the impact angle less than 18.5 ° and other for more than 18.5 °. Within the impact angle of 18.5° it can be further reduced to pipe flow conditions as follows

$$E.R\big|_{\text{single particle}} = \frac{\rho_{pipe}.m_p(v_p \sin\alpha - v_{cr})}{2P}\left[v_p \cos\alpha - \frac{3}{2}\left(v_p \sin\alpha - v_{cr}\right)\right] \quad 5.16$$

Where:

V_p = particle velocity can be couple to flow velocity

α = impact angle and can be assumed from the MCS

V_{cr} = critical velocity assumed to be 0.668 m/s for pipeline s/s (Nesic, 2001).

P = the flow stress

M_p = average particle weight.

A new procedure is proposed in the Future works to convert the single particle model into multi particle through Monte Carlo Simulation (MCS).

5.3 Synergistic effect

Erosion occurs when the shear stress exceeds the critical shear stress. Nesic et al (Nesic, 2001) modified Finnie's erosion model and include critical shear stress by subtracting critical velocity (v_{cr}) from the particle velocity v_p as in the above formula 5.16. There won't be any erosion if the particle velocity is less than the critical velocity. However most of the previous studies, to my knowledge, ignore the stress caused by the particle impact with a velocity less than critical velocity. The author believes this disregards stress causes the synergistic effect.

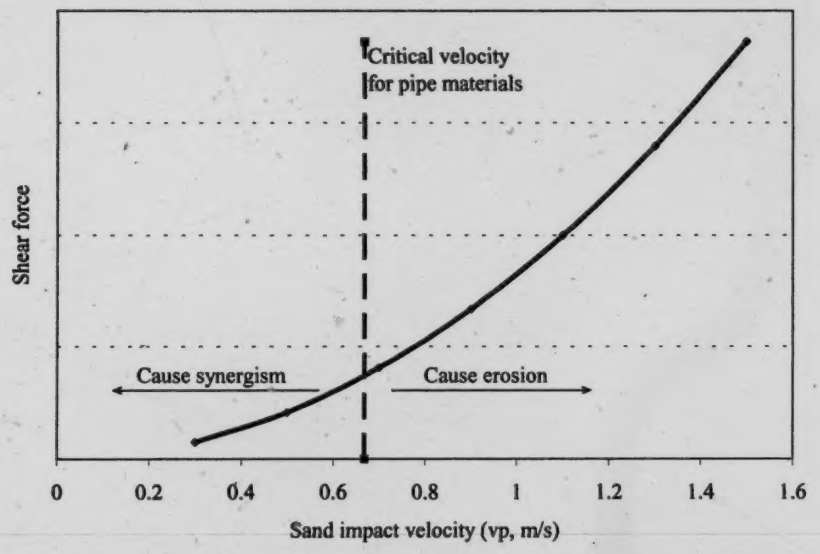

Figure 5.7 : Shear fore with flow velocity for a single particle impact

For instance consider an average particle of 300μm and the impact area of 50μm diameter, within the slurry flow range, assume no particle interaction, no rotation, angle of impact of 10°. The particle velocity can be calculated from Figure 5.6 (Wong, 2003).

The shear force acting on the surface due to single impact can be calculated and schematically represented as in Figure 5.6. (This equations used in this calculation is annexed in Appendix II and is based on the expressions adapted from Shirazi et al, 2001)

This shows that there is a substantial internal force even below the critical velocity. The particle impact with a velocity less than critical velocity causes difference in stress levels between the two adjacent impact and non impact surfaces. Therefore the same acted in a micro scale in every single sand impact below the critical velocity. The impact area becomes anode, increase iron dissolution rate and cause synergistic effect. Lets call this as `*micro stress corrosion*` and the process (iron dissolution rate) can be compared with pitting corrosion. Further more corrosion due to difference in stresses was well documented in textbooks and observed in barbed wires, bend steels, nail heads etc. Again iron dissolution rate corresponding to a particular stress level or single impact is a material property and is the reason why different materials do not show the same synergistic effect.

The severity and the distribution of stress beneath the single particle impact were studied by Levy (Levy, 1995). The Figure 5.8 extracted from this study shows the stress beneath the single particle impact and is around five times higher than the surrounding surface.

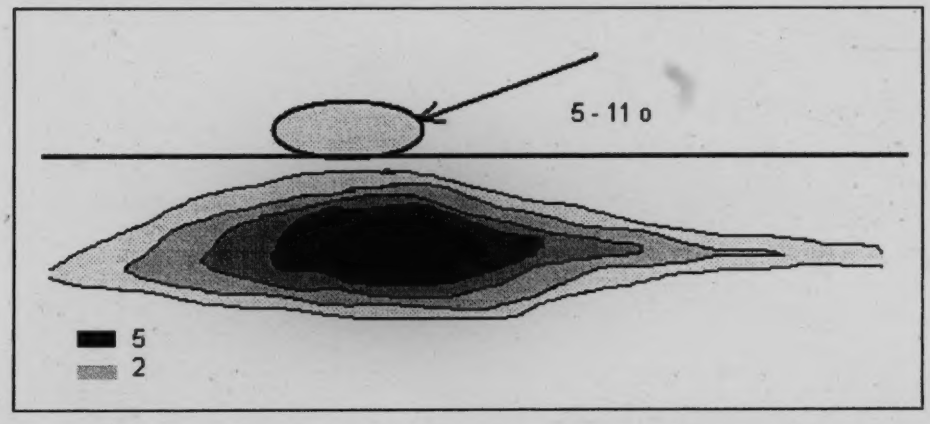

Figure 5.8 : Stress distribution of a single particle impact (Extracted from Levy, 1995)

The results of this study (previous section Figure 4.19) and reported works by Lu (2004), Heitz, (1991) in pipeline materials and He (2002), Burstein (2000) in stainless steel confirm that the synergistic effect is a form of pits and support this mechanism. Burstein further demonstrate that the synergistic effect enhanced by more oblique angle of impact than normal incidence.

A single particle impact was simulated by micro indentation as shown in Figure 5.9 (a) to further investigate the proposed mechanism. The indented specimen was kept in a similar environment for five minutes and the surface was analyzed. The micrograph in Figure 5.9(b) and (c) shows that more corrosion occurs in and around the stressed area. The surrounding is relatively clean and is a considerable evidence to support the proposed synergistic mechanism.

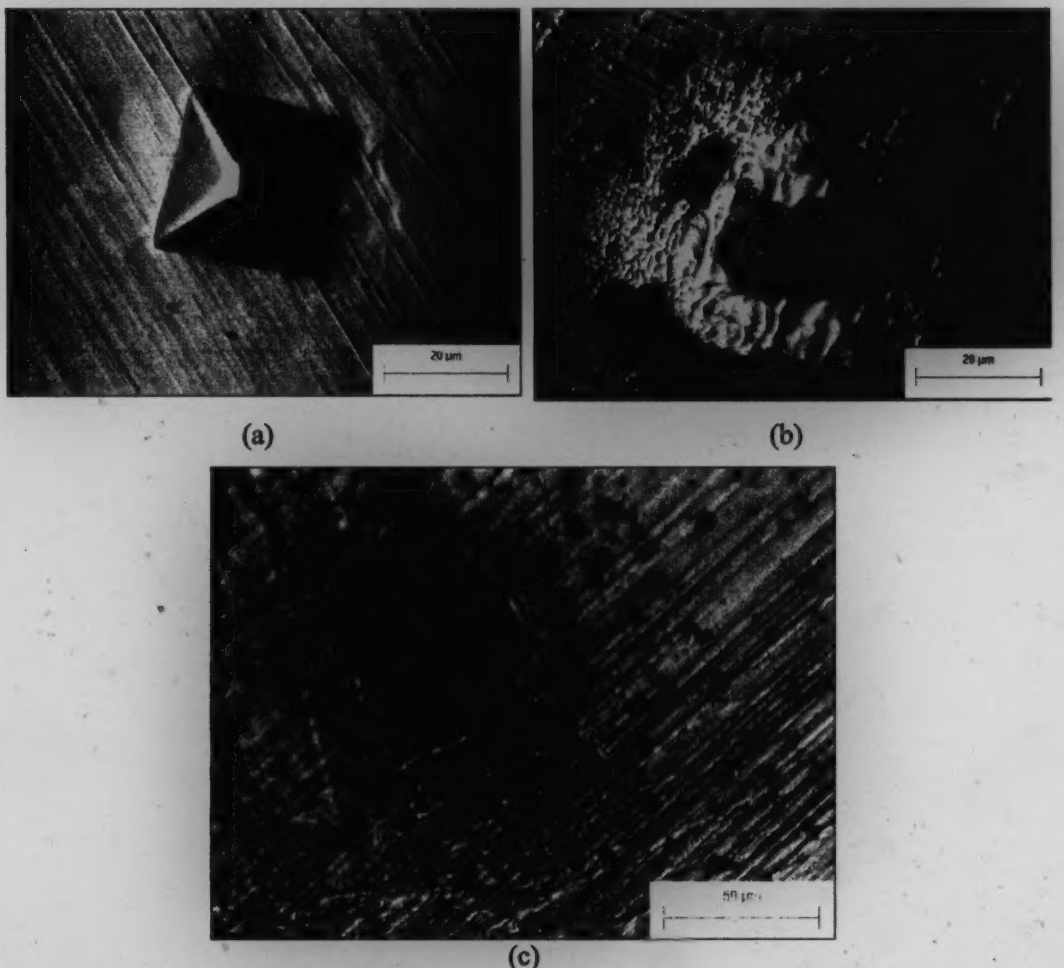

(a) (b)

(c)

Figure 5.9 : Single particle impact simulation

In addition to these findings, the results in Figure 4.15 in the previous chapter show that the contribution of synergistic effect on total erosion-corrosion is higher than pure erosion and almost 30%. The mechanism shows that any material or property that resists micro-stress-corrosion will reduce synergistic effect. To respond this however the literature survey shows, there were not many studies on synergistic effect resistance properties of pipeline materials. Therefore comparison of stress corrosion resistant of pipeline materials is another study proposed in the future.

6. Mitigation of Erosion-Corrosion

This chapter discusses the possible techniques in detail that can be effectively and economically used to control erosion-corrosion in slurry transportation.

6.1 Control of temperature

Temperature plays a big role in erosion-corrosion and a 20°C increment from the room temperature, increases three times the erosion-corrosion rate. Syncrude is now processing the North Mine ore at 50°C and planned to process Aurora mine extraction facility at 25°C. If the process requirements permit to feed oilsand at low temperature and if the flow parameters, pumping requirements were not much affect at lower temperatures, transporting oilsand at lower temperatures would significantly reduce erosion-corrosion.

6.2 Reduction of oxygen

Corrosion and corrosion due to erosion are the main controllable mechanisms for the accelerated damage of pipe wall in slurry transportation. Corrosion depends primarily on the presence of oxygen in the slurry and the temperature. Control of these parameters or transfer of the corrosion to a known place is one of the best options to mitigate erosion-corrosion.

Postlethwaite (Postlethwaite, 1986) suggested that measures to prevent corrosion of straight slurry pipeline should concentrate on controlling the corrosion component than on choosing erosion resistant piping. He further proposed that the erosion-corrosion could be controlled by inhibitors and/or de-aeration resulting in a smooth rust and scale free pipe. However economic considerations influence the above control methods in many slurry lines. De-aeration and inhibition are effective in closed circulating systems like boiler feed water lines, cooling water lines etc but how this techniques can be effectively applied in a long slurry transport line is still not clear.

This study proposes a new innovative approach to control the erosion-corrosion based on the observation in slurry lines and from the principals of cathodic protection. The concept behind this proposed method is by accelerating the corrosion in the first few lengths (km) of the pipe to remove the oxygen from the flow regime and thereby protect the rest of the pipeline. The same concept was successfully used in the past in other areas in the forest fire control, noise control in the airports, immunization!, etc.

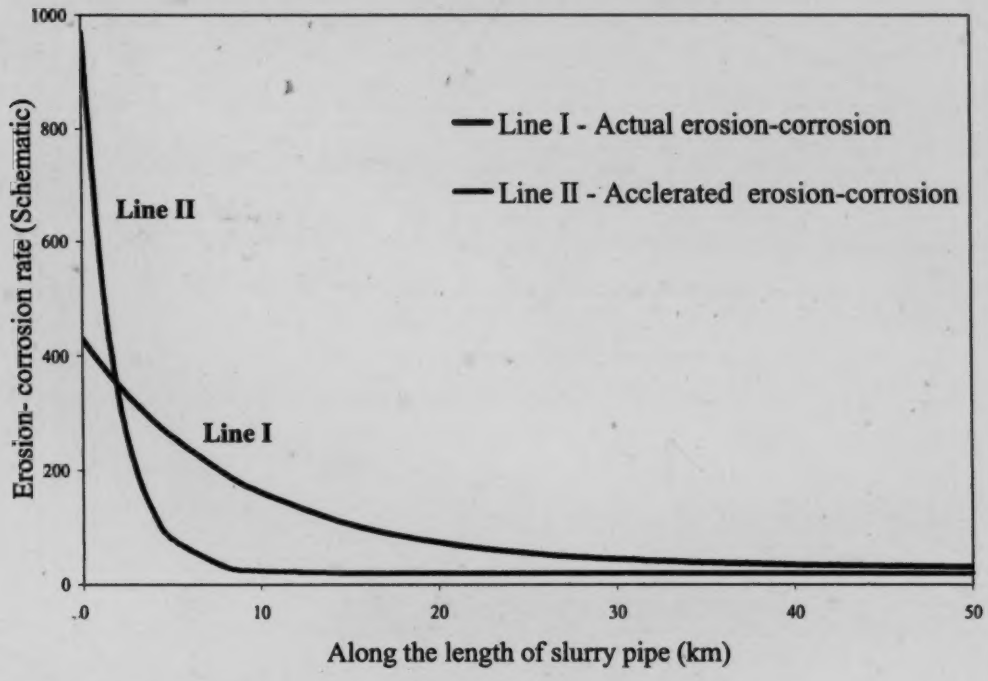

Figure 6.1 : Schematic erosion-corrosion distribution along the slurry line

Observations in the slurry line shows that more erosion-corrosion occurs at the entrance and decrease through the length as shown in line I, Figure 6.1. The line II show the expected corrosion rate as proposed by the above proposed control technique.

Further more the Pourbaix diagram support that the oxygen can be removed by applying a potential within the shaded region as in Figure 6.2. This accelerates the corrosion and promotes the oxygen reduction reaction.

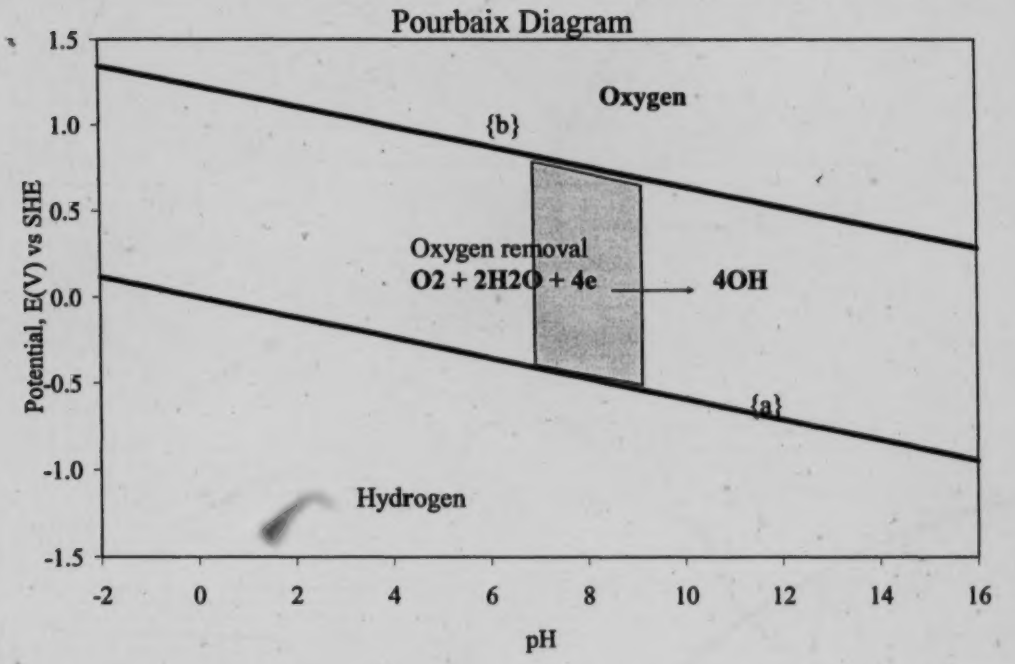

Figure 6.2 : Schematic potential / pH diagrams

Below line {a}, in the lower region, hydrogen is evolved and water is thermodynamically unstable and decomposes to hydrogen. The reaction in acidic solution becomes

$$2H^+ + 2e \rightarrow H_2 \qquad 6.2$$

And in neutral or alkaline solution

$$2H_2O + 2e \rightarrow H_2 + 2OH^- \qquad 6.2$$

As potential becomes more noble (positive), in the intermediate region in between line {a} and line {b}, in neutral or alkaline solution and the equivalent reaction is

$$O_2 + 2\,H_2O + 4e \rightarrow 4OH^- \qquad 6.3$$

In this region water is stable and becomes thermodynamically feasible and dissolved oxygen is reduced to water if present.

This proposed control method can be easily put in to effect as in Figure 6.3. The initial few lengths of the slurry pipe can be sacrificed and replaced time to time to protect the rest of the pipe from erosion-corrosion. (comparable to the economist Pareto's 80/20 theory). Or pipe-sleeves can be used for this purpose. Accelerating the corrosion can be

made by using a cathodic protection transformer rectifier with reversing the connections as of cathodic protection, positive to the pipe and negative to the anode.

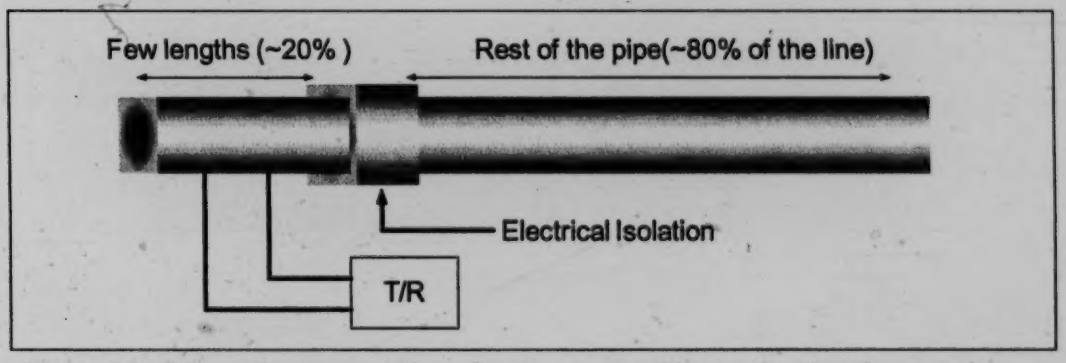

Figure 6.3 : Schematic representation of oxygen removal by accelerating the corrosion

6.3 Preferential protection

Cathodic protection reduces or almost stops corrosion if properly introduced and maintained inside the pipeline. Few smaller diameter pipelines have been protected from internal corrosion with ribbon type sacrificial anodes (Morgan, 1987). However internal cathodic protection for larger diameter pipe with low conductivity slurry is the biggest challenge presently faced by cathodic protection engineers.

Sacrificial anodes were designed and installed in very harsh environment like near the propeller in the ships. In internal pipeline protection, positioning the anode in the centre of the pipe as in Figure 6.4b is the best place in terms of current distribution, however it reduce the flow rate almost half and not practical.

(a) Flow rate = Q_1

(b) Flow rate =½ Q_1 (anode in the centre)

Figure 6.4 : Flow profile

Erosion-corrosion pattern from this study and literature review shows that the most of the damage in slurry lines take place in the bottom half of the pipe. This is due to the gravitational effect of sand in horizontal pipes. Therefore protecting this bottom half by considering the bottom half in cathodic protection design and introducing sacrificial anodes will definitely improve the lifetime of the pipe. Let us called this as *`preferential protection`*.

Preferential protection design concentrate only on the bottom half surface area, current distribution, anode distribution, protection level etc. The proposed schematic distribution of current and anode are shown on Figure 6.5 and Figure 6.6 respectively. This study proposes two anode distribution options. One is based on the available ribbon type anode as in Figure 6.6, option I and the other is based on custom design as in option II, considering flow and slurry erosion effects on anodes.

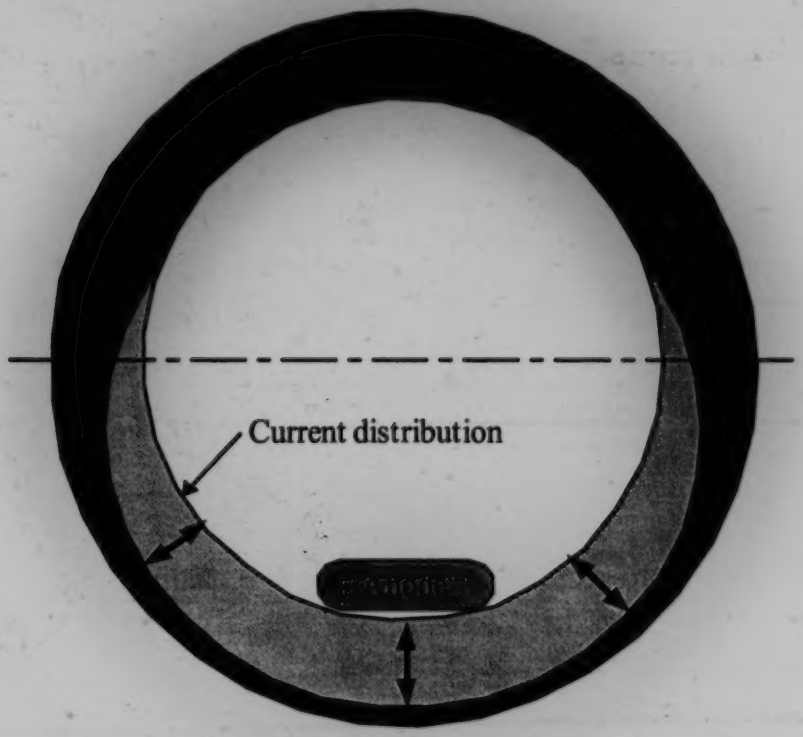

Figure 6.5 : Preferential protection anode position and current distribution

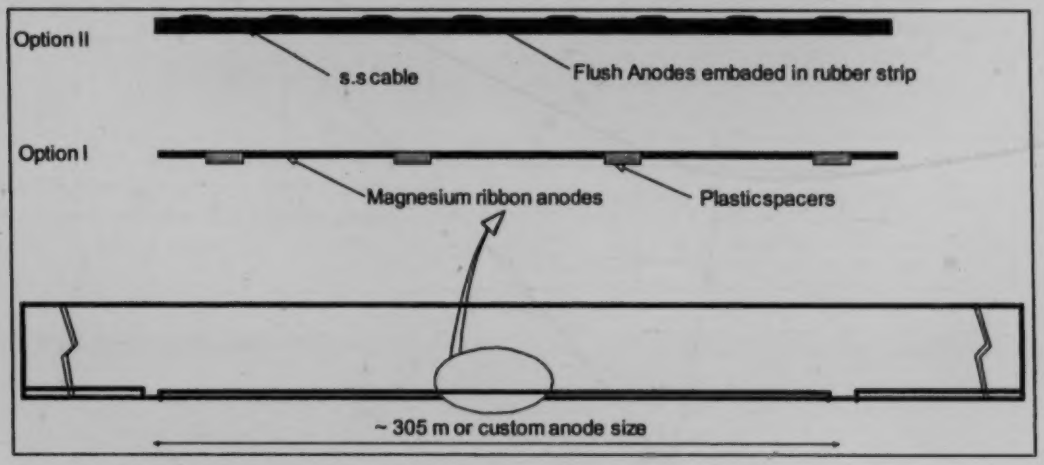

Figure 6.6 : Preliminary preferential protection design

7. Conclusions and recommendations

The first two chapters of this study present the overview of the significance of erosion-corrosion in slurry transportation and mitigation techniques proposed in the past. The relevant methods to simulate the slurry erosion-corrosion were reviewed in the third chapter and the forth chapter described the results in detail. The mechanism and the mitigation techniques were discussed in the next two chapters.

With ever increasing level of oilsand extraction, the need to transport oilsand economically, efficiently and effectively will become of greater importance. The use of pipelines with their many advantages can only increase and therefore the main objectives of this study – 'modeling and controlling erosion-corrosion', becomes more important than ever before. These objectives were achieved by understanding the erosion-corrosion in slurry transportation and the following conclusions were made from this study.

- The flow-loop, designed and fabricated for this study, decimates between erosion, corrosion and synergism and simulates the service conditions. The flow-loop could be easily expanded to permit simultaneous study on different materials.

- Temperature plays a big role in erosion-corrosion and a 20°C increment from the room temperature increases three time the erosion-corrosion rate. This study proposes to transport oilsand at lower temperatures, if the process and flow requirements permit to feed oilsand at lower temperature.

- The results in this study show that corrosion and synergistic effect are the dominant mode of erosion-corrosion in aerated slurry transportation and contribute almost 75% of the total material damage. The erosion contributes only around 25% of the total material damage within this test range.

- A mechanism has been proposed to explain the synergistic effect of erosion-corrosion in slurry transportation and is called as '*micro-stress-corrosion*'. This was

substantiates with the simulation and correlates with similar stress-corrosion situations.

- Two unique techniques to control erosion-corrosion are proposed. One is called '*oxygen removal*' and is reducing the oxygen by accelerating the corrosion in the first few length of the pipeline and thereby protects the rest of the line. The other method is called '*preferential protection*' and is by applying the cathodic protection only for the bottom half of the pipeline and there by protects the severely damaged bottom half of the slurry pipe.

- The results in this study shows that controlling the flow parameters like sand concentration, flow velocity will have less effect on controlling erosion-corrosion at higher temperature above 40°C, which is close to the actual oil-sand transporting temperature (50°C).

- The results also show the introduction of 5% or more sand to the pipeline carrying aerated saline water above 32°C almost doubles the total metal loss compare to the same pipe without sand. This lead to another conclusion and the reason why small amount of sand cause sever damage at 6 o'clock position in oil exploration and transportation lines in Alberta

- Additional evidence is shown in this study to support the previous findings that the corrosion of carbon steel pipe in aerated saline water flow is a mass transfer controlled process.

- A modified hypothesis from the pervious findings on the role of erosion is proposed in this study as follows: within the standard pipe flow velocity of 0 – 3m/s, the role of erosion is to reduce the formation of rust film and increase the exposed surface area for corrosion attack by the forming groves along the flow direction.

Control of erosion-corrosion in Alberta's oilsand transportation offers huge potential for wealth generation and enduring environmental and social benefits. Significant inroads were made in this study towards the control of erosion-corrosion. Putting in action, the plan developed on this research will help to unlock this potential and realize the benefit, while technical hurdles remain to be overcome; innovative approaches are expected to revolutionize the control of erosion-corrosion in oilsand transportation.

8. Future works

Mechanism: The proposed mechanism can be substantiated further with surface scanning using Scanning Reference Electrode Technique (SRET) available at Syncrude and video clipping of a single particle impact in the simulated environment.

Oxygen removal: Set-up and develop a prototype model and demonstrate the proposed oxygen removal technique to control erosion-corrosion.

Preferential protection and erosion resistance anode materials: Anode material erosion is the one of the concern in preferential protection even though the design based on current calculations. A study is proposed to reduce the erosion effect on the standard anodes by adding erosion resistance materials without loosing the electrochemical capacity of the anode. Yttrium is proposed for this and used in various metallurgical applications in magnesium and aluminum alloys. In addition to this, proposed preferential protection system should be tested on larger scale slurry flow-loop, or with spool piece in the actual plant slurry line.

Pipeline Material: The synergistic effect has higher influence than erosion in slurry transportation. Improving the synergistic resistance properties of material will definitely remove some of the erosion-corrosion effect. As the synergistic mechanism is known, this study proposes to focus and compare the synergistic effect (or micro-stress-corrosion) resistant properties of pipeline materials including stainless steel.

Flow-Loop modifications: A modification as shown Figure 8.1 is proposed by adding two by pass lines to overcome the difficulties faced during this study. The bypass Line I is for oxygen measurements. The bypass line II allows control and monitor the temperature and flow rate. Once the required parameters were met, it can be open to the test piece section. Also improved methods should be developed to mechanically polish the internal surface of the test piece.

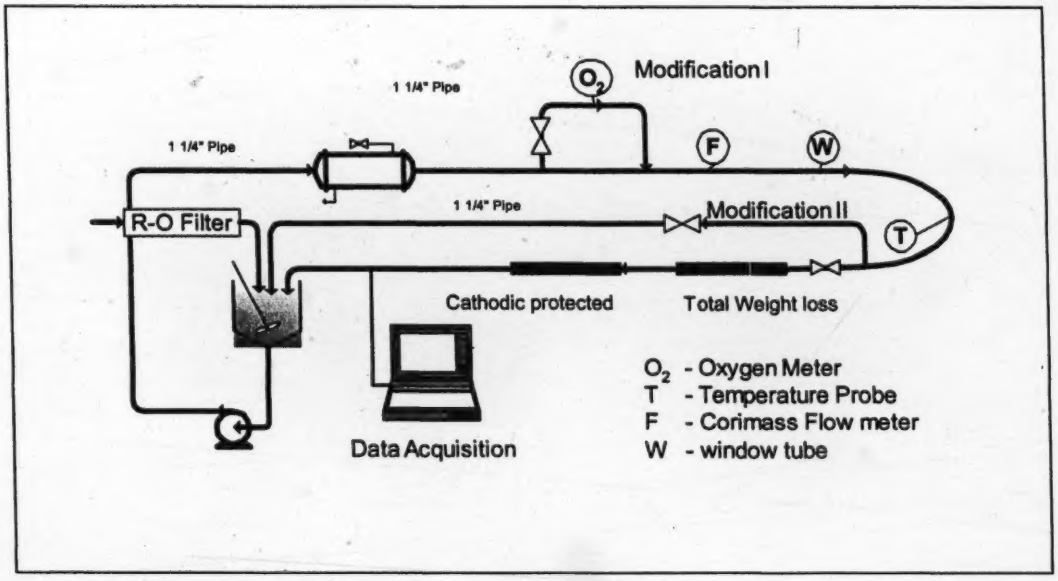

Figure 8.1 : Proposed slurry flow-loop modification

Corrosion model:

<u>Continued from section 5.1.2</u>

The difference between the rotating cylinder limiting current and the flow-loop corrosion current was calculated and plotted against the square root of the velocity as in Figure 8.2 This shows that the difference ($i_{lim} - i_{cor}$) also follows the linear relationship. Therefore ($i_{lim} - i_{cor}$) can be further correlated empirically as follows

$$i_{\lim} - i_{cor} = B + Cv^{1/2} \qquad 8.1$$

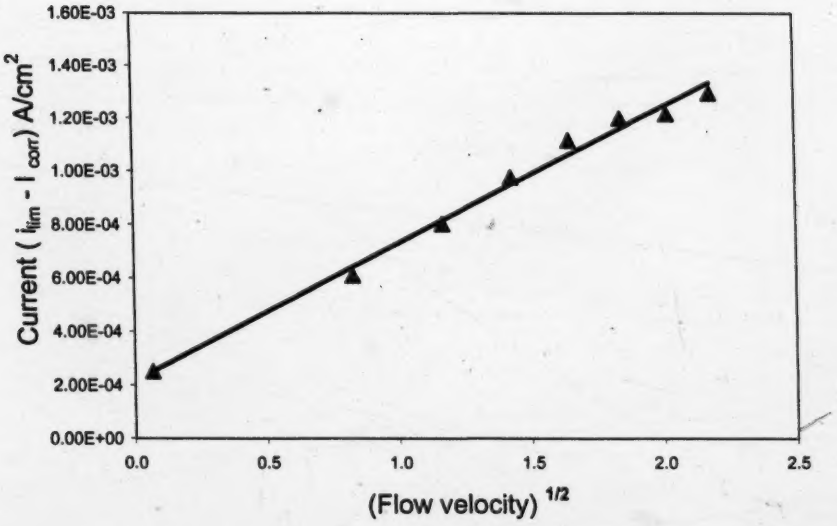

Figure 8.2 : The difference between limiting and corrosion current (i_{lim} - i_{cor})with velocity

Therefore I_{cor} becomes

$$i_{cor} = (i_{\lim_o} - B) + Dv^{1/2} \qquad 8.2$$

Where:

D = A-C, again an empirical constant

In diffusion controlled corrosion process the diffusion coefficient K_d can be expressed as

$$k_d = \frac{i_{cor}}{n_e F C_{O_2_b_rot}} \qquad 8.3$$

Where:

i_{corr} = corrosion current density

n_e = reacted electrons

F = Faraday constant

$C_{O2_b_rot}$ = bulk concentration of oxygen in the rotating cylinder

Therefore the oxygen diffusion coefficient K_d becomes

$$k_d = c_1 i_{\lim_o} + c_2 v^{1/2} + c_3 \qquad 8.4$$

Where:

$$C_1 = \frac{1}{n_e F C_{b_rot}} \qquad 8.5$$

C_1 can be calculated by measuring the oxygen concentration or assuming saturated concentration at room temperature. C_2 and C_3 are constants and C_3 is assumed to be depending only on temperature. K_d can be calculated back from weight loss measurements in the simulated environment using the above equation 5.9, C_2 and C_3 can be extracted from the plot of K_d vs. $v^{½}$. The diffusion coefficients can be further expanded to include temperature variations and considered for the future works.

Corrosion rate (C.R)

Once the mass transfer rate is known, the actual corrosion rate can be easily predicted based the following model assuming two moles of Fe reacts with one mol of oxygen.

$$CR_{Plant} = \left[\frac{2C_{O_2_b_plant} M_{Fe}}{\rho_{Fe}}\right] k_{d_plant} \qquad 8.6$$

Where:

$$k_{d_plant} = c_1 i_{\lim_o} + c_2 v_{plant}^{1/2} + c_3 \qquad 8.7$$

M_{Fe}	=	average molecular weight of the pipe material
$C_{O2_b_plant}$	=	bulk oxygen concentration in the pipeline
ρ_{Fe}	=	density of the pipe material
v_{plant}	=	actual plant fluid flow velocity
T_{plant}	=	actual plant temperature

The corrosion rate expression at room temperature (22°C) for the flow-loop becomes

$$CR_{Plant} = \left[(4.57E-05) i_{\lim_o} + 15.5 v^{1/2} - 164\right] C_{O_2_b_plant} \qquad 8.8$$

Where Corrosion rate is in mpy, v is in m/s, C_{O2} in ppm, i_{lim_o} in A/cm^2 and equals to 3.64E-04A/cm^2 for flow-loop slurry, Fe = 7865, kg/m3, n = 2, M_{Fe}= 55.8)

This model depends on the limiting current, which represents the oxygen diffusion rate, the bulk oxygen concentration corresponding to corrosion potential of the flow regime and velocity correlate flow and oxide layer thickness variations.

This shows that any pipeline flow-assisted-corrosion in aerated or partially aerated environment can be easily modeled through the following equation:

$$CR_{Plant} = \left[Ai_{\lim_o} + Bv^{1/2} + C \right] \left[\frac{2M_{Fe}}{\rho_{Fe}} \right] C_{O_2_b_plant} \qquad 8.9$$

Where A is a material property calculated from equation 5.11. i_{lim} can be calculated from the simulated laboratory limiting current test. B and C can be extracted from the plot of K_d vs. $v^{½}$. Weight loss measurements can be either from the rotating cylinder, rotating plate or from the flow-loop. To predict the corrosion rates over a long period of time, this model should be compared against the data from the plant operations.

Also the proposed corrosion model can be expanded to temperature variations

Erosion model: The author strongly believes and proposed by Chiovelli (Chiovelli, 2003) of Syncrude research, the number of sand impact, the angle of impact and distance between two successive impact called mean free path can be calculated through Monte Carlo simulations (MCS), a technique for simulating real-world situations involving elements of uncertainty and been used extensively in science, engineering, manufacturing and risk analysis for many years.

Electron trajectory simulation by Monte Carlo analysis in Scanning Electron Microscope (SEM) is much similar to the sand particle trajectory in slurry flows and the same can be followed to simulate the erosion. Beam energy or the supply voltage and the current or electron volume in SEM can be compared with the flow velocity and slurry concentration. The interaction volume in SEM can be related to the volume removed by erosion and can be compared with the erosion results. Also Monte Carlo simulation

software packages were used in risk analyses (Crystal ball 2000) can be easily introduced in this. The modified single particle erosion model can be written as

$$E.R\big|_{\text{single particle}} = \frac{\rho_{pipe}.m_p(v_p \sin\alpha - v_{cr})}{2P}\left[v_p \cos\alpha - \frac{3}{2}(v_p \sin\alpha - v_{cr})\right] \quad 8.10$$

MCS allows converting the single particle erosion model into multi particle. The number of impact per unit cross section area per unit time can be coupled to standard flow parameters like sand concentration and flow velocity. Therefore the erosion rate can be represented in mean velocity and material parameters of the pipe as follows:

$$E.R\big|_{\text{Loop}} = \frac{\rho_{Fe}.m_p}{2P} f(v_m, \chi) \quad 8.11$$

Where:

m_p = average mass of a single particle

χ = slurry concentration

v_m = mean slurry velocity

When the velocity and concentration remain same, Faddick proposed the wear rate is inversely proportional to the cross section area of the pipe (Faddick, 1975) and the above equation becomes

$$E.R\big|_{\text{Plant}} = \frac{\rho_{Fe}.m_p}{2P}\left[\frac{d_{loop}^2}{d_{plant}^2}\right] f(v_m, \chi) \quad 8.12$$

Finally, the future work will also should concentrate on the economic feasibility of the two control techniques proposed in this study and the commercial implementation.

Literature Cited

1. Amarnath T, Namboodhiri T, Upadhyay S N, Flow assisted corrosion of API X52 steel ion 3.5% NaCl solution, **Canadian Journal of Chemical Engineering**, pp456-463, Vol. 80, June 2002

2. ASTM D888-03, Standard Test Methods for Dissolved Oxygen in Water, **Annual ASTM standards**, vol. 11.01, 2003

3. ASTM G1-90, Standard practice for preparing, cleaning and evaluating corrosion test specimen, **Annual ASTM standards**, vol. 03.02, 1999

4. Berger F P, Hau L, Mass transfer in turbulent pipe flow measured by the electrochemical method, **International Journal of Heat and Mass Transfer**, pp 1185-1192, Vol.20 1977

5. Bitter J G A, A study of erosion-corrosion phenomena, part I: **Wear**, vol-6, Jan 1963 and Part II: **Wear** vol-6 Jan 1964.

6. Bonnel A, F.Dabosi Corrosion study of carbon steel in neutral chloride solutions by impedance techniques, **Journal of Electrochemical Society**, pp 753- 761, vol. 130, No.4 April 1983

7. Bruce C F, Corrosion products analysis – A road map to corrosion in oil and gas production, pp 56-58, **Material Performance**, August 2002

8. BS7361, Cathodic protection, **Code of practice for land and marine application** pp 20, part I, 1991

9. Burstein G T, Effect of impact angle on slurry erosion-corrosion of 304L stainless steel, pp 80-94, **Wear** 240, 2000

10. Callister D W, **Materials Science and Engineering**, pp 102, Fifth edition, John wiley & sons Inc publication (1999)

11. Chexal B, **Flow assisted corrosion in power plants**, Electric power research institute, Pleasant Hill, CA 1996.

12. Chiovelli S, Anderson M J, Materials for resource recovery and transport, pp 451-464, **The metallurgical society of CIM**, 1998

13. Chiovelli S, **Group Progress Meeting**, Syncrude Research, 24 October 2003.

14. Corradetti B, Ercolani S, Corrosion in coal water slurry pipeline, **The pipe protection conference**, edited by J.Tiratsoo, Elsevier applied science,1991

15. Denny A Jones, **Principles and Prevention of Corrosion**, Macmillan Pub. Co, New York, 1992

16. Edward J Wasp, Kenny J P, Gandhi R L, Solid liquid flow slurry pipelines transportation, **Series on Bulk Materials Handling** pp141- 151, Vol. 1, No 4, 1975

17. Efird K D, Disturbed Flow and Flow Accelerated Corrosion in Oil and Gas Production, **Journal of Energy Resources Technology**, pp.72-77, vol. 120, No. 1, March, 1998

18. Efird K D, Jet impingement testing for flow accelerated corrosion. Paper No.00052, **Corrosion** 2000

19. Efird K D, Wright E J, Hailey T G, Correlation of steel corrosion in pipe flow with jet impingement and rotating cylinder tests Vol.49, No.12, pp 992- 1003, **Corrosion**, December 1993

20. EPCOR weekly water quality report for March, **www.epcor.ca** 2003

21. Faddick R R, Pipeline wears from abrasive slurries, **International Conference on Internal and External Protection of Pipe**, BHRA, Durham, September 1975

22. Ferrini F, Giommi C, Ercolani D, Corrosion and wear measurements in slurry pipeline, pp 133-144, **Hydrotransport 8**, South Africa, August 1982

23. Finnie I, Erosion of surface by solid particles, vol. 3, pp 87-103, **Wear** 1960

24. Finnie I, Some reflections on the past and future of erosion, **Wear**, vol. 186-187, no. 1, pp. 1-10, July 1995

25. Goosen P, Malgas I, An experimental investigation into aspects of wear in boiler ash disposal pipeline, BHR Group, pp684-697, **Hydrotransport 14**, 1999

26. Hale D.W, Slurry pipelines in north America, International Conference on the Hydraulic Transport of Solids in Pipes, **Hydrotransport 4**, 1976

27. He D, Jiang X, Guan H, Erosion and erosion-corrosion behaviors of several stainless steel in duel phase fluid, **Corrosion**, march 2002

28. Heitz E, Chemo-mechanical effects of flow on corrosion, **Corrosion**, pp135- 145, Vol.47 No. 2, 1991

29. Husband W.H.W, **Slurry Pipeline Manual** - Design and Construction, Saskatchewan Research Council, 1986

30. Joseph I Goldstein, Dale E.Newbury **Scanning Electron Microscopy and X-ray Microanalysis**, Second edition, Chichester publications, New York, 1987

31. King R, Jacobs B., Factors affecting the design of slurry transport system for minimum wear, **The pipe protection conference**, edited by Tiratsoo J, Elsevier applied science,1991

32. Levy A V, **Solid particle erosion and erosion-corrosion of metals**, pp 7-43, ASM International, 1995

33. Lina A, Moinereau D, Delaune X, Phalippou C, The influence of water flow on the impact/sliding wear and oxidation of PWR control rods specimens, **Wear** 251, pp 839-852, 2001

34. Lu Jin Fang, Synergy between erosion-corrosion of carbon steel in tap water slurry, **M.Sc. Theses, University of Alberta**, spring 2004

35. Luis Efrain, **PhD Thesis,** MIT, The mechanism of erosion-corrosion in steam extraction lines of power stations pp 161. 1984

36. Luo J, Zhao X Z, Cui N, Chiovelli S, Effect of erosion on corrosion of type 430 and 316 stainless steel in aqueous environments, **British Corrosion Journal** Vol.36, No.4, 2001

37. Matsumura.M, Sakamoto A, Yamasaki T, Erosion-corrosion tests on copper alloys for water tap use, **Wear** pp 548-554, 1995

38. McCabe L W, Smith C J, Harriott P, **Unit Operations of Chemical Engineering,** pp 1102, Fifth edition, McGrow Hill publications, 1993

39. Melchers.R.E, Mathematical modeling of diffusion controlled phase in marine immersion of mild steel, pp 923- 940, **Corrosion Science** 45, 2003

40. Meyer U, Atrens A, Influence of environmental variables on erosion-corrosion of carbon steel in spent liquor re-heaters in Bayer plant, pp 107-116, **Wear** 189, 1995

41. Morgan John.H, **Cathodic Protection**, Second Edition, NACE International, pp 390-400, 1987

42. NACE RP-02-78, Design and operation of stripping columns for removal of oxygen from water, **NACE International**, 1978

43. NACE RP0775-87, Preparation and installation of corrosion coupons and interpretation of test data in oilfield operations, **NACE International**, 1987.

44. Nandakumar K, C.K. Huang, P. Minev, J.L. Luo, K. S. Chiovelli, A comprehensive phenomenological model for erosion in jet flows", submitted to **Wear**.

45. Nanjo H, Kurata, Y, Asano, O, Sata, N, Ikeuchi, J, Sanada, N, The effect of Velocity & pressure vibration on erosion-corrosion of mild steel in water. **Corrosion**, vol. 46, no. 10, pp. 837-842, Oct. 1990

46. Nesic S, Keting A, Numerical prediction of erosion-corrosion in bends, **Corrosion**, pp 621-633, vol.57, No.7. 2001-a

47. Nesic S, Nordsveen M, Nyborg R, Stangeland A, A diffusion based model for corrosion, **Defect and Diffusion Forum**, pp 1661-1674, vol.194-199, 2001-b

48. Nesic S, Solvi G T, Skjerve S, Comparison of rotating cylinder and loop methods for testing CO2 corrosion inhibitors, **British Corrosion Journal**, pp 269 -272, vol.32, No.4, 1997

49. Neville A, Hodgkiess T, Characterization of high grade alloy behavior in severe erosion-corrosion conditions, pp 596-607, **Wear**, 1999

50. Neville A, Hodgkiess T, Shrestha S, Electrochemical & mechanical interactions during erosion-corrosion of high velocity oxy-fuel coating and a stainless steel, pp 623-634, **Wear**, 1999

51. Neville A, Hodgkiess T, Study of effect of liquid corrosivity in liquid - solid impingement on cast iron and austenitic stainless steel, Vol. 32, No.3, pp 197-205 **British Corrosion Journal**, 1997

52. Neville A, Hu X, Mechanical and electrochemical interactions during liquid solid impingement on high alloy stainless steel, pp 1284-1294 **Wear**, 2001-a

53. Neville A, McDougall B A B, Tribo corrosion of Ti and its alloys, pp 46-50, **Material Performance**, December 2003

54. Neville A, McDougall B, Erosion and cavitations corrosion of titanium and its alloys, pp 1-10, **Wear**, 2001-b

55. PETWA, water treatment solutions, manufacturers catalog

56. Postlethwaite J, Brady B J, Studies of erosion-corrosion wear patterns in pilot plant slurry pipeline, paper no J2, **Hydrotransport 4**, 1976

57. Postlethwaite J, Dobbin M.H, Bergevin K, The role of oxygen mass transfer in the erosion-corrosion of slurry pipelines, **Corrosion**, pp514-521, Vol. 42, No.9, September 1986

58. Postlethwaite J, Nesic S, A predictive model for localized erosion-corrosion, Vol.47, No.8, **Corrosion** August 1991-a

59. Postlethwaite J, Nesic S, Hydrodynamics of disturbed flow and erosion-corrosion, Part I- Single phase flow study, **Canadian Journal of Chemical Engineering**, pp 698-702, Vol. 69, June 1991-b

60. Postlethwaite J, The control of erosion-corrosion in slurry pipelines, **Materials Performance**, pp 41-45, December 1987

61. Postlethwaite J, Nesic S, Erosion in disturbed liquid- particle pipe flow, pp850-857, Vol 49, No. 10 **Corrosion**, Oct 1993.

62. Poulson Bryan, Electrochemical measurements in flowing solutions, 'Electrochemical techniques in corrosion testing and research' **Conference UMIST**, pp 391-424, Jan 1982

63. Roco M C, Cader T, Numerical method to predict wear distribution in slurry pipeline, paper no 8, **Advances in Pipeline Protection**, published by BHRA, 1988

64. Sastri V S, Malaiyandi M, **Canadian Metallurgical Quarterly**. vol 22, pp 241, Studies on Molybdate as pipeline corrosion inhibitor in coal water slurry, 1983

65. Shirazi S.A, McLaury B S, Ali M M, Sand monitors evaluation in multiphase flow, paper No. 00084, **Corrosion**, 2000

66. Shirazi S.A, McLaury B S, Jeremy K.E, Modeling solid particle erosion in elbows and plugged tees, pp 277-284, vol. 123, **Journal of energy resources technology**, December 2001.

67. Shirazi, Shadley J R, Dayalan E, Ismail M, Rybicki E F, Erosion-corrosion of carbon steel elbow in CO_2 environment, paper no 119, **Corrosion 95**, 1995

68. Shook.C A, Gillies R G, Modeling High concentration settling slurry Flows, **The Canadian Journal of Chemical Engineering**, pp 709-716, vol. 78, August 2000-a

69. Shook.C A, Gillies R G, Sumner R J, Deposition velocities for Newtonian slurries in turbulent flow, **The Canadian Journal of Chemical Engineering**, pp 704-708, vol. 78, Aug 2000-b

70. Silverman D C, On estimating conditions for simulating velocity sensitive corrosion in the rotating cylinder electrode, pp 1115-1118, **Corrosion**, vol. 55, December, 1999.

71. Spitzer.D.W, **Flow Measurement**: Practical guideline for measurement and control, Instrument Society of America, 1991

72. Sundararajan G, Shewmon P G, A comprehensive model for the solid particle erosion of ductile materials, **Wear**, vol. 149 pp111-127, 1991

73. Walker C.I. Development of a wear test to simulate slurry erosion, paper K1, **Hydrotransport 11**, Stratford upon Avon, U.K, October 1988

74. Wang M.H, Group progress meeting, **University of Alberta**, 27 June 2003.

75. Wood R J K, Jones T F, Miles N J, Ganeshalingam J, Upstream swirl-induction for reduction of erosion damage from slurries in pipeline bends, pp 770-778, **Wear**, 2001

76. Zheng Z, Cheng X, Zheng Y, Numerical simulation of erosion-corrosion in liquid solid two phase flow, **Chinese Journal of Chemical Engineering**, pp 347-355, Vol. 8, No.4, 2000

Appendix I

Slurry flow-loop operating Procedure

STARTUP PROCEDURE

1. Set up the test pieces
2. Connect the cathodic protection by positive red cable to 1" long pipe (anode) and negative white cable to all test pieces
3. Close the drain valve of the mixing tank
4. Filled the water to the mixing tank up to the mark
5. Put the calculated amount of NaCl in to the mixing tank
6. Put the calculated amount of sand in to the mixing tank
7. Open the bypass valve
8. Open the loop valve
9. Start the pump
10. Set the cathodic protection potential to 2.5 volt
11. Start the DAQ
12. Start the Oxygen monitoring if necessary
13. Start the mixer
14. Increase the pump speed to the required flow rate
15. Close the bypass valve
16. Adjust the cathodic protection potential
17. Monitor the temperature and if is low adjust the temperature by adding hot water
18. Monitor every 30minutes

The pH values of these should me measured and maintained at 7

SHUTDOWN PROCEDURE

1. After the test period, reduce the pump speed its lowest frequency (5Hz)
2. Stop the pump by pressing the button Q on the control panel
3. Open the by pass valve on the flow-loop
4. Close the loop valve on the flow-loop
5. Drain the water in the loop by open the drain valve from the circulation tank
6. Clean the circulation tank

EMERGENCY SHUTDOWN PROCEDURE

1. Stop the pump by pressing the button Q on the pump control panel or off the three phase circuit breaker
2. Close all the loop valves
3. Drain the water in the loop by open the drain valve from the circulation tank

Appendix II

Force excreted by single particle impact

This calculation is based on the following expressions adapted from Shirazi et al (2001) published presentation.

The major component of the force acting on a particle is the drag that is excreted on the particle by the fluid. Assume same transferred on the metal surface during impact.

$$F_D = \frac{\pi d_p^2 \rho_p C_D \left| v_p - v_f \right|}{8} \left(v_p - v_f \right)$$

The drag coefficient C_d is given by

$$C_D = \frac{24}{\mathrm{Re}_s} \left(1 + 0.15 \mathrm{Re}_s^{0.687} \right)$$

The Reynolds number based on the relative (slip) velocity between the particle and the fluid and Re is defined by

$$\mathrm{Re}_s = \frac{\left(v_p - v_f \right) d_p}{\nu}$$

Where:

- ν = kinematic viscosity
- v_f = local fluid velocity and assumed to be zero
- v_p = local sand particle velocity (assumed Wong CFD simulations, 2003)
- d_p = average particle diameter
- ρ_p = particle density

However force due to particle mass is not included in this calculations and the trend is shown in Figure 5.7 without actual force excreted on the surface.

Figure 4.17 : Micrograph of the corrosion at 2.5 m/s and 32°C after 22 hrs

Figure 4.18 : Erosion-corrosion after 30 hrs

Figure 4.24 : Flow-loop reciprocating pump rotor

Rotor after 6 months – almost 50% of the hard chrome coating was removed

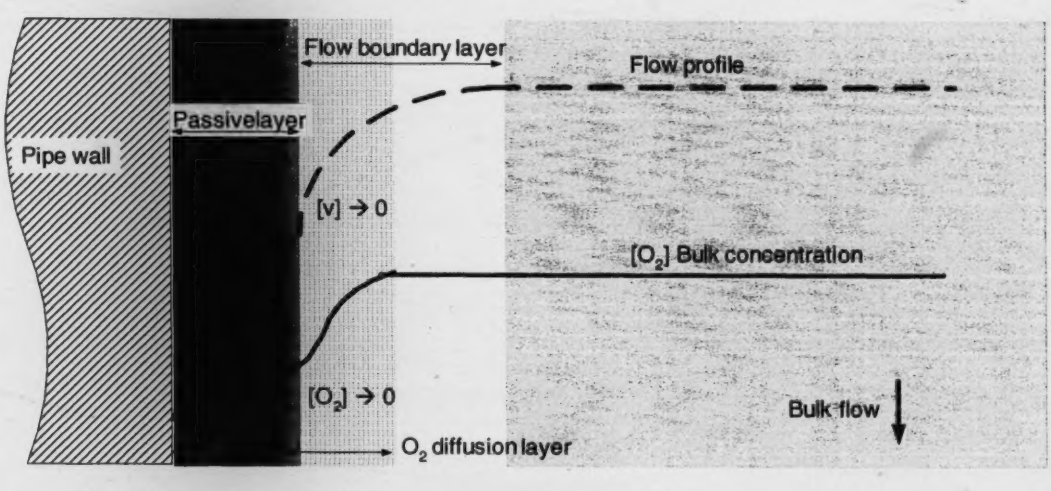

Figure 5.4 : Schematic O_2 diffusion, flow profile and oxide layer near pipe wall